



**A HOLISTIC APPROACH TO REMOTE
CONDITION MONITORING FOR THE
ACCURATE EVALUATION OF RAILWAY
INFRASTRUCTURE AND ROLLING STOCK**

By

Patrick Valley

A thesis submitted to
The University of Birmingham
for the degree of
DOCTOR OF PHILOSOPHY

School of Metallurgy and Materials
College of Engineering and Physical Sciences
University of Birmingham
September 2019

UNIVERSITY OF
BIRMINGHAM

University of Birmingham Research Archive

e-theses repository

This unpublished thesis/dissertation is copyright of the author and/or third parties. The intellectual property rights of the author or third parties in respect of this work are as defined by The Copyright Designs and Patents Act 1988 or as modified by any successor legislation.

Any use made of information contained in this thesis/dissertation must be in accordance with that legislation and must be properly acknowledged. Further distribution or reproduction in any format is prohibited without the permission of the copyright holder.

SYNOPSIS

The rail industry needs to address a number of important operational challenges in the foreseeable future. First of all, the safety of rail transport needs to be maintained at an absolute maximum matching the achievements of the European airline industry of zero fatalities. Secondly, promote sustainable growth to support increasing demand for both passenger and freight rail transport. Thirdly, support the implementation of measurable innovations and improvements that help increase capacity of current infrastructure through enhanced availability. Finally, maximise the environmentally benign character of railway transport through exploitation of novel technologies such as hydrogen trains and advanced electrification employing renewable energy sources.

This project, primarily focused on the UK Rail infrastructure, investigated the benefits arising from a holistic approach in the application of Remote Condition Monitoring (RCM) as a critical means for the accurate, efficient, reliable and cost-effective evaluation of key railway infrastructure assets and rolling stock. This work involved the use of several techniques and innovative methodologies based primarily on Acoustic Emission (AE) and vibration analysis in order to address the evaluation requirements for different components of interest. The results obtained have been very promising and present rail infrastructure managers and rolling stock operators with new opportunities for improved and more reliable operations.

This work has led to the instrumentation of multiple sites across the UK rail network enabling measurements to be carried out on various assets under actual operational conditions. At

Cropredy an integrated high-frequency vibro-acoustic RCM system has successfully been installed on the Chiltern railway line on the way from London to Birmingham. This customised system has been fully operational since 2015 measuring more than 200 passenger and freight trains every day moving at speeds up to 100 miles per hour (MPH). Prior to the installation of the system at Cropredy a Certificate (PA05/06524) of Acceptance was issued by Network Rail which after being renewed recently is now valid until September 2021. The system is due for an upgrade in the following stage of development, employing wireless sensors and advanced energy harvesting devices which are being developed under a collaborative Engineering and Physical Sciences Research Council (EPSRC) project between Exeter and Birmingham Universities, Network Rail, Swiss Approval UK and Quattro.

The widespread implementation of the techniques and methodologies researched will give rise to significant potential impact with respect to the effectiveness of maintenance strategies, particularly in terms of cost efficiency, improved availability of railway assets and better planning of available resources. As modern rail transport moves towards 24-hour railway, the inspection, maintenance and track renewal and upgrade regime will need to be re-thought at a fundamental level. Effective RCM will be a key factor in realistically enabling true round the clock operations.

The results presented in this thesis have been part of a six-year research effort with a clear focus on addressing the true industrial need. The findings of this work have led to a re-think within Network Rail regarding the new possibilities arising from the effective use of RCM in designing and implementing more efficient and cost-effective railway operations whilst helping reduce

the cost. The use of autonomous sensing systems in the future will change the inspection and maintenance strategies currently used shifting towards a truly prognostic operational strategy.

ACKNOWLEDGEMENTS

I wish to express my gratitude to my mother. She has always fully supported my academic journey. She is my inspiration, the greatest scholar I have ever known. Without her support it would have been impossible for me to complete my research.

I also want to say a very big thank you to my supervisor and friend Dr Mayorkinos Papaelias. Without his support, encouragement, patience, expert guidance, knowledge and feedback this PhD would not have been achievable. Thank you.

I gratefully acknowledge the financial support provided by Network Rail. This was facilitated by my industrial supervisor Brian Paynter. Brian gave me the support, space and time to focus on this piece of work.

I would like to thank my colleague's Dr Zheng Heung and Dr Arash Amini, initially for being great mentors whom I now count as great friends. It was my pleasure working with the both of you.

I would finally like to thank all my colleagues at Network Rail who helped me to collect vital information that I needed to complete this work. There are too many to name them all, however special thanks to Ciara Eves, Caroline Higgins, Jenna Davies, Brian Whitney, Tara Scott, Dr Ian Coleman, Chris Scharf and many others.

PUBLICATIONS

- M. Papaelias, Z. Huang, S. Kaenwunruen, M. Kongpuang, S. Kerkyras, F. P. Garcia Marquez, S. Shc, P. Vallely “*Online assessment of the structural integrity of railway crossings using high frequency acoustic emission sensors*”. Proceedings of the 6th Conference of the Combined Australian Materials Society, New South Wales, Australia, 27th - 29th November 2018
- M. Papaelias, A. Amini, R. Culwick, J. Heesom, Z. Huang, V. L. Jantara Junior, S. Kaenwunruen, S. Kerkyras, M. Kongpuang, F. P. Garcia Marquez, S. Shc, A. Upton, P. Vallely “*Advanced remote condition monitoring of railway infrastructure and rolling stock*”. In Proceedings of the 1st International Conference on Welding & NDT, Athens, Eugenides Foundation, 22-23 October 2018
- P Vallely & M Papaelias “*A Qualitative Comparison of Advantages and Disadvantages of Structural Health Monitoring of Railway Infrastructure over Conventional Inspection Methods*”. Proceedings of the 12th European Conference of Non-Destructive Testing (ECNDT2018), Gothenburg, Sweden 11th - 15th June, 2018

- J Davies, P Vallely, M Papaelias & Z Huang “*Addressing future rail network performance challenges through effective structural health monitoring*” Proceedings of the 2018 ASME Joint Rail Conference (JRC2018), Pittsburgh, PA, USA, April 18th - 20th 2018
- P. Vallely “*The UK Experience with RCM*” 2nd invitation presentation at the British Council- TUBITAK Knowledge Transfer on RCM for Railways Workshop, December 2017, Istanbul, Turkey
- P. Vallely “*The UK Experience with RCM*” 1st invitation presentation at the British Council- TUBITAK Knowledge Transfer on RCM for Railways Workshop, March 2016, Istanbul, Turkey.
- P. Vallely and M. Papaelias “*Integrating Remote Condition Monitoring of Railway Infrastructure with High Speed Inspection*” In Proceedings of WCCM 2017, London, UK, June 2017.
- P. Vallely, M. Papaelias, Z. Huang, S. Shi, S. Kaewunruen, J. Davies “*The Stephenson Conference: Research for Railways*”. IMechE, April 2017, London, UK.

- S. Shi, Z. Han, Z. Liua, P. Vallely, S. Souza, M. Papaelias “*Quantitative monitoring of brittle fatigue crack growth in railway steel using acoustic emission (Proceedings of the Institution of Mechanical Engineers*”. Part F: Journal of Rail and Rapid Transit).
- S. Shi, Z. Huang, S. Kaewunruen, P. Vallely, S. Souza and M. Papaelias “*Quantitative monitoring of brittle fatigue crack growth in railway steel using acoustic emission*”. In Proceedings of WCCM 2017, London, UK, June 2017.
- E. Giannouli, Z. Huang, A. Amini, P. Vallely, S. Souza, F. P. Garcia Marquez, M. Papaelias “*Remote condition monitoring of railway axle bearings based on data fusion from several sensors*”. In Proceedings of WCCM 2017, London, UK, June 2017.
- M. Papaelias, A. Amini, Z. Huang, P. Vallely, D. C. Dias, S. Kerkyras “*Online condition monitoring of rolling stock wheels and axle bearings*”. Proceedings of the Institution of Mechanical Engineers, Part F: Journal of Rail and Rapid Transit, Vol. 230, No. 3, pp. 709-723, March 2016.
- M. Papaelias, Z. Huang, A. Amini, P. Vallely, N. Day, R. Sharma, S. Kerkyras, Y. Kerkyras “*Advanced wayside condition monitoring of rolling stock wheelsets*”. In the Proceedings of ECNDT 2014, Prague, Czech Republic, 2014, October 2014

LIST OF ABBREVIATIONS

A	Amp
AC	Alternating Current
ACFM	Alternating Current Field Measurement
AE	Acoustic Emissions
AEA	Applied Electronic Applications
AI	Artificial Intelligence
AL ₂ O ₃	Alumina
ANN	Artificial Neural Networks
BNC	Bayonet Neill-Concelman
CF	Crest Factor
CM	Condition Monitoring
CP5	Control Period 5
DAQ	Data Acquisition Card
dB	Decibel
DC	Direct Current
DCPD	Direct Current Potential Drop
DfT	Department for Transport
DFT	Discrete Fourier Transform (DFT)

DNO	Distribution Network Operator
EC	Eddie Current
ECO	Electrical Control Operator
ECR	Electrical Control Room
ECT	Eddie Current Testing
EPSRC	Engineering and Physical Sciences Research Council
FAG	Fischers Aktlen-Gasellschaft
FFT	Fast Fourier Transform
FOC	Freight Operating Company
FRC	Fibre Reinforced Composite
HABD	Hot Axle Box Detector
HS1	High-Speed 1
HS2	High-Speed 2
H _v	Vickers hardness
Hz	Hertz
kHz	Kilohertz
km/h	Kilometres per Hour
kN	Kilonewton
kSamples/s	Kilo Samples per Second
kV	Kilovolt

LPI	Liquid Penetrant Inspection
MEMS	Micro Electronic Mechanical Systems (MEMS)
MeV	Mega Electron Volt
MFL	Magnetic Flux Leakage
MHz	Megahertz
mm	Millimetres
MnS	Manganese Sulphides
MPH	Miles Per Hour
MPI	Magnetic Particle Inspection
mS	Milliseconds
mV	Millivolts
N	Newton
NDT	Non-Destructive Testing
NR	Network Rail
OLE	Overhead Line Equipment
ORBIS	Offering Better Rail Information Services
PAC	Physical Acoustics Corporation
PLPR	Plain Line Pattern Recognition
PPA	Peek to Peek Amplitude

PSP	Principle Supply Point
PZT	Lead Zirconate Titanate
R&D	Research and Development
RCF	Rolling Contact Fatigue
RCM	Remote Condition Monitoring
RCM	Remote Condition Monitoring
RMS	Root Mean Square
RSSB	Rail Safety and Standards Board
RTU	Remote Terminal Unit
SCADA	Supervisory Control and Data Acquisition
SE	Spike Energy
SFT	Stress Free Temperature
SHM	Structural Health Monitoring
SK	Spectral Kurtosis
SKF	Svenska Kullagerfabriken
SNR	Signal to Noise Ratio
SSP	Signalling Supply Point
TAG	Track Acoustic Detectors
TOC	Train Operating Company
UOB	University of Birmingham

UK	United Kingdom
USB	Universal Serial Bus
UT	Ultrasonic Testing
V	Volt
VAC	Volt Alternating Current
VTG	Vereinigte Tanklager und Transportmittel

TABLE OF CONTENTS

PUBLICATIONS	6
LIST OF ABBREVIATIONS	9
LIST OF FIGURES	19
CHAPTER 1: THE INDUSTRIAL NEED	30
1.1 Introduction.....	30
1.2 The industrial need.....	33
1.3 Common root causes of railway accidents	39
1.4 Aims and objectives.....	41
1.5 Thesis structure	41
1.6 Chapter 1 Summary	42
CHAPTER 2: ROLLING STOCK FAULTS	44
2.1 Introduction.....	44
2.2 Types of rolling stock	45
2.3 Wheel Defects.....	48
2.3.1 Rolling Contact Fatigue Cracks	48
2.3.2 Sub-surface fatigue cracks	49
2.3.3 Thermomechanical Fatigue Cracks.....	50
2.3.4 Wheel Flats.....	50
2.3.5 Pitting	52

2.3.6 Shelling.....	52
2.3.7 Metal Build-Up	53
2.4 Axle Bearing Defects.....	53
2.5 Axle Defects	56
2.6 Faulty suspensions	58
2.7 Chapter 2 Summary	59
CHAPTER 3: STRUCTURAL DEGRADATION OF RAILWAY INFRASTRUCTURE AND MAIN TYPES OF DEFECTS.....	60
3.1 Introduction.....	60
3.2 Rail defects	61
3.3 Sleepers and Rail Pads.....	67
3.4 Cast manganese crossings.....	69
3.5 Chapter 3 Summary	71
CHAPTER 4: REMOTE CONDITION MONITORING SYSTEMS FOR ROLLING STOCK	72
4.1 Introduction.....	72
4.2 Hot Axle Box Detectors (HABDs)	73
4.3 Wheel Check Systems	75
4.4 Trackside Acoustic Detectors	77
4.5 Overhead line system monitoring	77
4.6 Train Detection Systems	79

4.7 Remote Condition Monitoring of Signalling / Principle Supply Points	80
4.8 Onboard RCM.....	83
4.9 Chapter 4 Summary	84
CHAPTER 5: RAILWAY INFRASTRUCTURE INSPECTION TECHNIQUES	85
5.1 Introduction.....	85
5.2 Visual inspection.....	87
5.3 Ultrasonic testing	87
5.4 Radiography.....	88
5.5 Thermography.....	89
5.6 Eddy Current Testing.....	89
5.7 Magnetic Flux Leakage (MFL).....	90
5.8 Magnetic Particle Inspection (MPI).....	91
5.9 Liquid Penetrant Inspection (LPI)	91
5.10 Chapter 5 Summary	92
CHAPTER 6: ACOUSTIC EMISSION AND VIBRATION ANALYSIS	94
6.1 Introduction.....	94
6.2 Acoustic Emission (AE)	95
6.3 Vibration Analysis	102
6.4 Chapter 6 Summary	105
CHAPTER 7: SIGNAL PROCESSING OF ACOUSTIC EMISSION AND VIBRATION DATA.....	106

7.1 Introduction.....	106
7.2 Peak-Peak amplitude (PPA).....	106
7.3 Moving Root Mean Square (RMS).....	107
7.4 Moving Crest Factor (CF).....	108
7.5 Moving Kurtosis	110
7.6 Power spectral analysis using Fast Fourier Transform (FFT)	111
7.7 Spike energy (SE)	112
7.8 Cepstral analysis	113
7.9 Spectral Kurtosis.....	113
7.10 Signal Correlation	113
7.11 Wavelet analysis	114
7.12 Statistical analysis for parametric data	115
7.13 Chapter 7 Summary	115
CHAPTER 8: EXPERIMENTAL METHODOLOGY	116
8.1 Introduction.....	116
8.2 Laboratory trials.....	117
8.2.1 Three-point fatigue bending tests	117
8.2.2 Amsler rolling tests	119
8.3 Rolling stock wheel and axle bearing testing at Long Marston.....	121
8.4 Cast manganese crossing tests	125
8.5 Cropredy rolling stock wheel and axle bearing monitoring system	128

8.6 Chapter 8 Summary	131
CHAPTER 9: RESULTS AND DISCUSSION	132
9.1 Introduction.....	132
9.2 Three-point fatigue bending laboratory trials	133
9.3 AMSLER rolling tests	143
9.4 Long Marston Field Trials under simulated operational conditions.....	156
9.5 Cropredy site field trials under actual operational conditions	171
9.6 Cast manganese crossing trials under actual operational conditions	175
9.7 Chapter 9 Summary	186
CHAPTER 10: CONCLUSIONS AND FUTURE WORK	187
10.1 Conclusions.....	187
10.2 Future Work.....	190
REFERENCES	192
APPENDIX 1	207

LIST OF FIGURES

Figure 1: Map showing the sites between Birmingham New Street and Milton Keynes on the UK Rail Network instrumented with existing Hot Axle Box Detector (HABD) RCM systems (courtesy of Nick Pinder, Network Rail)	36
Figure 2: The main categories of RCM technology used on the UK Rail Network.....	38
Figure 3: Railway accidents considered in D-RAIL FP7 project classified based on their root cause [14].	39
Figure 4: Rolling stock related accidents classified by root cause [14].	40
Figure 5: Photograph of a Falcon Wagon	45
Figure 6: a) Ballast side tipper wagon and b) Virgin BR Class 390 'Pendolino' EMU	46
Figure 7: The Summit Tunnel accident and subsequent fire caused by the derailment of a train carrying fuel. The derailment was initiated by a faulty axle bearing that led to the rupture of the axle while the train was moving through the tunnel derailing the train [28].	47
Figure 8: The Rickerscote accident in the UK in 1996 [16] and b) the Viarregio accident in Italy involving a tanker freight train carrying fuel [29].	48
Figure 9: Schematic showing the basic characteristics of a monoblock wheel (courtesy of NSW Transport RailCorp).	50
Figure 10: Photograph of a freight wagon monoblock wheel containing multiple wheel flats.....	51

Figure 11: Examples of shelling on freight (left) and passenger wheels (right).	52
Figure 12: Metal build-up on the surface of the tread of a freight monoblock wheel.....	53
Figure 13: Tapered Roller Bearing (Courtesy of Roller Bearing Industries Inc.).....	54
Figure 14: Derailment due to axle bearing failure (courtesy of Mr. Nick Pinder, Network Rail).	55
Figure 15: Photograph showing a sheared axle bearing (Courtesy of Mr. Nick Pinder, Network Rail).	56
Figure 16: Photograph of fatigue cracks on the surface of the axle (Courtesy of Dr John Rudlin, TWI Limited).....	57
Figure 17: Photographs of pitting corrosion on a freight axle.	58
Figure 18: RCF cracks with high level of plastic flow (photo courtesy of Brian Whitney, Network Rail).....	62
Figure 19: Shelling of the running surface of the rail [53].....	62
Figure 20: Photograph of a plain rail that fractured as a result of a crack which developed in the base of the rail. The rail sat on a sleeper with a degraded rail pad in an area of voiding on a transition to a bridge structure (photographs courtesy of Brian Whitney, Network Rail).	63
Figure 21: Photograph showing classic tache oval fatigue crack (courtesy of Brian Whitney, Network Rail).....	64
Figure 22: a) Rail foot corrosion (courtesy of Brian Whitney, Network Rail) and b) bolt hole cracking [53].....	64

Figure 23: a) Heavy RCF cracking on rail section revealed from service [53] and b) the site of the Hatfield accident [50].....	65
Figure 24: Aluminothermic weld preparation, Shugborough Tunnel, December 2012.	67
Figure 25: Photograph of a failed rail pad.....	68
Figure 26: Photograph of damaged crossing showing evidence of porosity due to the manufacturing process (the photograph is from Hardface Technology Presentation on Repair and Rebuild of Manganese crossings using Hardface Welding, 2003).	70
Figure 27: Typical HABD arrangement (the schematic is courtesy of Mermec).....	74
Figure 28: Photograph of a Wheelcheck system (the photograph is courtesy of Network Rail).	76
Figure 29: Pan Check Alarm Window (the screenshot is courtesy of Network Rail LNW Route Control)	78
Figure 30 : A Treadle system installed on the Chiltern rail line between Banbury and Leamington Spa station.	80
Figure 31 : Alarm status at Headstone Lane Principle Supply Point (screenshot courtesy of Rugby Electrical Control Room)	83
Figure 32: PLPR Linescan and Thermal Camera Design (this schematic is courtesy of Nick Pinder, Network Rail).....	86
Figure 33: Image produced by the cameras from the PLPR system (these images are courtesy of Nick Pinder, Network Rail)	86

Figure 34: a) a visual inspection being carried out at night by a NR Engineer, b) the undercarriage of a NR ultrasonic test unit, c) images produced by a thermographic inspection [125], d) Inspection using the Eddie Current roller search unit, and e) an inspection in progress where liquid has been applied to a crossing bolt hole under inspected at NR’s recycling depot at Whitmoore, Cambridgeshire (images a, b, d & e courtesy of Network Rail). 93

Figure 35: The Acoustic Emission principle (Schematic is courtesy of Physical Acoustics Corporation) 98

Figure 36: Schematic diagram showing the architecture of a typical AE sensor mounted on a test piece using an appropriate couplant, such as water-based gel, grease or araldite (Schematic diagram courtesy of Physical Acoustics Corp). 99

Figure 37: Schematic diagram showing a typical architecture of an accelerometer [123]. 104

Figure 38: Schematic diagram showing a standard three-point fatigue bending sample. 118

Figure 39: a) Experimental setup with PAC and customised acoustic emission system. The sample is in place and undergoing cyclic loading. Crack length is continuously monitored with the DCPD instrument. b) this photograph shows a close-up of a failed sample. The two acoustic emission sensors are visible together with the DCPD instrument connections. The sample has been loaded using three-point cyclic loading. 119

Figure 40: a) Example of Amsler rolling testing setup, b) Reference sample geometry, and c) Test sample geometry. 121

Figure 41: Tanker freight wagons with several axel bearings artificially damaged in the roller or race using a power tool. 122

Figure 42: The customised data acquisition equipment used during trials at Long Marston. 123

Figure 43: AE sensors and accelerometer installed in one of the axle bearings of the tanker freight wagons tested in Long Marston.	124
Figure 44: Wayside installation of AE sensors and accelerometers at Long Marston.	125
Figure 45: Crossing tested in a) Wembley, b) Hatton, c) Watford and d) Newark.....	126
Figure 46: Certificate of Acceptance issued by Network Rail for the customised AE and vibration system built in-house, enabling trials to be performed at various site on the UK railway network....	128
Figure 47: Photographs showing the installation of the customised 12-channel AE-vibration system at the Cropredy site, direction from London towards Birmingham.	130
Figure 48: Schematic diagram of the Cropredy system sensor layout.	131
Figure 49: AE activity for the reference sample over 10s long acquisition at 1 MS/s. The thickening of the signal occurs during the loading stage and arises from the bending moments. During unloading the signal amplitude drops to background noise. There are no other visible peaks indicating crack growth. Some minor peaks visible in the signal are due to noise from the DARTEC servo-hydraulic mechanism. The peak-peak value does not exceed ± 0.11 V.....	134
Figure 50: Raw dataset together with moving RMS and moving Kurtosis graphs. No crack indication is visible	135
Figure 51: Plot showing crack growth with normalised cumulative AE activity up to the point of failure for a pre-cracked cast manganese steel sample.....	136
Figure 52: Raw acoustic emission dataset at mid-stages of the test for one of the pre-cracked cast manganese steel sample. The AE activity is clearly intense with crack growth occurring at every loading cycle.	137

Figure 53 : Raw AE dataset, moving RMS and moving Kurtosis at the middle stage of the fatigue test for the cast manganese steel sample.....	138
Figure 54: The Paris-Erdogan law plot for some of the R260 grade steel samples tested under three-point fatigue bending testing.	139
Figure 55: Normalised AE cumulative energy detected with respect to crack growth measured with DCPD and increasing loading cycles plot for R260 rail sample S1 up to final failure	140
Figure 56: Normalised AE cumulative energy detected with respect to crack growth measured with DCPD and increasing loading cycles plot for R260 rail sample S3 up to final failure. Sensor 1 operation stopped earlier due to loss of coupling and hence the discrepancy in the trend also	141
Figure 57: Normalised AE cumulative energy detected with respect to crack growth measured with DCPD and increasing loading cycles plot for R260 rail sample S5 up to final failure.	142
Figure 58: Raw AE waveform for Amsler test on wheel samples with no defects present.	144
Figure 59: Moving RMS plot of the AE signal. The low intensity peaks visible are largely related to the background noise arising from a known faulty Amsler bearing and not from the sample wheels.	145
Figure 60: Power spectrum of the AE waveform captured for the wheel samples with no defects present. The peaks evident are associated with the background noise arising from the Amsler machine itself, particularly the known faulty bearing	146
Figure 61: Spike energy plot showing some low intensity peaks (max amplitude does not exceed 10^{-3} V ²) which are associated with the bearing fault only in the Amsler machine itself and not the wheel samples which are in good condition.	147

Figure 62: Raw AE waveform for the healthy wheel samples after load has been removed. This leads to much lower background noise since the Amsler bearing does not get as stressed as when under load. 148

Figure 63: The moving RMS plot with no peaks related to the bearing being evident. 148

Figure 64: Plot of the power spectrum. It is evident that all peaks have disappeared, and the signal contains very little noise. 149

Figure 65: No peaks are evident in the spike energy plot either. 149

Figure 66: Raw AE waveform for the defective wheels after an 8 kg load has been applied. Some low intensity peaks are evident just above the background noise. 150

Figure 67: Moving RMS plot with several peaks present indicating the presence of a fault. 151

Figure 68: Power spectrum showing a much richer frequency content when the wheel defect is present in comparison with the healthy wheel setup. 152

Figure 69: Spike energy plot indicating peaks at additional frequencies. However, the peaks for the bearing fault remain dominant. 153

Figure 70: Raw AE waveform with multiple peaks evident above the background noise. 154

Figure 71: Moving RMS plot. Notice the much higher amplitude of the peaks present when higher load is applied on the experimental setup. 154

Figure 72: Power spectrum analysis of the AE waveform indicating an increase in the frequency content and some higher intensity peaks at certain frequencies. 155

Figure 73: Spike energy plot with noticeable peaks at lower rotational frequencies associated with the rotation of the wheels. The peaks associated with the bearing fault are also still present but not as dominant as before in comparison with the wheel defect. 155

Figure 74: Onboard raw vibration signal for a healthy axle bearing..... 156

Figure 75: Moving RMS of the onboard vibration signal. The peaks are associated with joints on the track as the test train moves over them. 157

Figure 76: Power spectrum of the vibration signal. Some peaks evident are associated with the vibration arising from the movement over the joints. 158

Figure 77: Spike energy plot with no peaks evident, suggesting that the monitored bearing is healthy. 158

Figure 78: Raw vibration signal plot for faulty bearing. No much difference in comparison with the vibration signal for the healthy bearing is evident. 159

Figure 79: Moving RMS of the vibration signal for the faulty bearing. Again, the plot resembles that of the healthy bearing, with peaks associated with the transition over the track joints..... 160

Figure 80: Power spectrum of the vibration signal for the faulty bearing showing considerable peaks at particular frequencies which are associated with the bearing fault rather than the impacts arising during the transition over the jointed parts of the track 160

Figure 81: Spike energy plot for the vibration signal associated with the faulty bearing. 161

Figure 82: Raw AE waveform taken onboard for the healthy bearing. Notice the low level noise and almost complete absence of peaks associated with the jointed track. 162

Figure 83: Moving RMS indicating very low amplitude peaks indicating that there is no fault present.
..... 162

Figure 84: Power spectrum of the AE waveform. Notice the almost complete absence of frequency information in the power spectrum with the exception of a few low amplitude peaks at certain frequencies associated with background noise arising from the movement of the train..... 163

Figure 85: Spike energy plot of the AE signal. Notice the absence of any peaks with the exception of a very low amplitude peak at approximately 33.5 Hz. It is unknown what has given rise to this particular peak, but it is likely related to a background source, possibly the power axles of the locomotive pulling the test freight wagon..... 163

Figure 86: Raw AE waveform with multiple peaks present above the background noise level. 164

Figure 87: Moving RMS plot with several peaks present. These peaks are clearly associated with the bearing defect present..... 164

Figure 88: Power spectrum of the AE waveform for the faulty bearing. Notice the rich frequency content of the signal particularly between 130 kHz to 200 kHz in comparison with the power spectrum for the healthy condition. 165

Figure 89: Spike energy plot not showing any useful information in this particular instance..... 166

Figure 90: Wayside vibration signal for rolling stock with contaminated axle bearings. Clear peaks above the background noise are detectable. 167

Figure 91: Moving RMS of the vibration signal indicating the high energy content of the peaks observed in the raw AE signal. These are associated with the axle bearing defect as well as the vibrational response to the transition of the wheel trains over each joint along the track section being monitored. 167

Figure 92: Raw AE waveform taken wayside. Multiple peaks are clearly observed.....	168
Figure 93: Moving RMS signal showing the presence of the axle bearing defects as well as the presence of the artificially induced flat in one of the wheels of the test train.	169
Figure 94: a) Raw AE data acquired from a healthy bearing and b) its moving RMS plot using a filtering time window of 60 points.....	170
Figure 95: a) Raw AE data acquired from a bearing with a 4 mm roller defect and b) RMS processed results. Notice the amplitude of the strong RMS peaks	171
Figure 96: Raw AE signal for passenger train. The peak observed at the end of the signal is associated with a power axle causing sliding of the wheel as it moves along the track, generating additional noise captured by the AE sensor.....	172
Figure 97: The corresponding moving RMS signal for a passenger train moving over the instrumented site.	173
Figure 98: Power spectrum with relatively low amplitude peaks associated with background noise sources alone.	174
Figure 99: Spike energy plot indicating no wheel or axle bearing defect is present.....	175
Figure 100: a) Photograph of the Newark flat crossing, b) the installation process of the AE system overnight and c) measurement setup and example rolling stock moving over the crossing at normal operational speed.....	177
Figure 101: a) and c) raw AE waveforms acquired at Newark flat crossing and b) and d) corresponding power spectra indicating low frequency content above 100 kHz. This suggests that there is no crack propagation occurring which would result in peaks at higher frequencies being clearly observed. ...	179

Figure 102: Photographs showing the: a) the crossing measured and b) indicative traffic..... 181

Figure 103: a) and c) raw AE waveforms acquired at Wembley crossing and b) and d) corresponding power spectra indicating low frequency content above 100 kHz. This suggests that there is no crack propagation occurring which would result in peaks at higher frequencies being clearly observed. ... 183

Figure 104: Photographs of a) defective crossing in Watford, b) experimental setup and c) captured signal indicating clear crack growth when the crossing was loaded by a heavy freight train. 185

Figure 105: Raw AE signal indicating crack growth events occurring..... 186

CHAPTER 1: THE INDUSTRIAL NEED

1.1 Introduction

Traffic on rail networks around the world has been continuously increasing in recent years. Rolling stock is travelling at higher speeds while there is also increased passenger and freight demand. The result is heavier axle loads and higher tonnage carried per year along the rail network. This also leads to an increase in the frequency of inspection and maintenance interventions [1].

The rail industry in the United Kingdom (UK) as well as the rest of the world is set to continue to grow at a strong pace until at least the middle of the 21st century. More high-speed lines with trains travelling at speeds in excess of 250 km/h are continuously being designed and constructed. The growth plans will not only connect major cities within a country but there are plans to connect Europe with the Far East and Asia as part of the modern Silk Road.

In the UK, following from the success of High-Speed 1 (HS1) the British government decided that there is a fundamental need to strengthen the high-speed capacity on the North-South axis of the rail network in an effort to try and reduce automotive greenhouse gases, improve air quality and ease off the strain on the national road system. This has resulted in the establishment of the High-Speed 2 (HS2) project which consists of three main phases. The first phase of HS2 which is currently under way will connect London Euston with Birmingham New Street reducing the travel time from 81 minutes to 49 minutes. The second phase planned for 2022 will connect London Euston with Manchester Piccadilly reducing travel time from 128 minutes

currently to 68 minutes, and London Euston to Leeds reducing travel time from 132 minutes currently to 83 minutes. Thus, once the second phase of HS2 is completed commuters will be able to reach Manchester in less time than those travelling from London to Birmingham today. If the third phase of the HS2 project materialises, London Euston will be connected with the city of Edinburgh. In September 2019 the Government announced that the first phase of HS2 could be delayed by up to 5 years to 2033. This would have a knock-on effect on the completion dates of all subsequent phases.

The increasing traffic density and operational speeds in the UK rail network suggest that any unexpected faults or failures in rail infrastructure (broken rails, damaged cast manganese crossings, cracked sleepers, damaged bridges and tunnels) or rolling stock (damaged wheels, cracked or corroded axles, faulty bearings and damaged bogie suspensions) can result in severe delays and disruption of normal operations. Furthermore, such faults can cause dangerous derailments involving human casualties, damage to the rail infrastructure or furniture and incur substantial unnecessary repair and restoration costs for the infrastructure maintenance delivery managers and operators.

Technological advances over the past few decades in train design and infrastructure engineering have enabled the extensive use of high-speed trains. The nature of rail freight operations has also been changing gradually with high-value goods conventionally transported from the site of production to the site of consumption via rail instead of road. The increasing market trend for the rail industry is forecast to continue at least until 2050 since rail transport is steadily becoming a more attractive option over other means of transportation for both passengers and

goods [2-4]. Train travel is generally cheaper than using a car, and usually the fastest option to reach a destination. It is also inherently safer and far more environmentally friendly in comparison to car travel, without compromising passenger convenience.

This chapter introduces the industrial requirement for enhanced RCM capability over existing state of the art inspection and maintenance methods. The maintenance strategy for the UK rail network is largely based on corrective and preventive methods rather than condition-based and prognostic. To maximise the operational capability of the UK rail transport industry, there is a need to implement effective condition-based and prognostic inspection and maintenance strategies. To achieve this it is necessary to move away from traditional approaches that have largely exhausted their potential for further improvement through additional research and development [1-5]. It is necessary to highlight the current technological barriers and demonstrate the potential of novel RCM technologies in delivering the necessary technical capabilities that promote further growth of existing rail infrastructure and help maximise available human, equipment and financial resources. Network Rail thanks to its multi-billion annual budget, in-depth technical know-how and management responsibility for the entirety of the UK rail network is uniquely placed to deliver a step-change in current practices through the introduction and implementation of measurable and meaningful innovation [6-7]. This Network Rail-sponsored project forms part of the investment required towards the implementation of this strategy in the foreseeable future.

1.2 The industrial need

In June 2013 as part of Control Period 5 (CP5), Network Rail (NR) set out its strategy for a substantial investment in Research and Development (R&D) activities as part of the modernisation of the UK rail network [6]. This strategy has been further consolidated in CP6 with a further increase of the R&D budget accompanied by a deep-level restructuring of the organisation which is currently under way.

Network Rail's vision is to take a holistic system approach by introducing and implementing advanced technologies that can generate data which will enable it to reduce disruptive maintenance intervention, improve safety, reliability and efficiency whilst help increase customer satisfaction.

As part of the implementation of the R&D-related activities, Network Rail has established collaborative relationships with national industry stakeholders such as the Rail Safety and Standards Board (RSSB), educational and research institutions and partnerships, principal contractor delivery organisations, Train Operating Companies (TOCs) and Freight Operating Companies (FOCs).

TOCs and FOCs play a supportive partnering role whereas the RSSB is a not-for-profit organisation established as a direct result of the Ladbrook Grove rail crash [8]. It has issued various research guides to support rail systems R&D and is primarily funded by the Department for Transport (DfT) [8-9].

The rail network is a complex system consisting of multiple critical components associated with both infrastructure and rolling stock. Faults or failure of infrastructure components, primarily those associated with cracked, corroded or broken rails, damaged crossings, faulty sleepers, rail head geometry deterioration and misalignment can result in rough rides, excessive noise, reduced passenger comfort, emergency speed restrictions, unplanned line closures and ultimately possible derailments [10].

Bridges and tunnels are also critical for the smooth operation of the rail network. In the UK alone there are thousands of bridges and many tunnels which form an integral part of every line across the rail network. A large number of rail bridges and tunnels currently in operation were constructed between the late 19th and early 20th centuries. There is a substantial programme of work in place by Network Rail (NR) to maintain, and were required enhance, these bridges and tunnels such that they are in a condition which can allow modern faster and heavier trains to use them many times every day safely and reliably.

Remote Structural Health Monitoring (SHM) can help the infrastructure manager maintaining these bridges and tunnels to evaluate their condition continuously without having to organise expensive inspection campaigns carried out by engineering teams normally during night-time access when traffic is stopped [11-13].

Occasionally operational emergencies may necessitate that inspections are carried out during the day when trains are running normally. To allow the inspection of a site, trains may be stopped or diverted for a short period of time. However, longer no train periods may be required

if the damage found is significant and the infrastructure manager is required to close the line. Any disruptive access required to correct the fault or failure results in substantial extra operational costs. These costs can increase exponentially as traffic density increases in order to accommodate the constantly growing demand for rail transport services [12-13]. Additional costs are incurred in the form of penalties or fines whilst passengers and goods will need to accept higher than normal travel times [12].

Rolling stock, passenger or freight can suffer from other instances of infrastructure faults and failures which can result in additional costs and higher than normal travel times. Railway wheelsets are prone to develop various types of faults on the wheel tread or the axle bearings. Wheel surface defects and axle bearing faults have serious consequences to rolling stock operations as they can cause impact damage on rail infrastructure, reduce passenger comfort, increase noise levels and derailments [14-15].

To evaluate the condition of wheels and axle bearings in service the rail industry employs various types of wayside condition monitoring systems including wheel impact load, wheel profile, hotbox and axle bearing fault acoustic array detectors [16-17]. Existing wayside systems are expensive assets installed in strategically selected locations of the rail network to optimise as individual checkpoints. Figure 1 is a map that shows the location of existing wayside RCM Hot Axle Box Detector (HADB) equipment installed between two key stations, Birmingham New Street and Milton Keynes, on the UK Rail network.

Although wheel impact load and wheel profile detectors provide reasonably reliable data this is not the case for hot axle box and acoustic array axle bearing fault detectors, which are prone to false alarms. Faults are detectable only when they result in a temperature rise within the region of the axle box or noise produced by the axle bearing is abnormal. This usually happens when the fault has become critical [16].

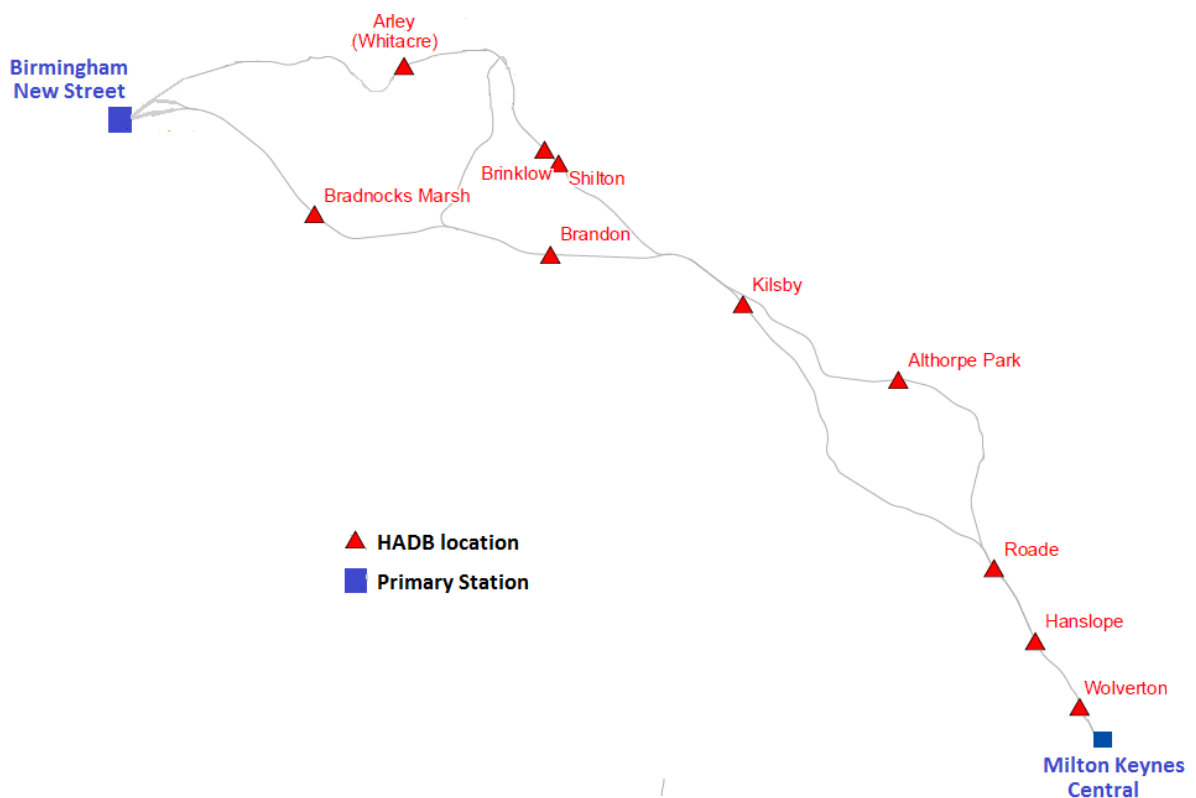


Figure 1: Map showing the sites between Birmingham New Street and Milton Keynes on the UK Rail Network instrumented with existing Hot Axle Box Detector (HABD) RCM systems (courtesy of Nick Pinder, Network Rail)

Infrastructure Route Control Managers have normally a few minutes to deal with a critical axle bearing fault before it may cause a derailment. For this reason, a high-density network of

hotboxes or acoustic arrays is currently required to cover the entire length of the active infrastructure [17-18].

Geometrical deterioration of the wheel tread is also one of the top causes of derailment related to rolling stock and therefore, regular checking and re-profiling of wheel tread geometry is required. This also avoids excessive noise being produced during train movement. Broken rolling stock suspensions which can result in rough rides and excessive noise may also increase the vulnerability of a train to derailment since lateral and vertical movement can surpass the allowed limits when a train is moving through a curve.

The importance of RCM has increased substantially in recent years. Since rail networks are complex systems, different types of RCM equipment need to be employed in order to address the various faults and failures that may develop during operation and which may be associated with either infrastructure or rolling stock.

The four main categories of RCM technology used on the UK rail network are shown in Figure 2. Different RCM equipment produce different types of data which may have fundamentally different storage and processing requirements including trending.

Most of the existing RCM systems which are currently being used, are designed to generate an alarm once a potential fault is identified. Moreover, in almost every case, each piece of equipment acts as a stand-alone unit. This means there is no possibility of trending or correlating with the other units that may be in place along the same line even if they are of the same type

[17-18]. There is very little, or no integration of the data being generated from existing RCM equipment. This limits the potential overall efficiency of these systems and the value of the information generated for the infrastructure manager.

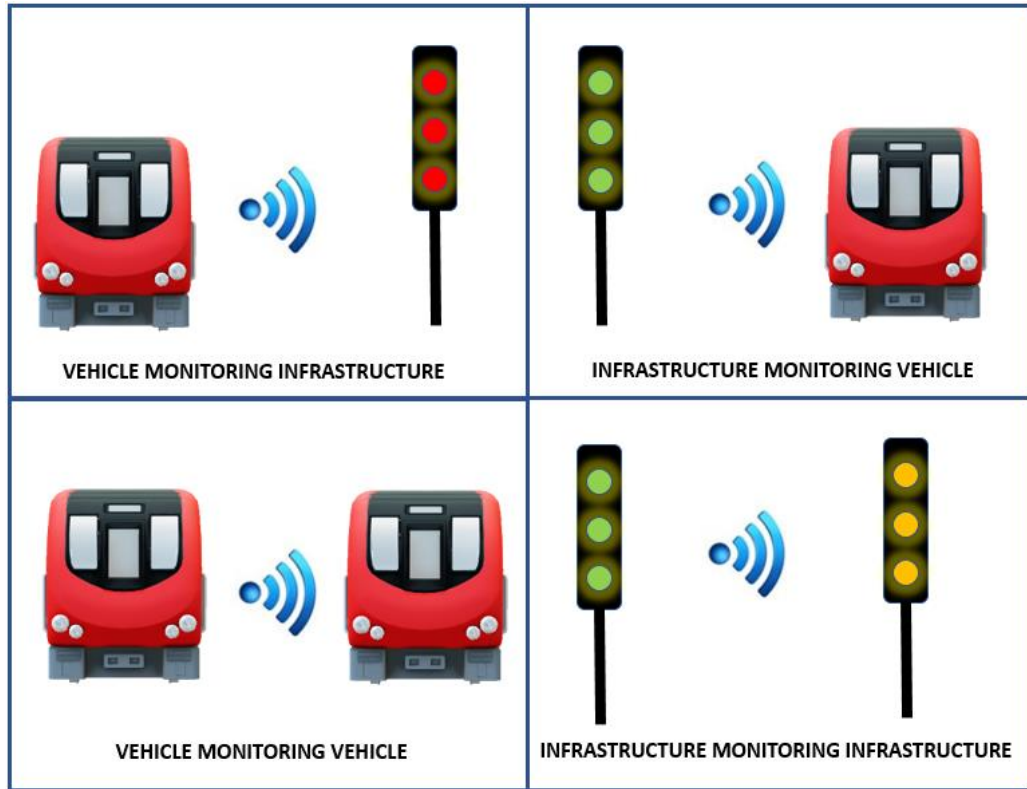


Figure 2: The main categories of RCM technology used on the UK Rail Network.

The introduction of asset information systems such as Offering Rail Better Information Services (ORBIS) in 2011 has provided NR with an opportunity to achieve this objective of integrating data and making the output easily available to their Infrastructure Managers. ORBIS seeks to use information from a range of sources to provide a holistic picture of the asset status in a given area. One of the primary objectives of the ORBIS initiative is to support safety by giving

infrastructure managers the ability to predict, prevent and respond to incident in a timely and effective manner.

1.3 Common root causes of railway accidents

A research study carried out in 2011 as part of the European D-RAIL FP7 project by Det Norske Veritas (DNV later merged with Germanischer Lloyd to become DNV-GL) considered railway accidents that had been reported in 23 countries over recent years. It was revealed that out of the 700 accidents considered, 37% had been the result of rolling stock faults Figure 3 [14]. Moreover, 84% of all rolling stock-related accidents were attributed to wheelset and bogie-related defects as shown in Figure 4.

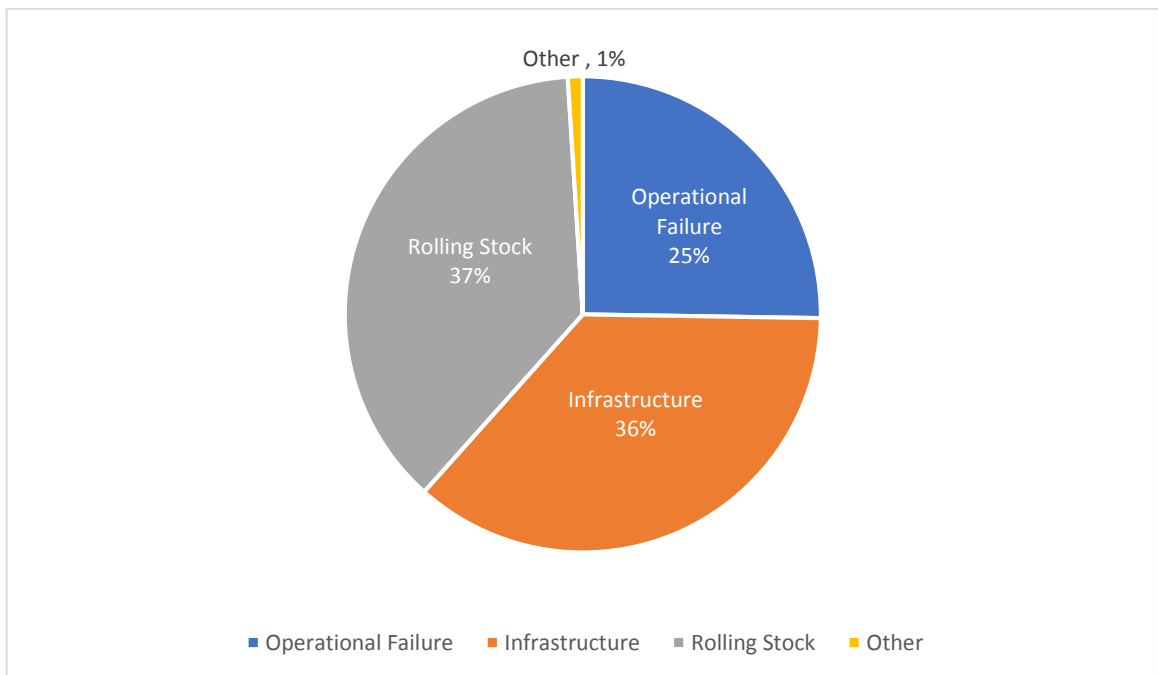


Figure 3: Railway accidents considered in D-RAIL FP7 project classified based on their root cause [14].

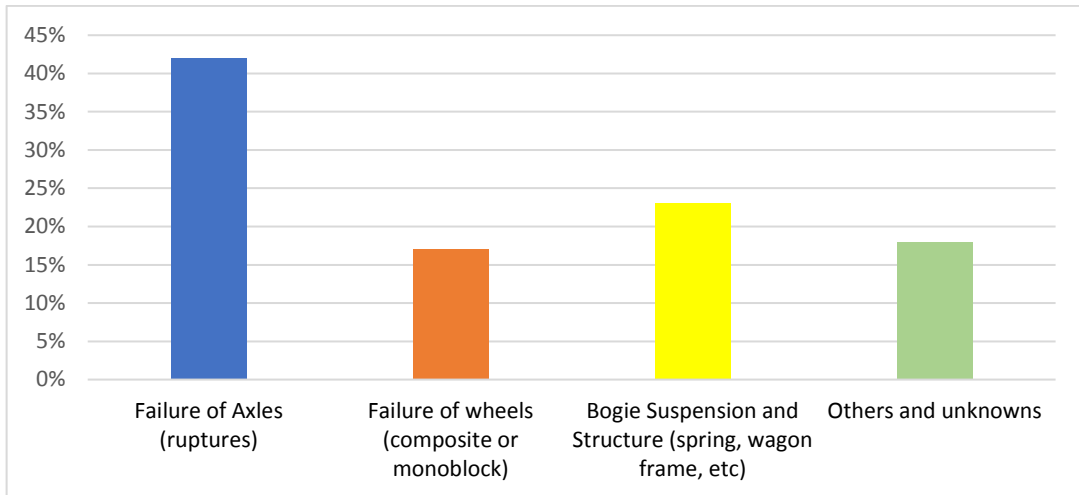


Figure 4: Rolling stock related accidents classified by root cause [14].

According to the findings of the D-RAIL FP7 project investigation, 41% of all rolling stock accidents were attributed to axle failure. Axle failure in the vast majority of cases was the result of a faulty bearing. Almost 60% of all rolling stock accidents were attributed to some form of wheelset failure, hence, accounting for one in five of all railway accidents considered in the study [14].

If a rail, crossing, wheel, axle or axle bearing defect is not detected promptly, it will gradually become more severe, leading to more serious damage that can eventually result in catastrophic failure and derailment. Early detection of infrastructure and wheelset faults helps rail infrastructure managers and rolling stock operators to schedule maintenance activities more efficiently without compromising the minimum fleet availability required in schedule planning. Poor maintenance scheduling can lead to reduced rail line and rolling stock availability, which in some cases can result in the severe disruption of normal train services and give rise to significant unnecessary financial losses.

1.4 Aims and objectives

The aim of this study has been to investigate the RCM requirements of modern rail networks as integrated complex systems and subsequently develop and implement appropriate technologies that address these requirements. In order to do this, the nature of the infrastructure and rolling stock faults that are of concern for the effective operation of the rail network have been identified and analysed. The capabilities and limitations of existing approaches and technologies employed have been considered and are discussed in detail. The exact needs of rail infrastructure managers with the primary parameters to increase efficiency and deliver operational improvements and investigate new techniques and methodologies which can enable the rail industry to deliver a step change in the safety, reliability, availability and efficiency of rail transport services. A holistic RCM approach is employed in this study, which has been primarily based on the application of acoustic emission and vibration analysis techniques. The results and associated analysis presented in depth in this thesis indicate that these techniques offer a number of new possibilities, which can greatly contribute towards the improvement of various aspects of the rail infrastructure system.

1.5 Thesis structure

This thesis consists of 10 chapters. Chapter 1 defines the industrial need together with the key aims and objectives achieved within this research study. Chapter 2 discusses the faults affecting railway rolling stock and the importance of identifying them in time. Chapter 3 goes on to discuss rail infrastructure faults, their root causes and how they can influence operations. Chapter 4 looks into the state-of-the-art RCM technologies and current technical barriers as well as the need to overcome them if conventional inspection strategies are to be gradually phased out. Chapter 5 discusses the state of the art technologies for the inspection of critical

railway infrastructure and rolling stock components together with their key technological limitations. Chapter 6 discusses the principles of acoustic emission and vibration analysis. These are two key RCM technologies that this research has focused on. These techniques can be effectively integrated with a wide range of existing systems, increasing the justification for employing them more widely in the field. Chapter 7 details the key signal processing methodology for analysing acoustic emission and vibration data and their applicability in fault detection. Chapter 8 discusses the experimental methodology employed. The laboratory experiments and field trials carried out are presented in detail. The materials, samples and components targeted together with the instruments employed during measurements are discussed in satisfactory detail. The permanent instrumentation of the site at Cropredy after the award of the relevant Certificate of Acceptance by Network Rail is discussed in particular detail. Chapter 9 presents the key results and associated analysis. The key findings are presented in a logical and comprehensive manner, justifying the widespread use of the technologies developed on the UK railway network. Finally, chapter 10 summarises the key conclusions drawn from this study and the results obtained. The thesis closes with a detailed outline of proposed future work that builds further on the achievements of the study.

1.6 Chapter 1 Summary

Chapter 1 has summarised the industrial need for this research study putting into context the experimental work carried out together with the key results obtained. The aims and objectives of the study have been defined and discussed in detail. Since this has been a Network Rail-sponsored doctoral research project from its inception, the fundamental aims and objectives of the study have been aligned with the actual industrial requirements for promoting long-term

operational capabilities. Finally, the structure of the thesis has been outlined, comprising ten chapters.

CHAPTER 2: ROLLING STOCK FAULTS

2.1 Introduction

Every day hundreds of thousands of trains run throughout the world's continuously growing railway networks connecting people and goods between major hubs. At the same time new and improved designs of more efficient trains are being developed and rolled out including the world's first hydrogen-powered locomotives. The improvement of modern railway systems is dependent on the continuous evolution to the better of both rolling stock and infrastructure. Rolling stock reliability and availability needs to be kept continuously at the maximum possible level in order to support growing demand for rail transport as well as ensure the safety of passengers. Rolling stock faults need to be avoided or at least be predicted in time so as maintenance planning can be optimised. In this way, the likelihood of catastrophic failure can be virtually eliminated, helping minimise disruption and maximise fleet availability. The most critical component of all rolling stock is the wheelset. There are various types of wheelsets but they all share the same main features, which are the wheels, axles and axle bearings (there are a few exceptions, such as certain metro trains of London Underground which do not make use of axle bearings in the wheelset design). In this chapter the key faults affecting rolling stock are discussed along with the importance of detecting them in a timely fashion to avoid disruption and eliminate the probability of catastrophic failure and hence derailment.

2.2 Types of rolling stock

There are numerous different types of locomotives, carriages and wagons cleared for use on the UK rail infrastructure and the majority of major railway networks across the world. The rolling stock used on the UK rail network has a variety of uses for both passenger and freight carriage services. A typical example of freight rolling stock is shown in Figure 5. This is a Falcon wagon that weighs 26 tonnes, has a maximum capacity of 60 tonnes and is approximately 17 metres long and can travel at speeds up to 100 km/h. Other types of passenger and freight rolling stock are shown in the photographs listed in Figure 6.



Figure 5: Photograph of a Falcon Wagon

Rolling stock are general similar in construction. The basic components (apart from the superstructure) are the bogies which comprise the wheelsets that carry the load and provide the interface with the rail. The wheelsets themselves consist of three critical components; the axle, the axle bearings and the wheels.

All three wheelset components are prone to developing damage while in service due to different reasons. If damage in any of these three components is left to progress beyond a certain point,

then failure will eventually occur [20-27]. Such a failure will almost certainly cause a derailment.



Figure 6: a) Ballast side tipper wagon and b) Virgin BR Class 390 'Pendolino' EMU

Each wheelset has a primary and secondary vertical spring arrangement. The primary springs are located within the bogie casting with one on each side of each wheel. This helps dampen the energy transfer between the wheels and the rail whereas the secondary suspension is centrally located on the bogie to manage the interface between the bogie frame and carriage. This two-tier suspension system reduces the impact effects however, defects can still occur.

A derailment, depending on the severity, can have a number of unwanted consequences ranging from simple and temporary delays until the concerned rolling stock has been re-railed, to severe disruption which can last for several months until damage has been repaired. An example of severe disruption is the Summit Tunnel accident, which happened on the UK railway network

during the late 1980s shown in Figure 7 [28]. The Summit Tunnel accident involved the derailment of a freight train carrying fuel. After the derailment, the fuel leaking from the tanker wagon that had tipped over to each side ignited catching fire. The fire and high temperatures involved caused extensive damage to the tunnel resulting in the closure of the North Eastern rail line for almost 6 months.

Certain severe derailments such as the ones shown in Figure 8 are likely to involve casualties e.g. the Rickerscote accident [16] and in certain cases can cause significant environmental damage e.g. the Viarregio accident [29].



Figure 7: The Summit Tunnel accident and subsequent fire caused by the derailment of a train carrying fuel. The derailment was initiated by a faulty axle bearing that led to the rupture of the axle while the train was moving through the tunnel derailing the train [28].

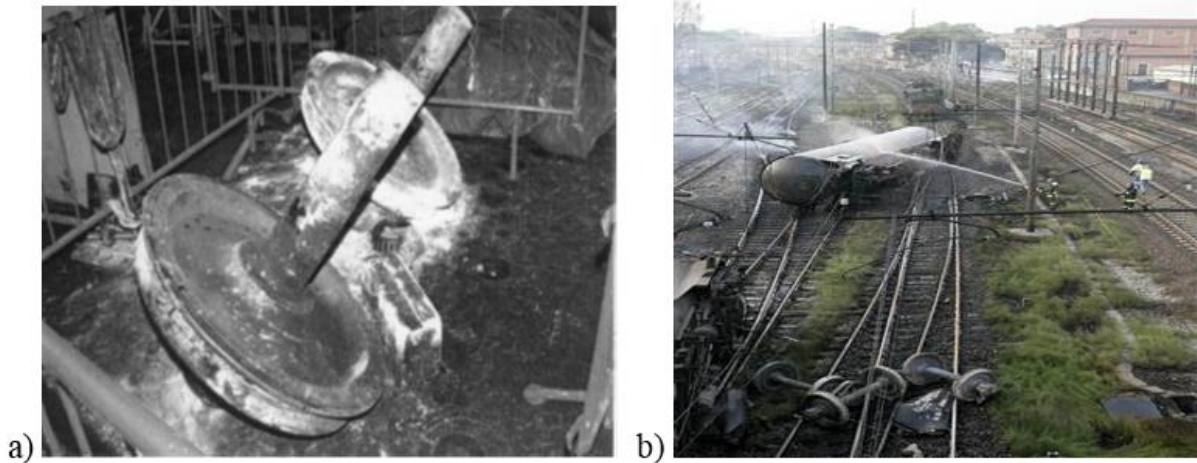


Figure 8: The Rickerscote accident in the UK in 1996 [16] and b) the Viarregio accident in Italy involving a tanker freight train carrying fuel [29].

The following sections briefly discuss the key wheelset defects of concern for rolling stock operators and rail infrastructure managers.

2.3 Wheel Defects

2.3.1 Rolling Contact Fatigue Cracks

Rolling Contact Fatigue (RCF) cracks are caused by imperfections in the wheel due to manufacturing defects. However, they are more often as a result of repetitive rolling contact loads which can cause initiation of defects in areas near the surface of wheel tread where inclusions such as manganese sulphides (MnS) are present [25, 30-32].

This type of defect usually occurs in the form of clusters with several cracks being spaced very closely to each other. RCF cracks initiate on or near the tread surface and tend to propagate during the early stage at a very shallow angle [25]. After having propagated 5 mm they tend to

turn downwards at a much steeper angle. This means that due to their complex nature, quantification can be difficult and largely depends on empirical determination.

RCF cracks do not share the same characteristics as thermomechanical fatigue cracks which are normally related to the braking characteristics of the train. Thermomechanical fatigue cracks are not uncommon in metro type rolling stock which is required to stop often at several stations and decelerate at a relatively high rate. RCF cracks can be detected using simple visual inspection, Alternating Current Field Measurement (ACFM) or Eddy Current (EC) testing [1, 33-41].

2.3.2 Sub-surface fatigue cracks

Due to imperfections in the wheel manufacturing material as a result of the RCF phenomena or failures in the manufacturing process, sub-surface cracks may develop. These cracks can occur at different depths below the surface. If such cracks are not detected early, they can rapidly propagate and cause the wheel to fracture. This type of defect can normally be identified with the use of Ultrasonic Testing (UT) equipment [42].

The schematic in Figure 9 shows the basic characteristics of standard monoblock wheels used in modern passenger and freight rolling stock. These wheels are normally made of plain carbon steel with a predominant pearlitic microstructure similar to that used in rails.

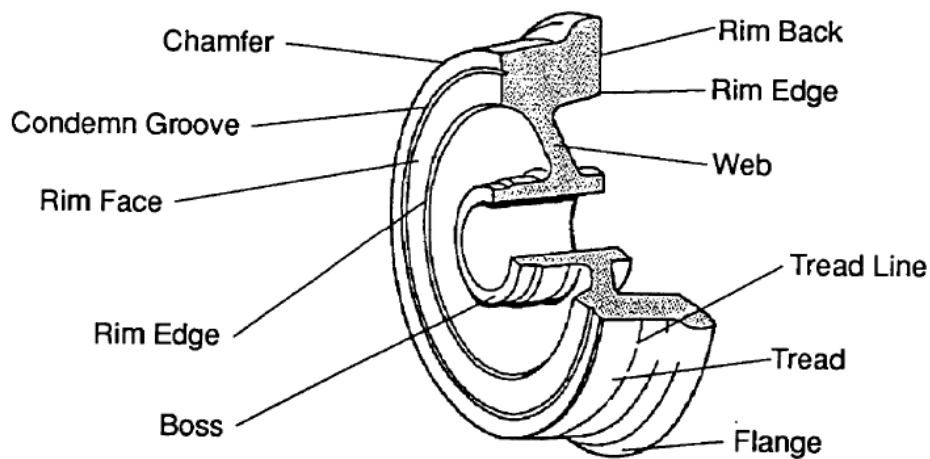


Figure 9: Schematic showing the basic characteristics of a monoblock wheel (courtesy of NSW Transport RailCorp).

2.3.3 Thermomechanical Fatigue Cracks

Thermomechanical fatigue cracks are the most severe form of wheel defects. They occur as the result of the combined effects of contact loads and repeating heating and cooling cycles experienced by the wheel tread and rim area during the braking process. Frequent braking or wheel slipping and the resultant friction forces can cause cracks to appear on the surface of the wheel tread. Minor cracks spotted early can be machined out whereas more severe cracks caused as a result of excess braking or slipping can eventually cause the wheel to fracture resulting into possible derailment.

2.3.4 Wheel Flats

Flat areas on the wheel tread normally occur when the wheels have locked due to hard braking events, causing the wheel to slip along the rail for some distance. Wheel flats may also occur as a result of poor adhesion between the wheel-rail interface and subsequent slipping but in this case the severity of the flats is usually much lower. The thermal effects can cause a build-up or

displacement of the metal to form a flat or indented surface on the circumference of the wheel [45-46]. This usually occurs on both wheels in the set.

Figure 10 shows an example of a wheel flat that occurred as the consequence of aggressive braking causing the wheels to lock. Wheel flats are often identified by the impact sound every time the affected wheels rotate. Wheel flats can cause collateral damage to the infrastructure or result in derailment of the affected train if not taken out of service in time.



Figure 10: Photograph of a freight wagon monoblock wheel containing multiple wheel flats

2.3.5 Pitting

Small corrosion pits can appear on the surface of the wheel. These can usually be ground out during wheel turning and do not normally cause any concern to rolling stock operators unless there is any associated cracking involved which nonetheless is extremely rare in this case.

2.3.6 Shelling

Shelling of the tread can occur when parts of the surface break off and are unevenly distributed along the surface of the wheel. RCF or thermal fatigue cracks can be a precursor to shelling.

Shelling can cause problems with the braking quality and adhesion of the wheel-rail interface. Moreover, in a similar way as flats, it can induce additional stress in the wheel rail contact area causing increased vibration and passenger discomfort.

The higher impact stresses can cause damage to the rail as well as the wheel itself causing its eventual fracture, albeit this is rare [16, 18-19]. The photographs in Figure 11 shows examples of wheel shelling.



Figure 11: Examples of shelling on freight (left) and passenger wheels (right).

2.3.7 Metal Build-Up

Extreme heat in the wheel arising as a result of friction from brakes sticking or wheel locking can cause metal overheating. Metal overheating can lead to the surface of the tread to become partially liquid. The stresses at the wheel-rail interface can cause the near-liquid metal to flow over the wheel and its circumference causing metal build-up or give the wheel a scaled appearance [19]. The photograph in Figure 12 shows a case of metal build-up on a freight wheel.



Figure 12: Metal build-up on the surface of the tread of a freight monoblock wheel.

2.4 Axle Bearing Defects

Axle bearings are lubricated rotating components installed between the axle and the wheel. The typical construction of a commonly used tapered roller bearing is shown in the schematic diagram in Figure 13. The bearing is attached to the journal of the axle and held in place by cap screw and locking plate.

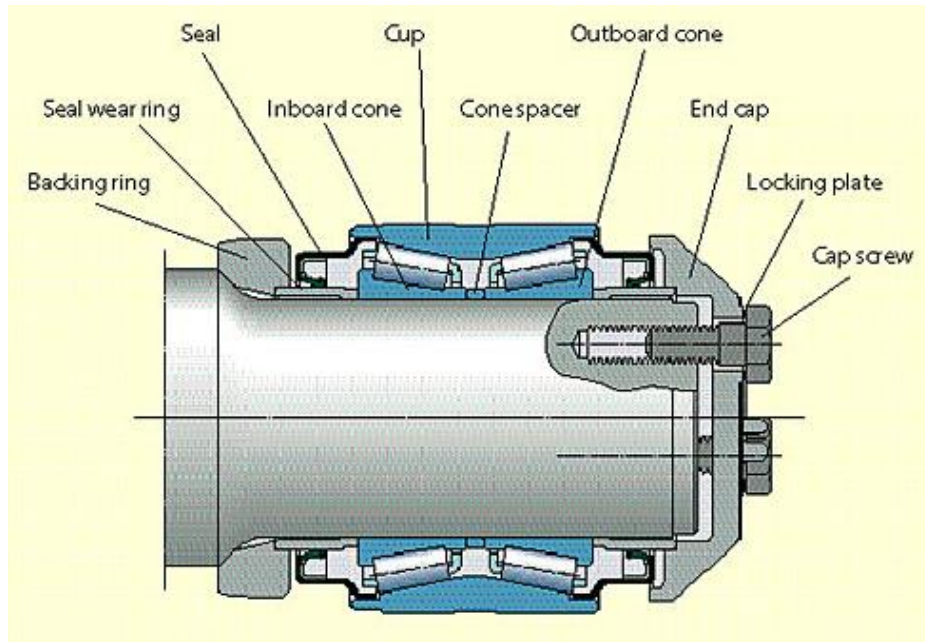


Figure 13: Tapered Roller Bearing (Courtesy of Roller Bearing Industries Inc.)

The axle bearing manufacturers specify the predicted axle bearing lifetime and maintenance intervention requirements. In reality rolling stock operators will normally use their own standardised maintenance procedures in order to increase availability and cost-efficiency [18-19].

These components need to sustain high stresses and occasional impact without loss of performance. Nonetheless, occasionally defects may initiate and evolve either due to poor maintenance or due to the aggressive in-service conditions that these components are exposed to. If left unchecked an axle bearing defect can evolve rapidly causing the bearing to seize and subsequently blocking the wheel. As soon as the wheel becomes blocked the axle of the affected wheelset will begin to move abnormally and experience very high stresses [18-19, 45].

This stress is caused because one wheel is rotating normally and the other is blocked. The abnormally high stresses sustained will very quickly cause the axle to rupture, most likely derailing the train affected. The photograph in Figure 14 shows a recent derailment of a freight train caused by the failure of an axle bearing.



Figure 14: Derailment due to axle bearing failure (courtesy of Mr. Nick Pinder, Network Rail).

Wheel flats are a common pre-cursor to axle bearing fault initiation due to the high impact loads caused by such defects to the axle bearing. Lubricant contamination is also a very dangerous factor as it can cause rapid degeneration of the lubricant due to overheating and hence result in the axle bearing failing rapidly.

The photograph in Figure 15 shows a freight train which was stopped in May 2012 in the area of Wantage, UK after a HADB generated an alarm. Subsequent inspection of the train

concerned revealed a seized axle bearing which resulted in such high forces that the axle bearing sheared completely. If the train had not been stopped it could definitely been derailed within a few miles.



Figure 15: Photograph showing a sheared axle bearing (Courtesy of Mr. Nick Pinder, Network Rail).

2.5 Axle Defects

Train wheelset axles are designed to have a minimum lifetime of more than thirty years. Modern trains employ two types of axles, solid or hollow. In the UK railway network, all rolling stock employ solid axles, the only exception being the Eurostar trains. Axles develop defects rarely and most of the ruptures that have been recorded in recent years are related to axle bearing failures which have subsequently led to the axle rupture as a result of the blocked wheel [16].

Axles can with time and under overloading conditions (above the permitted axle loads) develop fatigue cracks, see photograph in Figure 16.

If fatigue cracks develop then if they are shallow enough they can be removed by grinding away the affected region. Alternatively, the affected axles should be replaced with new ones.



Figure 16: Photograph of fatigue cracks on the surface of the axle (Courtesy of Dr John Rudlin, TWI Limited).

Pitting corrosion on the axle is another type of defect which is of concern apart from fatigue cracks as shown in the photograph in Figure 17. Corrosion pits can act as stress concentrators leading to crack initiation and possible failure of the axle.

Normally, in this case regardless of the depth of the pits the axle should be replaced. Axle corrosion is predominantly a concern in freight trains which can face long term storage and thus prolonged periods of inaction which can allow corrosion to initiate.



Figure 17: Photographs of pitting corrosion on a freight axle.

2.6 Faulty suspensions

The train suspension is a critical component of the bogie. It controls the vibration sustained by the superstructure as well as the amount of impacting loads from the superstructure to the bogie. If the suspension fails then the stability of the carriage is adversely affected causing excessive lateral and vertical movement to occur increasing the likelihood of derailments in curves. Also, much higher acceleration and decelerations need to be sustained by the bogies and consequently the wheelsets. Apart from increasing the likelihood of damaging the wheelset components, broken suspensions result in reduced passenger convenience and can potentially damage goods that are being carried by freight wagons. Normally, in the event of detecting a faulty suspension the carriage and bogie concerned are sent for immediate maintenance, so the problem can be rectified.

2.7 Chapter 2 Summary

Train wheelsets are the most critical components of all rolling stock since they are responsible for supporting train loads as well as ensuring adhesion with rails. However, the extreme operational environment to which train wheelsets are exposed to, coupled with the requirement for long service times, means that certain types of defects can evolve with time. If these defects are not detected in time this increases the possibility of catastrophic failure and consequently derailment. This chapter summarised the key types of wheelset defects which are of concern for both rolling stock and railway infrastructure managers. Technologies that are currently employed in wheelset inspection and RCM systems are discussed in detail in later chapters of this thesis.

CHAPTER 3: STRUCTURAL DEGRADATION OF RAILWAY INFRASTRUCTURE AND MAIN TYPES OF DEFECTS

3.1 Introduction

Railway infrastructure comprises several key components including the railway track, tunnels, bridges and viaducts. The UK network has a total length of almost 16,000km with approximately 33% (predominantly main network lines) having already been electrified. In addition, Network Rail is currently responsible for inspecting and maintaining in excess of 30,000 bridges, tunnels and viaducts [46-48]. The key components of the railway track are rails and cast manganese crossings. Both rails and crossings are subject to complex variable loading and environmental conditions throughout their intended service lifetime. As such, damage may initiate unexpectedly and subsequently propagate in a non-linear fashion [1, 17, 49]. Moreover, various types of defects may initiate and propagate. Therefore, infrastructure managers are required to promptly detect defects in rails and crossings, identify their type and quantify their severity. Maintenance planning cannot be optimised unless detected defects are identified in terms of their type and quantified in terms of their severity. If rail and cast manganese crossing structural defects are allowed to exceed a critical size, then catastrophic failure will occur. Catastrophic failure of a crossing or rail section can result in severe derailments such as the one that occurred in Hatfield, UK in 2000 [50]. In the aftermath of the Hatfield accident Network Rail was established in the place of Railtrack, resulting in the partial renationalisation of British railways. This chapter deals with the main defects of concern in rails and crossings.

3.2 Rail defects

Rails are prone to develop various types of defects with time either in the head, web or foot. Such defects can develop due to various mechanisms such as fatigue, Rolling Contact Fatigue (RCF), corrosion or high impact loads. Certain defects may initiate and evolve due to the combined effect of more than one of the aforementioned damage mechanisms.

The presence of manufacturing defects, albeit rare in modern rails thanks to the significant advances made in steelmaking technology over the last few decades, can cause initiation and propagation of cracks much earlier than expected. Similarly, mishandling of the rails during delivery, installation, maintenance or poor wheel-rail profile conformity due to the presence of tread defects or other wheel related problems can also result in damage initiating and subsequently propagating much earlier than anticipated by the design lifetime of rails. Most rails and crossings are expected to remain in service for a minimum of two decades without the need of any real maintenance other than rail head grinding in order to maintain the optimum profile [1, 10, 51-52].

Rails can suffer from various types of structural defects including RCF cracking Figure 18, shelling in the running surface of the rail Figure 19, rail fracture Figure 20. Figure 21 shows a classic tache oval fatigue crack where the right hand break occurred after the left had broken hence the different appearance, whereas you can also see the RCF propagating at an angle. Figure 22 shows rail foot corrosion and bolt hole cracking.



Figure 18: RCF cracks with high level of plastic flow (photo courtesy of Brian Whitney, Network Rail)



Figure 19: Shelling of the running surface of the rail [53].

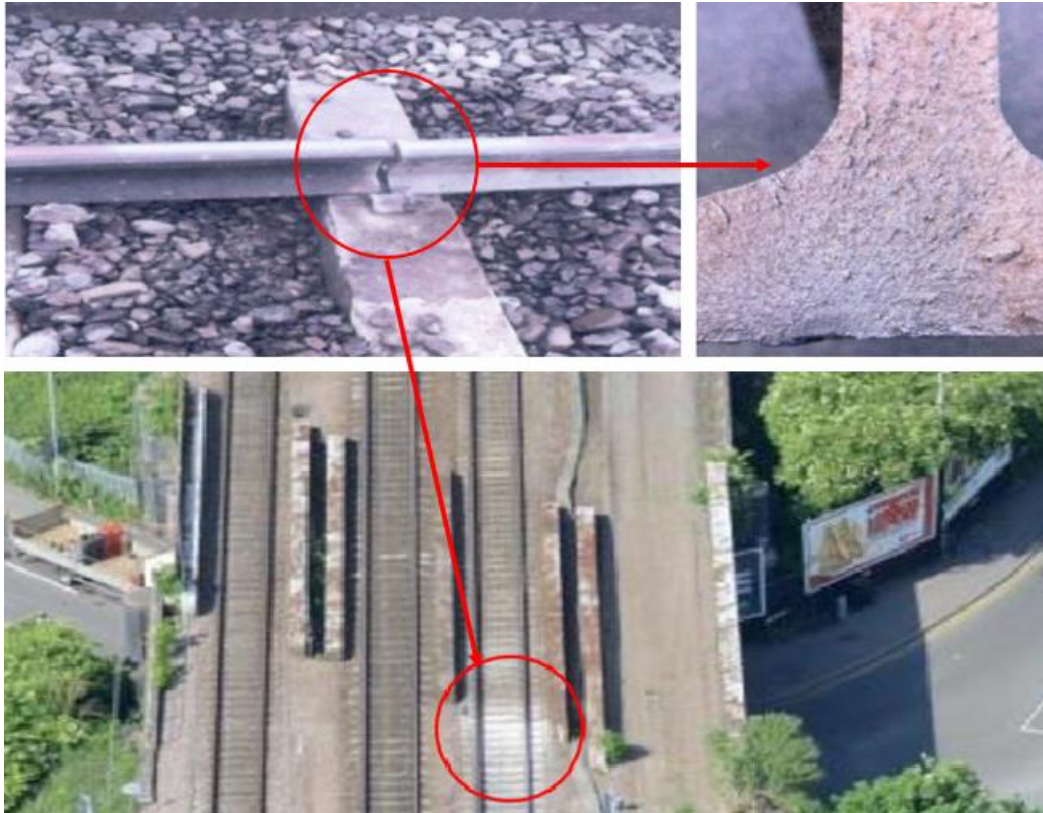


Figure 20: Photograph of a plain rail that fractured as a result of a crack which developed in the base of the rail. The rail sat on a sleeper with a degraded rail pad in an area of voiding on a transition to a bridge structure (photographs courtesy of Brian Whitney, Network Rail).



Figure 21: Photograph showing classic tache oval fatigue crack (courtesy of Brian Whitney, Network Rail)



Figure 22: a) Rail foot corrosion (courtesy of Brian Whitney, Network Rail) and b) bolt hole cracking [53].

All these defects if not detected in time will eventually result into final failure of the affected rail or rail section. An example of the consequence of rail fatigue failure is the Hatfield accident which took place in 2000 and led to the death of 4 people, including the partial renationalisation of Railtrack to form Network Rail. Moreover, one of the largest track renewal programmes ever recorded at global scale and whose value exceeded £5 billion had to be implemented in an extremely short time-scale [10, 50]. This unprecedented track renewal programme, was a direct result of the structural failure of a long rail section due to the presence of severe RCF cracking at Hatfield. The photographs in Figure 23 show an example of heavy RCF cracks on the surface of a rail head section removed from the railway network, and the train after its derailment in Hatfield. Multiple fractured rails from the section affected from RCF cracks are visible in the photograph.

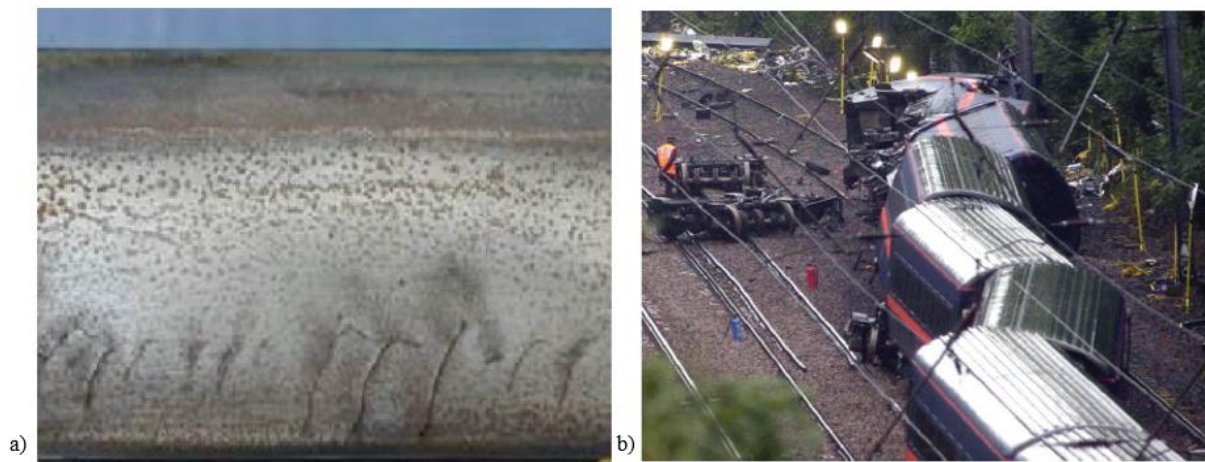


Figure 23: a) Heavy RCF cracking on rail section revealed from service [53] and b) the site of the Hatfield accident [50].

Modern high-speed rails are continuously welded and prestressed so as zero stress conditions are achieved at the predefined Stress Free Temperature (SFT). If the SFT is set too high, then rail breaks will occur in the winter due to excessive tensile stresses arising from the thermal contraction of the rails. If the SFT is set too low then buckling of the rails is likely to occur at lower than desirable temperatures during the summer due to excessive compressive stresses arising from the thermal expansion of the rails. Thus, it is important that the operational SFT is chosen carefully to accommodate stresses arising from thermal contraction and expansion as temperature varies.

Jointed tracks are currently employed only in rail stations or secondary lines where speeds are relatively low or historic sites not yet renewed. Rails are normally flash butt welded. Aluminothermic welding is used for repairing or splicing together continuously welded rail.

Rail welds pose a significant challenge for inspection engineers due to their microstructure which highly attenuates interrogating ultrasonic beams. Radiography due to its health and safety requirements as well as the time-consuming processes involved is applied in selective cases only [1, 10]. Thus, radiographic inspection results can only be used as a statistical tool to evaluate the quality of the general population of welds found throughout the rail network [10, 41]. Figure 24 below shows two welders preparing a Aluminothermic weld during a 9 day blockade to renew the Track in Shugborough Tunnel during December of 2012.



Figure 24: Aluminothermic weld preparation, Shugborough Tunnel, December 2012.

Rail geometry is a critical operational parameter and needs to be maintained within acceptable limits at all times. The majority of rail infrastructure related derailments is attributed to poor geometry of the rail head resulting in poor contact with the train wheels. The same applies when the wheel tread geometry has deteriorated beyond the acceptable limits [1, 10].

3.3 Sleepers and Rail Pads

Modern rail networks make use of three types of sleepers; wooden, steel or concrete with the latter being the most common type now installed in the UK rail network. Other types of sleepers used on the rail network include those made of fibre-reinforced composite (FRC) materials, however FRC are not common in the UK rail network. Sleepers support the rails and provide part of the stiffness required to support the passage of trains.

Accidental impacts and vibrations combined with the presence of failed rail pads or manufacturing defects can cause concrete sleepers to crack and eventually fail. Normally one failed sleeper will not pose a problem but two or more consecutive sleepers are a cause for concern necessitating repairs to take place. Sleepers can also be influenced by ‘wet beds’ which is where water is captured beneath the sleepers causing the track system to pump each time a train passes over.

Wet beds apart from causing decreased stiffness of the rail track also result in much higher bending moments to be experienced by the rails increasing the likelihood of fatigue cracks initiating and propagating in the affected areas. Wet beds can also reduce passenger comfort and increase vibration and noise particularly when the train is travelling at high speeds. Figure 25 shows an example of a failed rail pad sleeper.



Figure 25: Photograph of a failed rail pad.

3.4 Cast manganese crossings

Cast manganese steel grades (otherwise known as Hadfield steel) due to their high resistance to impact damage, are commonly used for manufacturing rail crossings. Cast manganese steels used for manufacturing crossings contain 11-14% Mn. Mn apart from being an austenite stabiliser in steels increases the tolerance to fatigue crack initiation from impacts. This enables the crossings made from such a material to achieve an acceptably long-life span. More specifically crossings are required from their design to remain in service for at least 20 years before requiring any maintenance or replacement.

Although inspection of conventional rails is relatively straightforward, this is not the case for cast manganese crossings which have a predominantly large-grain austenitic microstructure due to the large content of Mn, causing scattering and attenuation of the interrogating ultrasonic beam [54-58]. Therefore, the signal to noise ratio (SNR) significantly deteriorates making ultrasonic inspection even with phased arrays unreliable at best and impossible at worst. UT could be carried out at lower frequencies, but this would result in very long near-fields and very poor sensitivity and resolution, which renders the inspection impractical and the results pointless from a maintenance point of view since the structural integrity cannot be determined with sufficient remaining fault tolerance.

For this reason, evaluation of the condition of cast manganese crossings is currently carried out visually or by using liquid penetrant inspection (LPI). Magnetic particle inspection (MPI) or magnetic flux leakage (MFL) are not applicable techniques as cast manganese crossings are paramagnetic. Radiography could be applied to inspect parts of the crossing but its application

is not easy in the field and does involve health and safety issues. Defects such as fatigue cracks and impact damage in cast manganese crossings predominantly occur in the nose and wings of the crossing. However, manufacturing defects can occur during the casting or welding process. These can result in structural failure of part of the crossing. A typical example of a defective cast manganese crossing nose is shown in Figure 26.



Figure 26: Photograph of damaged crossing showing evidence of porosity due to the manufacturing process (the photograph is from Hardface Technology Presentation on Repair and Rebuild of Manganese crossings using Hardface Welding, 2003).

Cracks initiating and propagating below the surface cannot be detected due to the limitations of ultrasonic testing. Even if the application of radiography for the inspection of cast manganese in the field was straightforward the presence of internal cracks could be easily missed due to the limitations of this technique in detecting relatively small cracks. Figure 26 shows cracking near the nose of a crossing which had to be replaced.

3.5 Chapter 3 Summary

Rail infrastructure consists of several different components including the rail track (rails, sleepers, rail pads, ballast and sub-ballast), cast manganese crossings, bridges and tunnels. In most cases, these railway components are required to remain in service for tens of years under adverse weather conditions and heavy variable loads, be tolerant to damage, receive infrequent and as little maintenance as possible, and virtually never fail catastrophically. It is relatively easy to understand the challenges that these requirements pose for rail infrastructure managers maintaining several thousands of kilometres of rail track, together with thousands of bridges and tunnels even without taking into consideration the maintenance of the various stations (parts of which also develop problems with time). In this chapter, the key aspects of structural degradation affecting rails and crossings has been illustrated and discussed in detail.

CHAPTER 4: REMOTE CONDITION MONITORING SYSTEMS FOR ROLLING STOCK

4.1 Introduction

Onboard or wayside RCM is used to determine the status of rolling stock or infrastructure either in real time or at fixed or random intervals. The principles of RCM involves the gathering of information automatically from the point of concerns followed by its communication to a central nodal point for action or recording based on alarm threshold settings which are dependent on the type of data obtained [18-19].

NR currently employs the following wayside RCM equipment:

- 206 Hot Axle box Detectors
- 26 Wheelchex® Wheel Impact Load Detectors monitoring 69 tracks
- 8 Gotcha Wheel Impact Load Detector sites installed
- 25 Panchex® Pantograph monitoring systems
- 2 Railbam® Acoustic Bearing Monitoring Systems (Installed in partnership with Siemens on the Wessex Route).
- 1 TADS Acoustic Bearing Monitoring System (on trial)

Apart from the aforementioned wayside systems, a number of onboard RCM systems are currently employed by rolling stock operators to monitor the condition of axle bearings. Eurostar high-speed trains operating on the High Speed 1 line are legally required to monitor the temperature of the axle bearings continuously and thus not rely solely on wayside hot axle

box detectors fitted along the track. South Eastern railway have recently installed the Perpetuum vibration-based equipment to monitor axle bearings in real-time. Manufacturer Swsvenska Kullogerfabrikin (SKF) offers the option to rolling stock operators to obtain axle bearings which have been fitted with its Axletronic system [59-60]. The SKF Axletronic system uses up to three types of detectors including acoustic emission, vibration and temperature sensors. The Fischers Aktien-Gesellschaft (FAG) bearing manufactured by Scahaeffler also offers the possibility to monitor axle bearings by integrating accelerometers on them.

The main purpose of the RCM systems is to provide either early warning of evolving damage on critical rolling stock components or if this is not possible act as a last line of defence against imminent failure which can cause unnecessary disruption to rail operations.

4.2 Hot Axle Box Detectors (HABDs)

The primary purpose of a HADB is to detect failed axle bearings, which have begun overheating and hence are about to seize or have seized already. In this way failed axle bearings can be detected on time in order to prevent the subsequent derailment of the train affected.

A HADB makes use of infrared radiation detectors normally mounted on a specially designed hollow sleeper. The infrared detectors can determine the temperature of the individual axle boxes as they pass by measuring the intensity of the radiation temperature within a particular frequency from the passing bearings or breaks. These include the bearings and the wheels.

Figure 27 shows a typical HADB arrangement. HADBs count the passing axle boxes and wheels and warn the Signal Box supervisor if one or more of the wheels are overheating beyond a pre-defined threshold, which is normally set at 90°C. Above this temperature a red alarm will be given. Overheating of the surrounding area (around the axle box) can occur due to recent braking or heavy braking just before the HADB is passed by a train [18-19, 63-65]. This may give rise to unwanted false alarms that can result in delays. However, in recent years through better data management and trending the occurrence of false alarms have decreased by up to 90% and is much less of a problem than it had been previously.

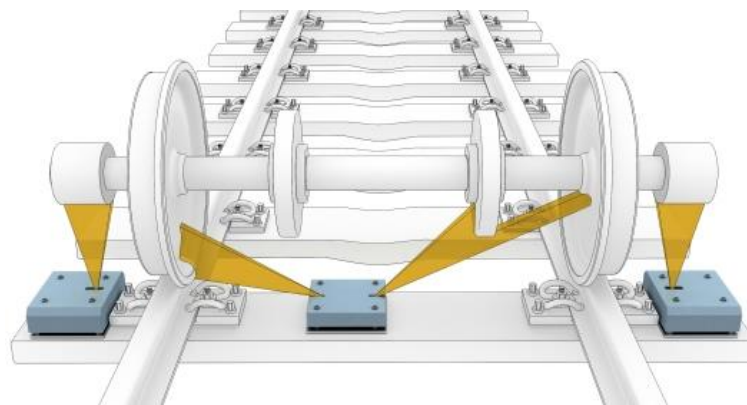


Figure 27: Typical HADB arrangement (the schematic is courtesy of Mermec).

However, it should be emphasised that HADB's are not capable of detecting the cause of the fault causing overheating but just the result. This means they are not really a fault detection system. Instead, they are a derailment prevention system, meaning they are the last line defence against accidents. This necessitates their installation at relatively frequent intervals, which are largely dictated by the type of the line as well as the budget available to procure such systems.

Data obtained from HABDs are relayed to a computer located trackside. A simple algorithm is used to determine if the temperature is out of pre-defined tolerance. If it is found that the axle box is overheating then an alarm is raised to the Signal Box. The Signal Box supervisor is then tasked to inform the Infrastructure Controller. It is the Infrastructure Controller who then decides whether to allow the train to run at a reduced speed or be stopped completely in order for the wagon concerned to be eventually taken out of service for repairs.

Failure of an axle box can cause significant damage to the railway infrastructure and wagon if it results in a ruptured axle and subsequent derailment. The key UK Group Standard which outlines the requirements of HABD's is GE/RT8014. This document, owned by the RSSB, mandates the design of hot axle box detection systems.

4.3 Wheel Check Systems

The objective of wheel check systems is to measure the critical dimensions of the wheel such as flange height & width, wheel profile, defect trends, wheel flats, thickness of the rim as well as recognise surface cracks, and pitting. There are a variety of wheel check systems in use on the UK infrastructure.

Damage to the rail network infrastructure can be caused by overloaded wagons or damaged wheels. This can result in significant cost to the rail for the repair or renewal of the infrastructure. Wheel profile distortion can occur as a result of breaking process, poor adhesion or incorrect break lock settings. The contact from the rail-wheel interaction causes friction and

the can lead to the formation of a crystalline martensitic structure on the surface of the wheel [18-19]. Figure 28 show an installed wheel check system.



Figure 28: Photograph of a Wheelcheck system (the photograph is courtesy of Network Rail).

The technology used by the different system manufacturers vary. The WheelChex systems (shown in Figure 28) employ strain gauges welded on the web which measure the change in resistance whereas the FactIS system (mostly found in Canada, USA, Brazil, and Australia), uses cameras to capture images of the wheels as they pass. This is similar to the Argus system which uses a combination of scanning laser and cameras. Other systems make use of accelerometers that measure vibration instead. Vibration-based wheel check systems employ a more complex data processing approach in comparison with strain gauge-based systems. However, they do not require temperature compensation during data analysis [66-68].

4.4 Trackside Acoustic Detectors

Trackside acoustic detection systems are predictive maintenance tools. They make use multiple microphone arrays placed trackside in order to detect axle bearing faults in passing rolling stock. The microphone arrays operate at a frequency of 20-40 kHz, which means that the signals captured can be contaminated by environmental noise from the engine or the surroundings.

There are two main types of trackside acoustic detectors used in the rail industry. Track IQ's (Siemens) Railway Bearing Acoustic Monitoring (RailBam) [68] and APNA Technology and Solutions Trackside Acoustic Detection System (TADS). The microphones identify sound characteristics emitted by bearing defects such as roller or ring surface defects that radiate noise containing their unique characteristic bearing frequencies [69-76].

Since 2012 trackside acoustic detector systems have been installed in 3 locations on the UK rail network. The first location Swaythling, installed in 2009 detected a number of faults during passage of a large number of trains.

4.5 Overhead line system monitoring

The purpose of monitoring the overhead line system is to detect faults before they occur and result in damage to the train mounted pantograph or a 'rip down' of wire from the overhead wire system.

NR has installed the Panchex system developed by Applied Electronic Applications (AEA) technology. The dynamic performance of the pantograph is measured by the displacement induced in the overhead wire system. The system accounts for other variables such as environmental elements, direction of travel and speed.

When a train passes the location of an installed system the Panchex measures the uplift, speed and wind conditions. This information is processed locally by the equipment’s computer to determine if the pan is within the standard tolerances. If it is outside of the tolerances an alarm is flagged to the Route Control Manager. A screen shot of an active Panchex system database is shown in Figure 29. The database records the alarm, the location of the system and the information gathered.

Site	Track	Warning	Low	High	Alarms	Low	High
Benfleet	Up line	Yes	-100	100	Yes	-100	120
Benfleet	Down line	Yes	-100	90	Yes	-100	120
Benfleet	Up line reverse	Yes	-100	100	Yes	-100	120
Benfleet	Down line reverse	Yes	-100	90	Yes	-100	120
Cathcart	Outer circle	Yes	-100	70	Yes	-100	120
Cathcart	Inner circle	Yes	-100	70	Yes	-100	120
Chadwell Heath	Up main	Yes	-100	45	Yes	-100	53
Chadwell Heath	Down main	Yes	-100	44	Yes	-100	44
Chadwell Heath	Up electric	Yes	-100	45	Yes	-100	55
Chadwell Heath	Down electric	Yes	-100	70	Yes	-100	70
Cheddington	Down fast	No	30	90	Yes	0	120
Cheddington	Up fast	No	30	90	Yes	0	120
Cheddington	Down slow	No	30	90	Yes	0	120
Cheddington	Up slow	No	30	90	Yes	0	120
Cheshunt	Down line	Yes	-100	90	Yes	-100	120
Cheshunt	Up line	Yes	-100	110	Yes	-100	120
Cuffley	Down line	Yes	-100	70	Yes	-100	120
Cuffley	Up line	Yes	-100	70	Yes	-100	120
Duddeston	Up line	No	30	50	Yes	0	120
Duddeston	Down line	No	30	60	Yes	0	120
Great Bridgeford	Down slow	Yes	-100	80	Yes	-100	120

Figure 29: Pan Check Alarm Window (the screenshot is courtesy of Network Rail LNW Route Control)

4.6 Train Detection Systems

Train detection systems normally form part of, or input to, the signalling system of railway infrastructure. The primary purpose of the systems is to detect the presence of the train (or otherwise) within an area of the infrastructure, i.e. if it is passing or has passed a specific location. Many systems can also determine the direction of travel of the train. NR uses a number of different types of train detection systems including, Axle Counters, Track Circuits, Constant Delay Systems, Rail Circuits, Block Systems and Supplementary Systems.

The running rails are used to provide a track circuit. A low power signal is transmitted from one end of the rail to a receiver at the other end; the adjacent rail operates as the return conductor in the circuit. Where there is no train in the section then the receiver is energised, however when the train enters the section the current short circuits through the bogie of the train and therefore the receiver is de-energised [47]. The track circuits transmit a signal via cables to the local Signal Box.

The Signal Manager is aware of any change in the track circuit. The normal position of the system is energised i.e. track clear and de-energised when a track is in section. The system can also be used to detect rail breaks as this will also lead to the receiver being de-energised and the track showing occupied when not. This is known as a 'right side failure'.

Another form of track monitoring where this method is employed is in a treadle system as show in Figure 30. The treadle is a mechanical device that is installed track side. Each time a train enters into the section its wheels strike the treadle arm activating a counter. The treadle 'counts-

The signaling power distribution system relies on the local Distribution Network Operator (DNO) for its main supply. In the event of a failure of this supply, and depending on the geographical location, the supply can be sourced from a single phase 25 kV 50 Hz AC Overhead Line Equipment (OLE) traction supply system or a diesel-powered generator.

.

The UK railway network has two main traction power supply systems. The most common is the single phase 25 kV 50 Hz AC OLE system. Power is supplied directly to the train via an overhead line contact wire that is in contact with the train mounted pantograph. The overhead line catenary system is fed sequentially from each phase of the 3-phase distribution network to ensure a balance across the external three phases supply. The other traction supply is a 650 v – 750 v DC supply. In this system the power is supplied to the train via a 3rd and/or 4th rail ground mounted distribution system which has direct contact with a gather pad mounted underneath the train. There is no phase application on a DC system.

The signalling power distribution rooms are typically connected to two primary feeds for resilience. The main feed is sourced from the DNO via a 3 phase 400 volt alternating current (VAC) metering section. The other feed is from the 25 kV AC OLE or in DC traction areas from a diesel-powered generator located on site.

The equipment within the supply point is monitored and managed using approximately 20 directly wired alarms. These alarms monitor the health status of the equipment and report this back to a terminal located in the Electrical Control Room (ECR).

Alarms are terminated on a distribution frame and routed via the Remote Terminal Unit (RTU) over Supervisory Control and Data Acquisition (SCADA) communication equipment to the ECR where the health of the equipment is displayed. The screenshot in Figure 31 shows the health status and the alarms at Headstone Lane PCP as reported to Rugby ECR.

If an alarm is triggered it will flash red on the screen and sound an audible tone until acknowledge by the Electrical Control Operator (ECO). The ECO will acknowledge the alarm, review the information provided and depending on the severity may dispatch a maintenance team to the fault location where they will attempt to rectify the fault using information downloaded locally from the management unit to a laptop.

Headstone Lane PSP Point Summary Page 01		
Description	Point Id	Current Status
Hdstn Ln PSP PROT 50v BC COMM ALM	H1D_BC50P_CA	ALM OFF
Hdstn Ln PSP PROT 50v BC Fail	H1D_BC50P_CF	ALM OFF
Hdstn Ln PSP PROT 50v BC High Volts	H1D_BC50P_HV	ALM OFF
Hdstn Ln PSP PROT 50v BC Lo Volts	H1D_BC50P_LV	ALM OFF
Hdstn Ln PSP PROT 50v BC SUP Fail	H1D_BC50P_SF	ALM OFF
Hdstn Ln PSP RTU 50v BC COMM ALM	H1D_BC50R_CA	ALM ON
Hdstn Ln PSP RTU 50v BC Fail	H1D_BC50R_CF	ALM ON
Hdstn Ln PSP RTU 50v BC Earth FLT	H1D_BC50R_EF	ALM ON
Hdstn Ln PSP RTU 50v BC High Volts	H1D_BC50R_HV	ALM ON
Hdstn Ln PSP RTU 50v BC Lo Volts	H1D_BC50R_LV	ALM ON
Hdstn Ln PSP RTU 50v BC SUP Fail	H1D_BC50R_SF	ALM ON
Hdstn Ln PSP Intruder Alarm	H1D_IA	ALM OFF
Hdstn Ln PSP RTU Power DIST Alarm	H1D_RTU_DIST	ALM OFF
Hdstn Ln PSP RTU OVRTEMP	H1D_RTU_OT	ALM OFF
Hdstn Ln PSP Mains Supl Avail	H1D_PSP_MSA	ALM OFF
Hdstn Ln PSP Mains Supl on Load	H1D_PSP_MSL	ALM OFF
Hdstn Ln PSP Traction Supl Avail	H1D_PSP_TSA	ALM ON
Hdstn Ln PSP Traction Supl on Load	H1D_PSP_TSL	ALM ON
Hdstn Ln PSP BH-21/BH-23A/AT/HL MOS Fail	BH21BH23AATHL_F	ALM OFF

Figure 31 : Alarm status at Headstone Lane Principle Supply Point (screenshot courtesy of Rugby Electrical Control Room)

4.8 Onboard RCM

High-speed trains operating at velocities above 250km/h are required to have their axle bearings fitted with temperature sensors. The purpose of this legal requirement is to avoid any faulty axle bearing seizing before it has a chance to be detected by HABD. In the UK the only line where temperature sensors are required to be operational is HS1 and in the future when it is completed HS2 [77-78]. All other lines operate at speeds below 250km/h and thus are not considered to be high-speed.

Southeastern railways have opted to use the Perpetuum system developed by the University of Southampton. Perpetuum is based on accelerometers installed on the axle box in order to monitor abnormal vibrations arising from faulty axle bearings. The data obtained are processed

using appropriate signal processing algorithms. An alarm is given when abnormal indications are evident in the signals analysed.

As mentioned above SKF has developed the Axletronic system. The system is integrated on bearings manufactured by SKF. It comprises up to three different detectors, including AE sensor, accelerometer and standard temperature sensor. In its simplest format the system comprises an accelerometer and a standard temperature sensor. The data collected from the sensors are fed to a computer onboard the train where they are subsequently processed and stored. In the case of an alarm the driver is alerted who subsequently informs the Signal Box.

FAG has also developed an onboard monitoring system based on an accelerometer being integrated on the axle box. High-speed train axle bearings are also equipped with temperature sensors by default.

4.9 Chapter 4 Summary

This chapter summarises the different wayside and onboard systems currently used to remotely monitor the condition of rolling stock wheelsets. The operation of various types of systems has been discussed together with their overall capabilities in some detail.

CHAPTER 5: RAILWAY INFRASTRUCTURE INSPECTION TECHNIQUES

5.1 Introduction

NR employs a wide range of non-destructive testing (NDT) procedures to identify infrastructure faults in order to evaluate the potential maintenance or renewal requirements. The inspection techniques used include both manual and automated techniques based on manual deployment of inspection equipment, via hi-rail vehicles or dedicated inspection trains. The NR inspection trains are deployed on a daily basis in order to record out of tolerance track geometry or physical defects in track components using ultrasonic probes based on the Sperry wheel design. Apart from the Sperry probes, the NR inspection trains use an advanced Plain Line Pattern Recognition (PLPR) automated vision system. The PLPR system captures and process images in order to detect defects and generates reports based on the visual inspection results. The reports generated contain lineside images, thermal capture and 3D camera information.

Images are processed using machine vision algorithms to identify and highlight potential defects [1, 10, 78]. The cameras are mounted on the undercarriage of the train as shown in Figure 32 and are oriented to give views that permit the machine vision algorithms to reliably detect the track components. An inspection engineer on board the train reviews images highlighted as potential concerns. The images shown in Figure 33 were captured using a PLPR system. The reports are fed directly into the detected defects statements, which are consulted in

order to determine accurately the maintenance activities or renewals interventions required to keep up reliability and safety of the railway network.

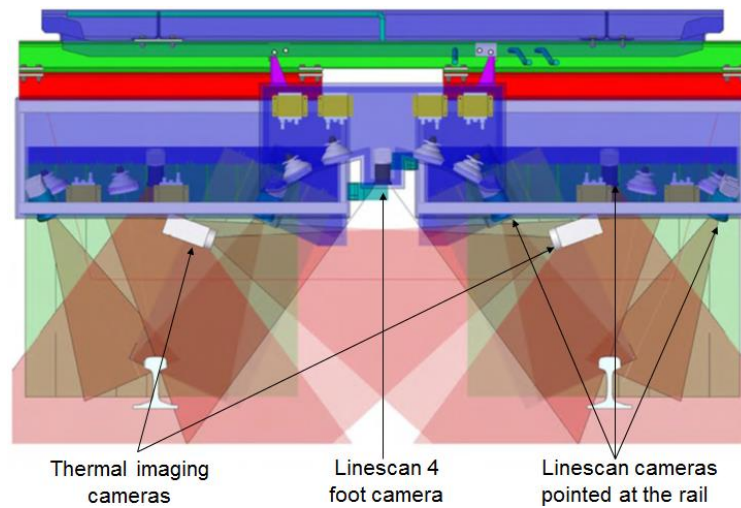


Figure 32: PLPR Linescan and Thermal Camera Design (this schematic is courtesy of Nick Pinder, Network Rail)

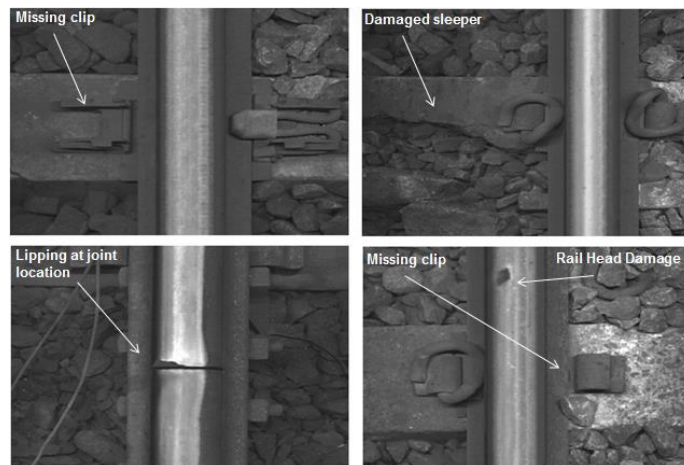


Figure 33: Image produced by the cameras from the PLPR system (these images are courtesy of Nick Pinder, Network Rail)

5.2 Visual inspection

In visual inspection the examiner views the rail section concerned to identify visible surface defects or missing components. It is often completed with the aid of magnification. This is a simple and easy to complete the test. This used to be a common inspection approach but is being gradually been phased out, Figure 34 a).

Automated inspection systems are widely used in modern networks, especially in order to confirm the rail head profile and ensure conformity with wheel profile. The majority of rail infrastructure-related derailments have been due to poor rail-wheel profile conformity. Poor rail-wheel conformity results in much higher stresses and wear on both the rail and the wheel reducing their lifetime. It also results in higher levels of noise and lower adhesion.

Automated inspection systems use cameras in addition to lasers in order to capture images of the track. The track images can be automatically analysed using advanced pattern recognition algorithms in order to detect missing components or other visible defects. Depending on the type of track and traffic density, visual inspections may be carried out as often as once a week or once a fortnight [1, 10, 49, 78].

5.3 Ultrasonic testing

Ultrasonic testing uses ultrasonic waves that propagate through the material. The ultrasonic waves are generated from lead zirconate titanate (PZT) crystals which are orientated in different angles. Typically, wheel probes designed by Sperry are used on the UK rail network. Alternatively manual single or dual crystal probes or phased arrays can be used for manual inspection where high accuracy in quantifying defects is required.

Wheel probes contain multiple single element (crystal) PZT transducers orientated at different angles, which are typically 0° , 37° and 70° . This ensures maximum coverage of the rail. However, due to the geometry of the rail, certain defects may be missed if they are out of the line of propagation of the interrogating ultrasonic beams. Each wheel probe can contain up to 7 transducers [1, 10, 49, 78].

Apart from wheel probes, the ultrasonic test unit, Figure 34 b) or sleds can be used to deploy the UT transducers on the surface of the rail head. Although sleds can be used at higher speeds than wheel probes, better control is required for sled deployment.

Although ultrasonic probes perform well in rail inspection, this is not the case in the inspection of cast manganese crossings due to the high levels of attenuation of the interrogating beam from the large grain austenitic microstructure. Some research groups have attempted to use ultrasonic phased arrays for the inspection of crossings but the results have not been particularly convincing. Reports of ultrasonic testing of cast manganese crossings applied in the field are yet to be confirmed. However, phased arrays have been more successful in the inspection of aluminothermic welds, with results being much more encouraging.

5.4 Radiography

In radiographic inspection, X-ray or gamma-ray radiation is used to examine the component with the help of films or digital detectors. Radiographic inspection is primarily used for the assessment of a small number of rail welds each year as a means of statistically extrapolating the condition of the general population of welds [1, 10]. The limited use of this technique on

the network is due to the various difficulties including health and safety issues associated with radiographic inspection.

Radiography is nonetheless, routinely used for the evaluation of the quality of cast manganese crossings. High-power X-ray systems in the range of a few megaelectronvolts (MeV) are required to inspect the entire crossing for the presence of various defects such as porosities and large inclusions.

5.5 Thermography

Thermography is based on the detection of temperature changes due to the presence of defects, Figure 34 c). The technique is based on the detection of infrared radiation emitted from the component being inspected. Thermography is primarily deployed on the rail network for measuring the temperature of rails on warm days in order to evaluate the risk of buckling.

Nonetheless, hybrid approaches involving the use of eddy currents together with thermography have been proposed for the detection of RCF cracks. However, such techniques have yet to be applied at a commercial level in the field [32-35].

5.6 Eddy Current Testing

Eddy Current Testing (ECT) employs a coil which is brought near the surface of a conducting material while being excited by an alternating current. This causes eddy currents to be induced in the specimen and an associated magnetic field to be generated. When there are no defects in the material, the magnetic field generated by the eddy currents will remain undisturbed. However, in the presence of a crack, the flowing path of the eddy currents induced in the

material will change causing variations in the magnetic field generated. This will cause changes in the impedance of the coil providing an indication which is directly related to the presence of a crack.

Eddy current inspection is widely used on the rail network for the detection of surface and very near-surface defects, particularly RCF cracking Figure 34 d). This is due to the very high sensitivity of the ECT technique in the detection of RCF and other surface and near surface defects. A similar technique is Alternating Current Field Measurement (ACFM) but it is applicable only to surface breaking defects such as RCF cracks.

ECT systems can be deployed either manually, using push trolleys or pedestrian walking sticks for localised measurement, via hi-rail vehicles or dedicated inspection trains. ECT and ACFM have the unique advantage of being largely inert to the speed at which the inspection is carried out [1, 10, 49, 79-82]. However, they are also particularly sensitive to lift-off variations and therefore, probe handling is particularly important during inspection with these techniques.

5.7 Magnetic Flux Leakage (MFL)

MFL uses powerful rare earth magnets or Direct Current (DC) electromagnets in order to magnetise the ferromagnetic rail. If there is no defect present then the flux lines will be retained inside the rail. However, in the presence of a defect some flux will leak which will be detectable by a sensing coil or Hall probe. This technique is appropriate for the inspection of the rail head for surface, near surface and shallow defects. MFL is widely used in the rail industry as it is simple and fairly reliable. However, it lacks reliable quantification capability. Also the

maximum inspection speed cannot exceed 15km/h as magnetisation drops and eddy current effects increase causing the flux to be pushed further out towards the surface of the rail head reducing detectability of defects lying deeper in the rail head [1, 10, 49].

MFL probes can be deployed either using push-trolleys or via hi-rail vehicles. Deployment via inspection trains is rare due to the limitations in the maximum speed of inspection, rendering ECT a more preferable option over MFL.

5.8 Magnetic Particle Inspection (MPI)

MPI is a manual inspection technique based on ferrous particles sprayed on the surface of the ferromagnetic rail [1,10, 49]. A powerful DC electromagnet then generates an electromagnetic field whose leaking flux in the damaged area will cause the ferrous particles to be attracted giving a visible indication. This technique is only applicable for surface-breaking or very near surface defects. Despite its simplicity, it is still widely used on the rail network.

5.9 Liquid Penetrant Inspection (LPI)

LPI is an alternative methodology to MPI, which is based on the application of special dyes on the surface to be inspected. It can be applied to any type of material regardless of whether it is conductive and ferromagnetic (or not) as long as it is not porous. Figure 34 e) shows an inspection in progress where liquid has been applied to a crossing bolt hole under inspection at a Network Rails recycling depot. The resolution of the technique is very high, with clear sensitivity even to very small surface-breaking defects [1,10]. However, it does require surface preparation in order to be accurate. LPI is not commonly used for the evaluation of rails, but it

is used for the evaluation of crossings. This is since cast manganese crossings are paramagnetic and hence MPI cannot be used.

5.10 Chapter 5 Summary

This chapter has summarised the key inspection techniques used by the railway industry for the evaluation of railway infrastructure. The industry tends to use combinations of the aforementioned techniques in order to obtain a clear understanding of the condition of the structural integrity of the key components of the track, namely rails, crossings and sleepers. The importance of ultrasonic inspection needs to be emphasised since is the only technique which is capable of evaluating the entire rail. Nonetheless, it performs poorly in cast manganese crossings due to the high level of attenuation caused by the large grain austenitic microstructure. Accurate quantification and characterisation of detected defects is of utmost importance in order to determine the optimum maintenance action [83].

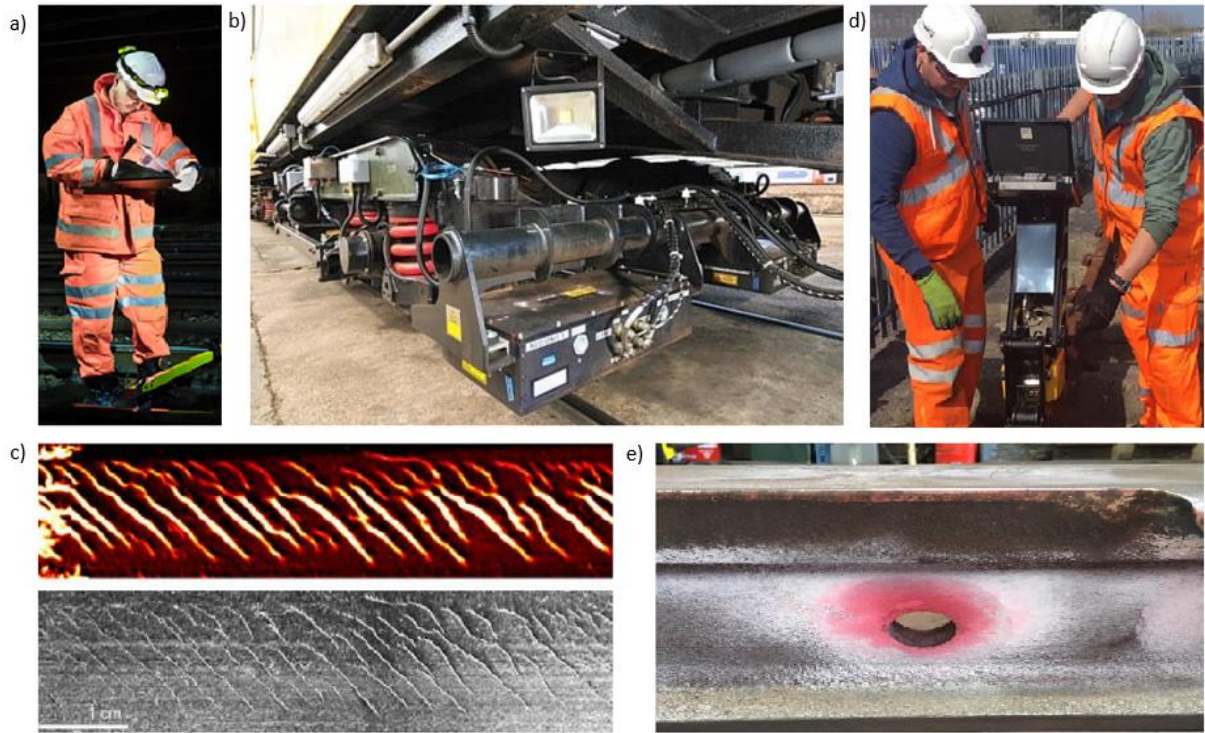


Figure 34: a) a visual inspection being carried out at night by a NR Engineer, b) the undercarriage of a NR ultrasonic test unit, c) images produced by a thermographic rail head inspection [125], d) Inspection using the Eddie Current roller search unit, and e) an inspection in progress where liquid has been applied to a crossing bolt hole under inspected at NR's recycling depot at Whitmoore, Cambridgeshire (images a, b, d & e courtesy of Network Rail).

CHAPTER 6: ACOUSTIC EMISSION AND VIBRATION ANALYSIS

6.1 Introduction

The railway industry has experienced unprecedented growth in recent decades. In the UK, the trend has been that of steady strong growth on an annual basis. Even though railway freight traffic has not reached the levels seen in the 1960s and 1970s, passenger numbers have increased considerably making up for the difference. Nonetheless, the trend for railway freight is also following an upward trajectory. With increasing traffic density, higher operational speeds and heavier axle loads, traditional inspection methods and tools are becoming more difficult to implement, resulting in reduced availability of railway infrastructure. Although inspection always aims to safeguard the reliability and safety of railway infrastructure, in the current operational environment it can be a cause of delay or even disruption if it is carried out unscheduled. However, even when scheduled inspection is carried out using test trains, the speed of inspection cannot match that of normal traffic. Hence, test trains generally need to move at lower speeds. The exception to this rule is when rail head geometry is measured, in which case the speed of the test train can keep up with the speed of normal traffic. However, UT and other forms of inspection are required to proceed at much lower speeds in comparison with normal traffic. Existing RCM technology also suffers from considerable limitations and therefore, there is significant room for improvement, especially in terms of reducing the overall cost of instrumenting the rail track in order to reduce the need for conventional inspection. With the gradual realisation of the 24-hour railway in the future, novel RCM technologies will need to be in place in order to ensure acceptable levels of operational reliability and safety [84-87]. Within this study, research has focused on the applicability of high-frequency AE and vibration

analysis. AE and vibration analysis are two promising RCM techniques which are capable of monitoring railway infrastructure and rolling stock equipment for a variety of faults. Both techniques can be implemented reasonably quickly and at a low cost. They are non-intrusive and can be integrated easily with existing RCM equipment. In addition, they can be complemented by existing inspection methodologies and procedures [88-110].

6.2 Acoustic Emission (AE)

AE testing is the most ancient method of NDT together with visual inspection. The introduction of AE in the modern industry has been rather slow. The first industrial applications of AE started in the 1960s. However, its wider implementation across the industry has been rather slow. The slow growth of AE in terms of number of industrial applications has been attributed in the past to the limitations in electronics, high-speed data acquisition and computing capacity for real-time data processing. Thanks to the advent of high-speed computers and advanced electronics equipment brought about by the unprecedented growth in semiconductors and integrated circuits, AE has experienced a boom with several industries taking advantage of the unique capabilities that this Condition Monitoring (CM) technique offers over traditional inspection methods and procedures. At the same time AE has benefited from significant developments in computer science and electronic engineering, especially in the field of advanced signal processing technology. Further, important developments have been associated with the improvement in manufacturing technologies of piezoelectric transducers with PZT crystals offering unique levels of sensitivity, which previously had been impossible to achieve.

The fundamental principles of AE testing are fairly straightforward and in their most basic form can be even implemented without the use of computers [111-113]. For example, during overloading of a wooden bridge, the audible sound that wood cracking produces is a basic form of detecting AE activity by just listening to the noise of the surroundings. It is impossible to accurately quantify the amount of damage sustained. However, it is still possible to extrapolate that certain parts of the bridge are cracking. As the bridge is loaded further the amount of audible activity produced by more wooden components cracking multiplies and intensifies. The increase in AE activity thus signifies an increase in the level of damage sustained. As the damage accumulated approaches critical levels, the amplitude of audible sound reaches a maximum and final failure occurs. This is a simple way of describing the principles of AE without having to employ any sophisticated equipment. Nonetheless, the principles of application of industrial AE are somewhat more complex.

When a load is applied to a solid structure, e.g. by internal pressure or by external mechanical means, it begins to deform elastically. The elastic deformation of any material or structure is associated with changes in the structure's stress distribution and storage of elastic strain energy. As the load increases further, some permanent microscopic deformation or crack growth may occur, which is accompanied by a release of stored energy, partly in the form of propagating elastic waves or AE [111].

If these emissions are above a certain threshold level, they can be detected and subsequently converted to electric signals with the use of sensitive piezoelectric sensors mounted on the structure's surface. The AE principle is shown in the schematic diagram of Figure 35. Although

there is an abundance of piezoelectric materials, the vast majority of AE sensors incorporate PZT crystals. The PZT crystals are encased in a stainless steel cylinder and are mounted against the back of a protective plate, which is normally made either of alumina (Al_2O_3) or stainless steel. The main requirement for the material selection of the protective plate in AE sensors is to ensure the maximum transmissibility of elastic waves propagating in the monitored structure to the piezoelectric crystal. The schematic diagram in Figure 36 shows the basic architecture of a typical AE sensor and its key features. As elastic waves propagate to the sensor the piezoelectric crystal will deform dynamically. As it experiences dynamic deformation, its polarisation will change producing electric signals. The electric signals acquired from AE sensors are very small, in the range of a few mV, in terms of amplitude. The amplitude of electric signals depends on the level of deformation experienced by the crystal as well as the surface area of the crystal. Hence, the higher the deformation and the larger the crystal, the stronger the electric signal generated. Modern PZT crystals are extremely tolerant to repetitive dynamic deformation and can survive trillions of loading cycles without appreciable degradation. However, accidental impact or misuse of the sensor can result in the crystal fracturing in which case the sensor can no longer be used.

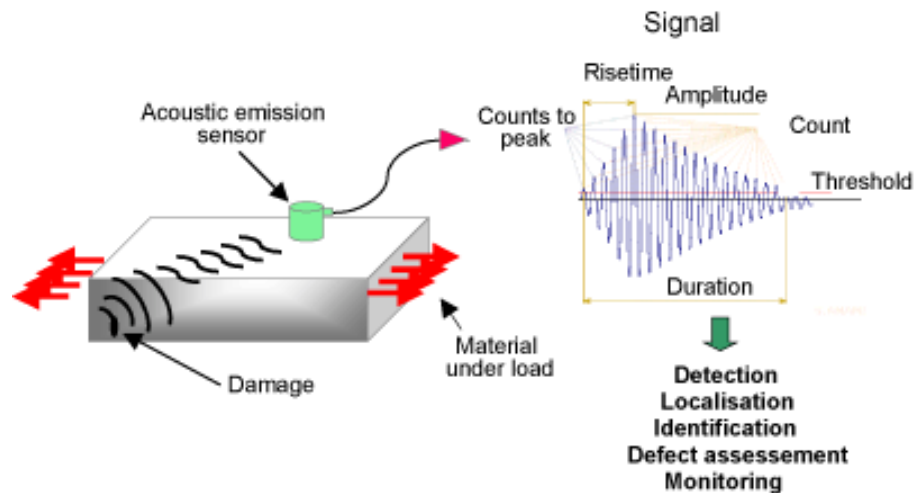


Figure 35: The Acoustic Emission principle (Schematic is courtesy of Physical Acoustics Corporation)

Depending on the type of AE application, either resonant or wideband sensors can be employed. Wideband AE sensors tend to have a rather flat response over a wide range of frequencies. Resonant sensors on the other hand exhibit a higher response at particular frequencies, which are known as the resonance frequencies of the sensor. For specialised applications requiring the removal of environmental noise, the use of resonant sensors can be particularly beneficial. For general applications wideband AE sensors are appropriate.

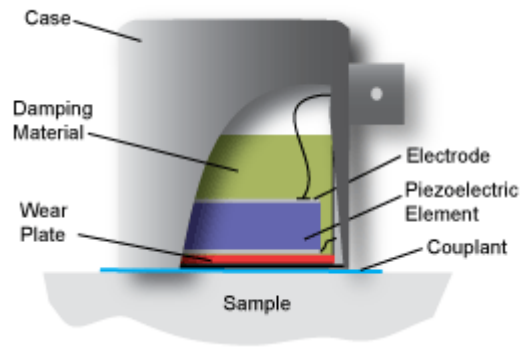


Figure 36: Schematic diagram showing the architecture of a typical AE sensor mounted on a test piece using an appropriate couplant, such as water-based gel, grease or araldite (Schematic diagram courtesy of Physical Acoustics Corp).

As mentioned earlier, the electric signals produced by the piezoelectric crystal are rather low in amplitude. Therefore, prior to being digitised and logged they need to be amplified. In modern industrial AE equipment this is achieved by incorporating a two-stage amplification with the use of a pre-amplifier and a main amplifier. The amplification level can be adjusted according to the needs of the test. It should be noted that the amplification of the signal does not only amplify the signal itself but also the background noise. Thus, the most important aspect is the SNR achieved during the monitoring process and the level of unwanted noise from the background.

AE is a passive technique. As such, it has several advantages including the fact that it is easy to apply, has no material limitations and can monitor a structure globally without having to move the sensors around. However, it has two key disadvantages. Firstly, it is prone to background noise contaminating the signals acquired. Secondly, it is difficult to quantify the

damage level sustained by the monitored structure. Nonetheless, despite the fact that it is a passive technique, from the data obtained, it is often possible to locate accurately the region of damage using either linear, zonal or point location techniques. Also depending on the nature of the AE signal it is possible to identify the type of source of the captured AE activity.

AE monitoring can result in a vast amount of data being produced, particularly since acquisition rates use are in excess of 500 kSamples/s and up to 20 MSamples/s. Therefore, during AE monitoring data acquisition can be carried out using two main strategies. Firstly and most commonly used is the parametric approach in which AE signals that conform to a particular pattern are detected and stored only. The remainder of the AE activity is discarded using high-speed real-time processing. If the AE signals do not confirm with the pattern parameters predefined by the user, then they are simply discarded. This has the advantage of reducing the amount of data generated, especially in applications where data acquisition is required to be performed over long periods of times which can be in the range of days, months or even years. However, if the predefined pattern parameters have not been selected appropriately for a particular application, important data can be missed or excessive data can be generated making analysis either extremely challenging or impossible. In parametric AE testing, various parameters associated with the detected AE signals are considered, including, amplitude, rise time, counts, counts to peak, duration, energy, peak frequency, etc. Parametric data are analysed using statistical methods and taking into account the loading history of the component or structure monitored where this is possible in order to quantify the level of damage that has accumulated.

AE data acquisition needs to be carried out at sufficient high sampling rates in order to overcome aliasing or folding back phenomena. Therefore, taking into consideration the Nyquist frequency an appropriate AE sampling rate needs to be chosen in the range of several hundreds of kHz to several MHz.

An alternative approach to parametric AE testing is the waveform-based AE testing. In waveform-based AE testing, the entire waveform of the AE signal is recorded over the time-period of the acquisition defined by the user. Due to the amount of data acquired, the waveform cannot be recorded for longer than a few tens of seconds with a conventional computer. The longer the waveform that is captured, the longer that the signal processing will take, depending also on the type of algorithm employed. AE waveform analysis is normally carried after data acquisition has been completed, but in very advanced application basic analysis can be carried out in real-time and in parallel with the acquisition.

Waveform analysis is advantageous in the fact that all the information contained in the AE signal is captured. In the case where data acquisition is only needed for a few seconds then waveform analysis has a clear advantage over parametric analysis. It is also easier to work with in the case where background noise levels are high and contaminate the signals of interest. In the case of railway applications, both parametric and waveform analysis can be employed. In this study, a customised waveform analysis-based system has been developed in collaboration with other researchers in the NDT and Condition Monitoring Group at the School of Metallurgy and Materials of the University of Birmingham. The customised AE system has been successfully tested under laboratory and field conditions on the railway network.

Within the rail industry AE testing has only recently begun being applied in the field. Only a few studies, including this one has so far reported results from measurements in the field. However, there are several studies of relevance on AE, which have been carried out in the context of different industrial applications [114]. These have also been taken into consideration as part of this study.

6.3 Vibration Analysis

Vibration analysis is a monitoring method, which has been extensively used for evaluating rotating and reciprocating machinery as well as static structures, such as bridges [115]. All structures once excited by an external stimulus, such as impact from a hammer will vibrate. The vibration signature of a structure can change with time depending on its condition. For example, a large crack in a metallic structure, can result in that structure producing a different vibration signature than that of an identical structure without a crack. Similarly, a bearing with a roller defect will produce a different level and pattern of vibration in comparison with a bearing without any faults. Vibration levels will change gradually and therefore, it is possible to carry out trending in order to identify how much damage has propagated. Industrial standards specify simple rules for the assessment and correlation of vibration levels with accumulated damage. The simplest of the approaches defined by standards are based on the evaluation of peak-peak or RMS values of the vibration signals captured. If a certain threshold has been exceeded, then an appropriate pre-defined maintenance action needs to be taken.

Vibration is different to AE as it relates to the oscillating response of a structure to excitation. AE on the other hand arises in the form of noise due to interactions occurring at the interface

of two different structures, such as the wheel-rail interface, or due to damage growth in the material, e.g. elastic waves being emitted from the tip of a crack growing in a rail.

Vibration signals are generally low frequency with ranges between 0.1 Hz to 18 kHz. High-frequency AE on the other hand has an operating frequency of 30 kHz up to several MHz, although in most applications the frequency range of interest is between 100 kHz to 500 kHz. Vibration analysis is based on the detection and acquisition of vibration signals using industrial accelerometers. Industrial accelerometers depending on their design, have different operational frequency ranges and therefore, need to be selected specifically as per the application requirements. Industrial accelerometers can be either uniaxial or triaxial. Triaxial accelerometers are capable of detecting vibration in all three directions whilst uniaxial can only detect vibration in the axis of their orientation. If vibration is required to be detected in all three directions, then either three uniaxial accelerometers, each orientated in a particular axis, will need to be used, or one triaxial accelerometer installed in an appropriate location.

In a similar fashion as with AE sensors, industrial accelerometers comprise a piezoelectric crystal which is connected to a proof mass Figure 37. If vibration occurs, the proof mass will oscillate accordingly generating a force, which will cause the crystal to deform dynamically. As with the AE sensors, the dynamic deformation of the crystal will give rise to electric signals due to changes occurring in polarisation. The most common type of piezoelectric material used for industrial accelerometers is PZT. Alternatively, low cost accelerometers based on MicroElectronicMechanical Systems (MEMS) can be employed but have inferior performance over conventional piezoelectric industrial accelerometers.

Vibration analysis normally requires data acquisition rates which are much lower depending on the frequency range of interest. Normally, data acquisition in vibration analysis does not need to exceed 25 kSamples/s. Therefore, much longer data acquisition is possible in comparison with high-frequency AE testing. The captured vibration can be analysed using similar algorithms as in AE waveform analysis. However, damage identification sometimes requires trending and therefore, a number of vibration measurements need to be carried out over time. AE does not suffer from this limitation. Still, vibration measurements and associated analysis complements the AE results in a very useful way.

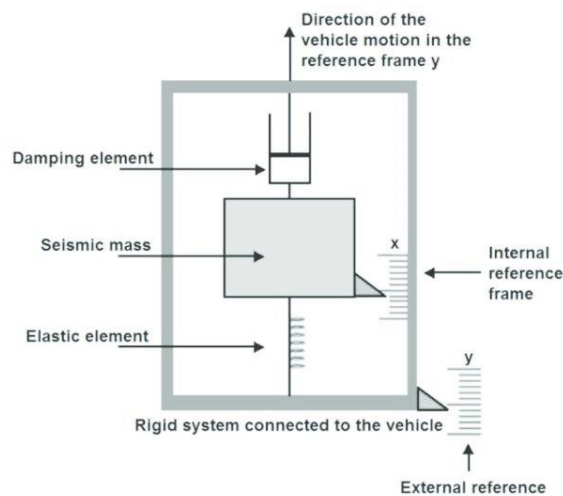


Figure 37: Schematic diagram showing a typical architecture of an accelerometer [123].

Vibration analysis as AE testing has very few practical limitations associated with materials and structures that can be monitored using this technique. Accelerometers depending on their type can be relatively inexpensive and can provide information for a wide range of conditions.

Vibration has already been used for some of the RCM systems used in the rail industry. However, only a very limited number of studies have investigated the integrated use of vibration analysis with AE, including this thesis.

6.4 Chapter 6 Summary

Chapter 6 summarised the main principles governing AE and vibration analysis testing. The key equipment required together with data acquisition parameters have been discussed. The differences and the complementary between AE and vibration analysis have been highlighted and analysed. The following chapter discusses the key signal processing algorithms to be used in conjunction with AE and vibration analysis data.

CHAPTER 7: SIGNAL PROCESSING OF ACOUSTIC EMISSION AND VIBRATION DATA

7.1 Introduction

This chapter focuses on the different methods that can be applied for processing AE and vibration data. Both AE and vibration signals can be affected by noise. Signal Processing is required to eliminate the effect of noise as irrelevant information may mask the useful part of the signal. This is necessary to identify the features of the signal that is associated with the presence of a fault. Signal processing can be carried out in the time, frequency or time-frequency domain, depending on what is required as a final output of the analysis. Therefore, to effectively analyse AE and vibration signals different algorithms can be employed, including peak-to-peak amplitude (PPA), moving Root Mean Square (RMS), moving Crest Factor (CF), moving Kurtosis, power spectral analysis using Fast Fourier Transform (FFT), Cepstral analysis, Spike Energy (SE), Spectral Kurtosis (SK), signal correlation and wavelet transforms [115-120]. As mentioned in the previous chapter there are two different strategies for acquiring AE data, namely parametric or waveform-based. For the waveform-based analysis all of the aforementioned algorithms are applicable. However, for parametric data, statistical analysis needs to be employed. Statistical analysis is discussed at the end of this chapter.

7.2 Peak-Peak amplitude (PPA)

Raw AE and vibration signals are typically plotted in the form of voltage versus time. Peak-peak amplitude based analysis is the simplest of all forms of time-domain analysis. In the measured signal of a healthy bearing or gear it is expected that the maximum amplitude will be

relatively low and no significant and periodic peaks will be evident. However, in the event of damage, it is common to observe peaks at regular intervals in the signal with noticeable higher amplitude than the background signal. The peak-peak amplitude can therefore be used as an initial indicator of damage being present as well as damage accumulation. Especially, in cases where the background noise is low, peak-peak amplitude can be used to draw reliable conclusions of whether a structure is healthy or not. Depending on the repeatability of the peaks at regular period or not it is also possible to extrapolate the possible fault type present. However, to affirm the exact nature of the fault in systems consisting of multiple elements, frequency analysis will always be necessary unless certain types of faults can be ruled out in the first place.

7.3 Moving Root Mean Square (RMS)

Peak-peak amplitude analysis does not reveal the energy contained in the various parts of the signal. Therefore, noise-related background events can generate strong signal peaks, which however, contain very little energy. With peak-peak amplitude analysis it is impossible to distinguish between peaks that are of interest and hence associated with damage and those that are simply associated with background noise. An easy way of evaluating the energy contained in the signal and hence individual peaks, is to use the moving RMS algorithm. However, it is important when using the moving RMS algorithm to define a window, which is representative for the system otherwise useful information may be filtered out or excessive noise may be contained in the post-processed signal. There is no specific standard on what the size of the window should be although as a general rule larger systems are likely to result in more high energy signals and therefore a larger window would be applicable. Normally, some trial and error will be necessary before the optimum window size is determined. The RMS can be calculated using Equation 1:

$$\mathbf{RMS} = \sqrt{\frac{1}{N} \sum_{n=1}^N x_n^2}$$

where N is the number of data points.

Equation 1: Calculating the RMS

For the window size defined an RMS value will be calculated. The window is then subsequently scanned across the entire data set point after point up to the end of the signal. The moving RMS plot is therefore, representative of the energy contained in the signal. Peaks with low energy considered to be noise will be filtered out and only important energetic events will remain in the RMS plot. Of course in more complex situations where noise also contains higher amounts of energy, moving RMS-based analysis is inadequate and more advanced signal processing algorithms are required.

7.4 Moving Crest Factor (CF)

An alternative time-domain processing algorithm to moving RMS is the moving Crest Factor. The Crest Factor is related to the ratio of peak amplitude with the RMS value. Crest Factor is a more computationally expensive algorithm in comparison with moving RMS. It also requires that an appropriate window size is set. Again if the window size is not optimised, important signal features can be lost or excessive noise may remain unfiltered, contaminating the Crest Factor plot.

Essentially the Crest Factor is used when it is desirable to ascertain how extreme the peaks in an AE or vibration signal are. A Crest Factor value of 1 would be obtained for a signal with no peaks as the peak amplitude and RMS values would overlap. However, the higher the ratio of peak amplitude to the RMS value, the more strong the peak in the signal will be. Equation 2 can be used to calculate the CF of a signal:

$$c = \frac{|x_{peak}|}{x_{rms}} = \frac{\|x\|_{\infty}}{\|x\|_2}$$

Equation 2: Calculating the CF of a signal

The value of the Crest Factor can indicate the extent of damage in a surface impacting upon each other, such as a worn roller impacting on the race of the bearing. Crest Factor can also be used for the identification and evaluation of crack related signals indicating how significant the energy released from a crack propagation event was. By using trending of Crest Factor values it is possible to evaluate the extent of damage since crack growth rate will increase as damage propagates and approaches critical dimensions. The advantage of the Crest Factor in comparison with the RMS is that the former has much higher sensitivity to sharp peaks, which may contain comparable energy levels with those peaks related to background noise signal. In such cases the moving RMS algorithm cannot cope but Crest Factor may identify peaks related to other events than background noise if they are sharp enough. Normally a Crest Factor value of 3 and above is indicative of a fault.

7.5 Moving Kurtosis

Kurtosis is another time-domain processing algorithm used to evaluate the peakedness or sharpness of peaks in an acoustic emission or vibration signal. Moving Kurtosis has similarities with the CF although it is a much more computationally expensive algorithm and therefore large files can take much longer to process than with moving CF. Normally, Kurtosis values above 4 are indicative of a fault being present, whilst values below 3 are indicative of a healthy system. Kurtosis can be calculated using Equation 3:

$$K = n \frac{\sum_{i=1}^n (X_i - \bar{X})^4}{\sum_{i=1}^n ((X_i - \bar{X})^2)^2}$$

Equation 3: Kurtosis time-domain processing algorithm

During the analysis with moving Kurtosis an appropriate threshold can be set, which is representative for the system. In simple cases setting $K > 4$ would be adequate. However, in more complex situations, where noise is largely overlapping with features of the signal associated with a fault, different values are likely going to be needed to be set as thresholds. Again there is no specific rule and trial and error will need to be employed in identifying appropriate threshold levels in each case.

7.6 Power spectral analysis using Fast Fourier Transform (FFT)

Although time-domain analysis can be used to reveal the presence of a fault in a system, it can rarely reveal its actual nature. In order to achieve this reliably, it is necessary to carry out signal processing in the frequency domain, particularly when rotating or reciprocating components are being monitored. In the case, where crack growth is being monitored in a component or structure, time-domain analysis may suffice since no other fault is anticipated to be present other than other cracks. However, even in this scenario, if the crack growth event-related signal features are hidden in the background noise more complex signal processing in the frequency or time-frequency domain is likely to be required.

The simplest method of carrying out frequency-domain analysis on AE and vibration signals is by applying the FFT algorithm. The FFT algorithm can be applied to decompose the time signal into its constituent frequencies and their amplitudes. All AE and vibration signals contained frequency-related information. An AE or vibration signal captured from a healthy component is expected to have a relatively smooth power spectrum with no distinct individual peaks evident at specific frequencies. However, in the case where there is a fault, the power spectrum will begin to change with certain peaks appearing at particular frequencies, which indicate the presence of a problem. Therefore, comparison of the power spectra for healthy and faulty conditions can be employed to rapidly ascertain whether changes in the system being monitored have occurred. If the peak amplitudes at the new frequencies increase or additional peaks become evident, these would represent indications of damage evolving further. The Discrete Fourier Transform (DFT) used in the FFT algorithm is represented by Equation 4:

$$X_k = \sum_{n=0}^{N-1} x_n e^{-i2\pi kn/N} \quad k = 0, \dots, N-1,$$

where $e^{-i2\pi kn/N}$ is a primitive N th root of 1.

Equation 4: The Discrete Fourier Transform

7.7 Spike energy (SE)

To ascertain which component has been affected by damage, power spectral analysis alone is not adequate. Instead, the spike energy algorithm needs to be used instead. The spike energy algorithm is based on analysing the power spectrum of the envelope of the signal. The peaks arising at the frequencies of interest are indicative of what the fault is. The higher the peak amplitude at a particular frequency, the more severe the damage will be. Also, the number of harmonics present are representative of the severity of the fault. As the damage progresses further, harmonics will become clearly evident in the analysed signal.

The algorithm is based on carrying out enveloping of the raw signal by applying the moving RMS algorithm and subsequently using the FFT algorithm in order to devolve the signal to its constituent frequencies. This is a very powerful and reasonably inexpensive computationally algorithm for filtering out unwanted background noise from the signal and identifying the features of interest. The amplitude values can be trended in order to evaluate damage progression. Threshold values can be set once confidence margins have been estimated reliably for a particular component or system.

7.8 Cepstral analysis

Cepstral analysis is based on the calculation of the Inverse Fourier Transform. Hence, the power cepstrum is the inverse of the power spectrum. It is also a frequency-domain analysis algorithm, which is routinely used to identify families of defects in cases where multiple defects are present at the same time in a rotating component. Power Cepstrum is defined as the squared magnitude of the inverse of the logarithm of the squared magnitude of the FT of a signal and is given by Equation 5:

$$\text{power cepstrum of a signal} = |F^{-1}\{\log(|F\{f(t)\}|^2)\}|^2$$

Equation 5: Power Cepstrum

7.9 Spectral Kurtosis

Time domain and frequency domain algorithms have their own specific limitations, which can be overcome in time-frequency domain analysis. Spectral Kurtosis is a powerful time-frequency domain analysis algorithm which can reveal not only the energy of the signal in the time domain but also relate it to the frequencies of interest. In this way the identification and quantification of a fault present in a rotating component can be rendered more reliable. The resulting plots are called kurtograms [18]. However, as in conventional moving Kurtosis analysis, an appropriate window size needs to be defined for optimum results.

7.10 Signal Correlation

The signal correlation algorithm is based on the extraction of features of interest from a signal which can then be used as a template for scanning the rest of the signal for apparent similarities.

For example, assume that there is a single peak in an AE signal which is known to be related to a crack growth event. The data associated around the range of the peak identified in the signal can be defined as the template, in a similar way as when a window is defined in moving RMS, etc. This is now the template where subsequent analysis will be carried out [19]. The template can be further processed using various types of algorithms including spectral analysis in order to reveal its frequency content. Subsequently the original signal is scanned and correlated with the template obtained. All background features should produce a low similarity index value. However, when the template scans the part of the signal from where it was extracted a very high similarity index value should be obtained. New signals can be scanned in the same way to reveal their similarity index values based on the template used. If low similarity index values are obtained, then no crack-related features are present. However, in the case where high similarity index values are obtained, then crack events are likely to have been detected. The technique can employ a variety of representative templates all of which can be correlated to a given signal. The more templates that a signal is correlated against, the more reliable the analysis will be. The technique has been successfully applied in the rail sector in a number of studies. However, it remains a relatively computationally expensive technique and requires optimisation of the templates used for the analysis.

7.11 Wavelet analysis

Wavelet analysis is an alternative method for analysing AE and vibration signals. However, it is more complicated to apply and more difficult to obtain quantifiable results in comparison with the aforementioned algorithms, which are more straightforward to use [121]. The wavelet transform of an AE or vibration signal can be described by Equation 6:

$$S(b, a) = \frac{1}{\sqrt{a}} \int_{-\infty}^{\infty} \psi' \left(\frac{t - b}{a} \right) s(t) dt$$

where ψ' denotes the complex conjugate of the complex-valued function ψ .

Equation 6: Wavelet transform

7.12 Statistical analysis for parametric data

AE parametric data cannot be analysed with the aforementioned algorithms. Instead statistical tools are required to be used instead. Therefore, AE data need to be plotted with respect to the parameters of interest or combinations of those. For example, AE hits captured during parametric acquisition can be plotted in terms of amplitude with time, strain, load, etc. Similarly, energy can be plotted in cumulative form with time, strain, load, etc. Parameters can also be trended to see if their values increase with increasing damage accumulation, e.g. the signal energy value, signal duration, signal counts, etc. Relationships between different parameters can also be investigated, such as the ratio of the rise-time with amplitude or other combinations.

7.13 Chapter 7 Summary

Chapter 7 discussed in some detail the different types of algorithms that can be used for the analysis of AE and vibration signals. These algorithms can be applied for the analysis of other types of data also meaning they have a wide range of applications. The signal processing used for the analysis of AE and vibration data captured during laboratory and field trials are discussed in more detail in the results and discussion section of this thesis.

CHAPTER 8: EXPERIMENTAL METHODOLOGY

8.1 Introduction

This chapter details the experimental methodology employed during this research study. A variety of experiments have been carried out starting from representative laboratory tests, moving onto trials in the field under simulated conditions and finally, carrying out measurement under actual operational conditions on the UK railway network. The laboratory tests were based on: a) three-point fatigue bending tests of rail and cast manganese steel standard samples and b) rolling tests using an Amsler rolling machine capable of rotating fixed speed cylindrical samples. The purpose of the three-point fatigue bending tests was to simulate crack growth in similar fashion as it occurs on rails and crossings in order to investigate the capability of AE in detecting crack growth events. The Amsler tests on the other hand aimed at identifying the capability of AE and vibration analysis in detecting wear defects on the tread of a cylindrical sample as it rolled against a reference sample. Subsequently, tests were carried out at the Long Marston test track with the help of Motor Rail Logistics using simulated wheel and axle bearing defects on freight rolling stock provided by the private rail car hire provider Vereinigte Tanklager und Transportmittel (VTG). Following from the successful trials at Long Marston, a site on the Chiltern Line in Cropredy was selected for the permanent installation of a customised vibration and acoustic emission system for monitoring the condition of wheels and axle bearings of passing rolling stock on a daily basis. Finally, AE measurements were carried out on actual cast manganese crossings at various sites on the UK railway network including Watford, Newark, Wembley and Hatton. With the exception of the crossing at Watford, which was found to be severely damaged and due to be replaced within a week after the measurements, all other crossings tested were found to be in acceptable condition. The results of the

measurements were reported to the maintainer within Network Rail. All trials on the UK railway network were performed following the issuing of a Certificate of Acceptance by Network Rail, permitting the tests of the customised vibration and acoustic emission systems on sites on the UK railway network.

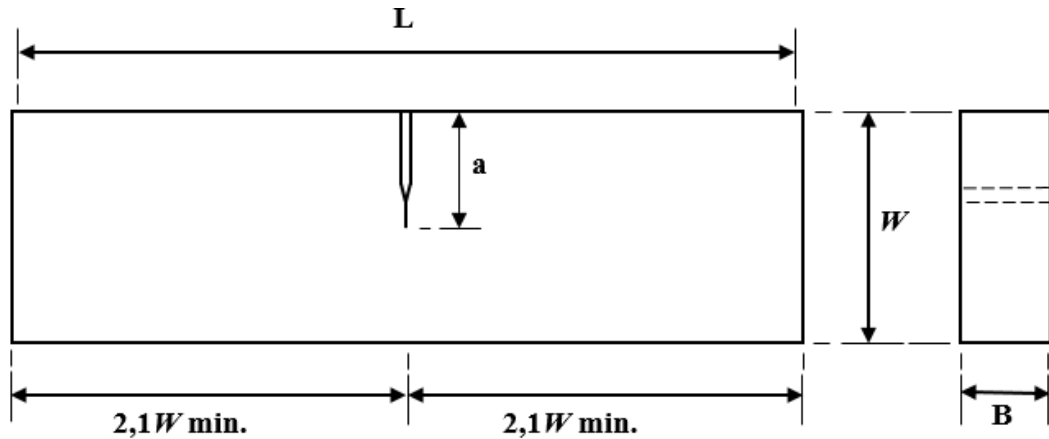
8.2 Laboratory trials

Laboratory trials were split into two types of tests. Firstly, three-point fatigue bending tests designed to cause crack growth on pre-cracked samples during cyclic loading. This type of test was considered to be representative of actual crack growth events occurring in actual rails and crossings being repeatedly loaded by rolling stock passing over them. The capability of AE in detecting the crack growth events was evaluated during these trials. Secondly, Amsler rolling tests designed to evaluate the capability of AE in detecting wear on the surface of rolling samples considered to be representative of rolling stock wheel and axle bearing damage.

8.2.1 Three-point fatigue bending tests

Standard three-point fatigue bending samples were cut from the web of actual rails and a plate of cast manganese steel procured from West Yorkshire steel. In the case of the cast manganese steel, samples were plasma cut. The dimensions of all three-point fatigue bending samples were 200 millimetres (mm) long, 10 mm wide and 20 mm thick. A 2 mm notch was spark eroded at the centre of all samples with an angle of 60° as shown in Figure 38. The samples were subsequently pre-cracked using a high-frequency Vibrophore operating at an appropriate load range, so cracks could initiate. Crack initiation and propagation were confirmed using metallographic replicas as well as AE. Subsequently, the pre-cracked samples were fatigue

tested until final failure occurred using a 50 kN DARTEC servo-hydraulic universal test machine. The loading range used was 0.5 – 5.5 kN at loading frequency of 1 or 5 Hz depending on the test.



B = thickness
W = width = $2B$
a = effective crack length = $0,45W$ to $0,55W$
L = loading span = $4W$

Figure 38: Schematic diagram showing a standard three-point fatigue bending sample.

During all fatigue tests, crack growth was monitored using Direct Current Potential Drop (DCPD) measurements in parallel with AE testing. For the AE measurements two R50a resonant piezoelectric sensors procured from Physical Acoustics Corporation were employed. Data acquisition was carried out using both a commercial PAC system as well as the customised AE system developed in-house. The amplification for measurements with both systems were set at 46 dB (40 dB pre-amplification and 6 dB main amplification). The sampling rates in both cases were set at 1 MSample/s per channel. Araldite was used for adhesion and ultrasonic

coupling for all tests. The photograph in Figure 39 a) shows the general experimental setup employed during three-point fatigue tests. The photograph in Figure 39 b) shows a sample tested after having failed.

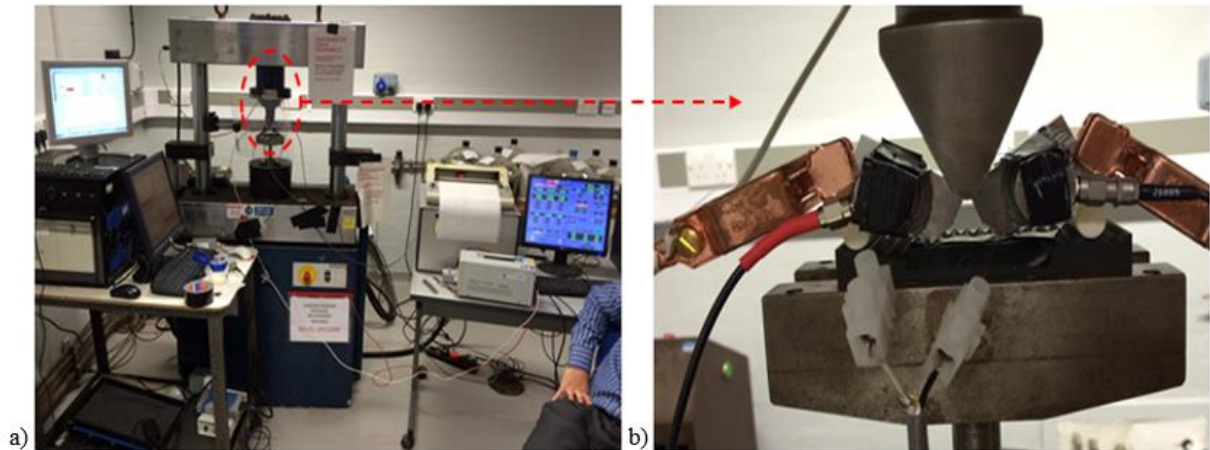


Figure 39: a) Experimental setup with PAC and customised acoustic emission system. The sample is in place and undergoing cyclic loading. Crack length is continuously monitored with the DCPD instrument. b) this photograph shows a close-up of a failed sample. The two acoustic emission sensors are visible together with the DCPD instrument connections. The sample has been loaded using three-point cyclic loading.

8.2.2 Amsler rolling tests

The Amsler test rig is a tribometer device designed to simulate kinematic conditions of rotating components such as the wheel-rail interface. The test rig requires the use of two cylindrical samples, one of which is the reference sample and the other is the test sample. The reference sample needs to be made of a harder material so wear damage occurs only on the test sample. In this case the reference sample was made of tungsten carbide whilst the test sample was made

EN24T steel. Although, the EN24T grade is not identical to wheel steel grade, it is still representative for the testing of interest required for the present study. The upper specimen rotates at 360 RPM whilst the lower specimen rotates at 400 RPM.

Cylindrical steel samples were manufactured for rolling tests using an Amsler rolling machine. The rolling samples employed were representative of good and damaged condition, i.e. without wear damage on the tread and artificially induced wear on the tread. The samples were rotated against a reference cylindrical sample in good condition. A load of 200 N was applied on the testing wheels during rolling tests. The contact stresses (calculated to be 2.77 GPa) arising from the application of the 200 N load are considered to be representative of the contact stresses sustained by the wheel tread of poor geometrical conformity for actual rolling stock travelling across the railway network. The samples were monitored using an R50a piezoelectric AE sensor procured from PAC. The sampling rate was set at 500 kSamples/s in this instance whilst the amplification was set again at 46 dB (40 dB pre-amplification and 6 dB main amplification). The custom-built system was employed for all measurements. Digital data acquisition was carried out using a four-channel Agilent 2531A USB DAQ capable of sampling up to 2 MSamples/s (500 kSamples/s per channel if all four channels are used simultaneously or up to 2 MSamples/s if only one channel is used). Adhesion and ultrasonic coupling of the AE sensor were achieved using araldite.

The photograph in Figure 40 a) shows the Amsler rolling example setup, Figure 40 b) shows the reference sample geometry and Figure 40 c) show the test sample geometry. In this

particular instance the healthy sample, i.e. the one with no tread defects is shown. The bottom wheel is the reference one.

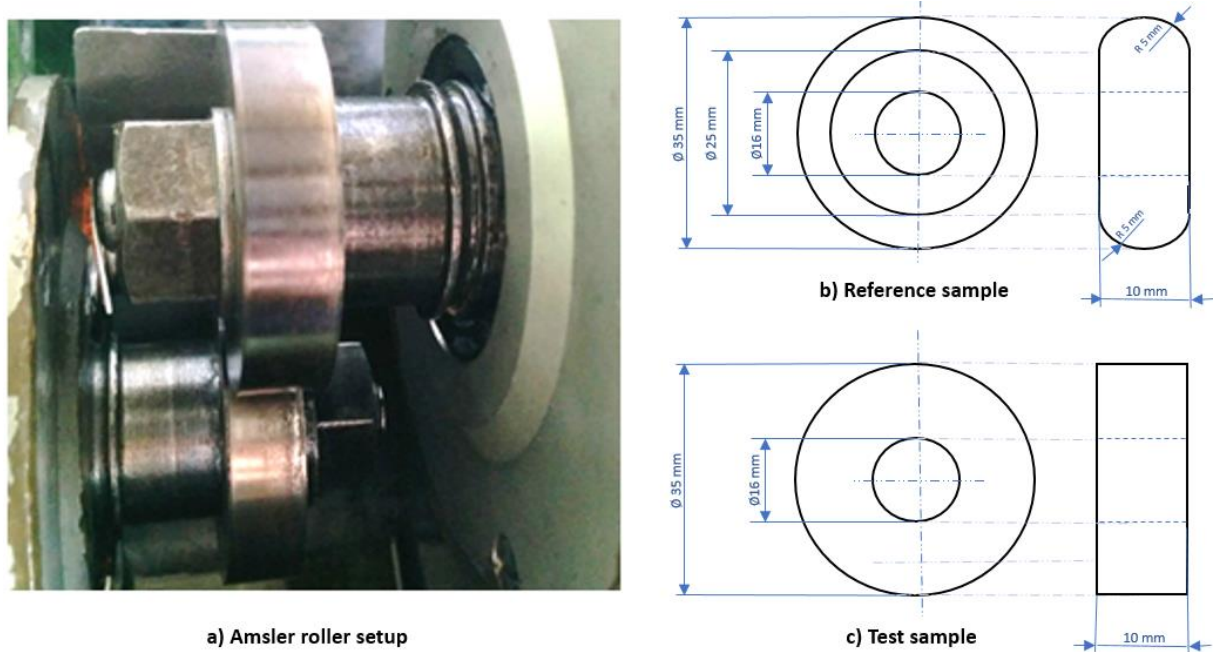


Figure 40: a) Example of Amsler rolling testing setup, b) Reference sample geometry, and c) Test sample geometry.

8.3 Rolling stock wheel and axle bearing testing at Long Marston

A customised AE and vibration analysis system for onboard and wayside evaluation of axle bearings and wheels, which can be rapidly installed and removed from the train tested using magnetic hold-downs was developed in-house in collaboration with other researchers. Experiments using simulated faults were carried out on freight rolling stock in Long Marston. The tanker wagons used during the tests were provided by VTG and contained a variety of artificially damaged axle bearings. The photographs in Figure 41 show an example of the rolling stock used during the Long Marston trials. Rolling stock used during the Long Marston trials

were clearly marked so they would not be returned for service by accident on the actual network with artificially induced faulty wheels or axle bearings.



Figure 41: Tanker freight wagons with several axel bearings artificially damaged in the roller or race using a power tool.

A customized integrated AE and vibration analysis system that was developed in-house was employed for the evaluation of wheel tread damage as well as various types of axle bearing defects including lubricant contamination, roller and race defects of different severity.

The customized AE/vibration analysis system shown in the photograph of Figure 42 consists of the following components: a) resonant acoustic emission sensors manufactured by Physical Acoustics Corporation (PAC), b) industrial accelerometers with sensitivity 100mV/g manufactured by Wilcoxon, c) pre-amplifiers manufactured by PAC, d) amplifiers manufactured by Krestos, e) accelerometer power supply manufactured by Krestos, f) Agilent four-channel decoupling hub manufactured, g) 2531A Agilent four-channel data acquisition

card with a maximum sampling rate of 2 MS/s in single channel mode and h) Amplicon industrial computer with customized data logging and analysis software [2-5, 18-19].



Figure 42: The customised data acquisition equipment used during trials at Long Marston.

Onboard AE and acceleration measurements were carried out in order to confirm the condition of the healthy and defective axle bearings, while the tankers were moved over a straight rail track section a few hundred meters long at a speed of 24 km/h. Various axle bearing defects were induced including roller defects of different magnitudes 2, 4 and 8 mm deep and outer race defects 2, 4 and 8mm deep were induced using a power tool. The photograph in Figure 43 shows the way the sensors were installed onboard. A similar set up was used for the wayside measurements, but in this case the accelerometers and AE sensors were mounted on the web of the rail.



Figure 43: AE sensors and accelerometer installed in one of the axle bearings of the tanker freight wagons tested in Long Marston.

The acquisition rate for the AE measurements was set at 500 kSamples/s per channel. For the vibration measurements the acquisition rate was set at 25 kSamples/s per channel. The photograph in Figure 44 shows the wayside installation of AE sensors and accelerometers.



Figure 44: Wayside installation of AE sensors and accelerometers at Long Marston.

8.4 Cast manganese crossing tests

The aforementioned customised AE system was used to test cast manganese steel samples under actual operational conditions on the UK railway network. Crossings at four different sites were measured including, Watford, Newark, Wembley and Hatton as shown in the photographs of Figure 45. The system employed consisted of: a) one commercially available 2531A Universal Serial Bus (USB) data acquisition card (DAQ) with decoupling procured from Agilent with maximum sampling rate of 2MS/s and capable of supporting up to 4 channels; b) signal pre-amplifiers and amplifiers procured from Physical Acoustics Corporation (PAC); and c) R50A acoustic emission sensors also procured from PAC. All connections were done using Bayonet Neill-Concelman (BNC) cables. The entire customised acoustic emission system was powered from the mains using 220 Volts (V) Alternating Current (AC).

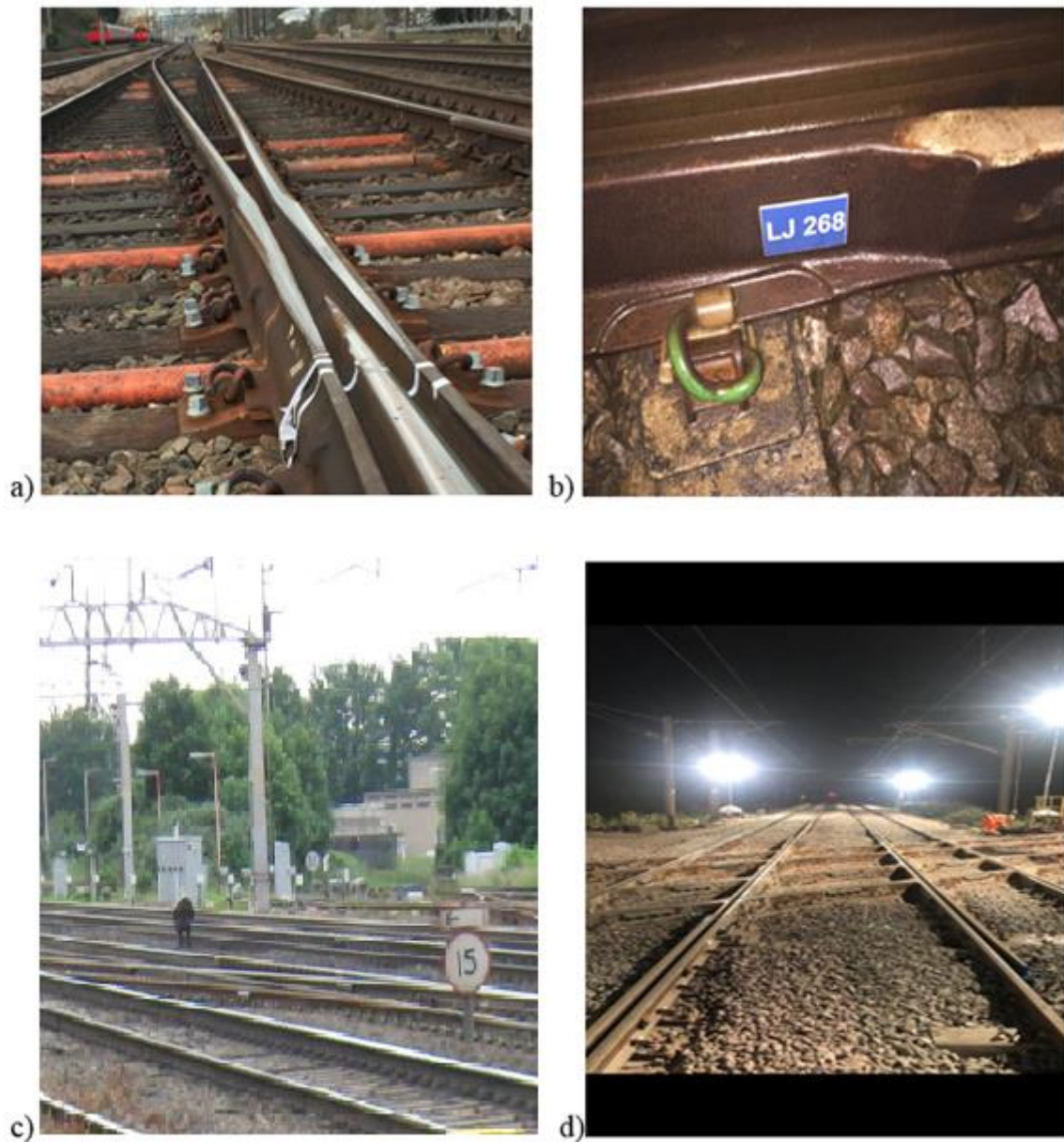


Figure 45: Crossing tested in a) Wembley, b) Hatton, c) Watford and d) Newark

An integrated customised data logger and signal analysis software package created in-house using MATLAB was employed. The software is capable of carrying out multiple measurements at duration and time intervals specified by the system operator.

The PAC AE system used in the laboratory trials monitors AE activity and then deletes the complete waveform keeping only the data related to the definition of an AE hit as defined by the user. In the case of the customised AE the entire waveform produced due to crack growth and background noise during loading and unloading of the crossing from passing trains is captured. Due to the large amount of data generated the recording cannot be maintained indefinitely since the system will crash due to the high sampling rate (at least 1 MS/s) or the hard disk will run out of free space.

However, under operational conditions in the field, loading only occurs whenever there is a wheel passing over the area of interest loading it. Thus, loading lasts for a few seconds and the AE activity that is of interest occurs only during this period. Hence, it is affordable in terms of computing resources to capture the entire waveform of the AE activity.

Although it is possible to also monitor the entire waveform throughout the test the duration that recording can be maintained is limited by the size of the hard disk. Moreover, the use of the waveform later on is not as straightforward since the PAC system has been designed with a different notion. All tests in the field were carried out after a Certificate of Acceptance, shown in Figure 46 had been issued for the customised CM system by Network Rail.



Figure 46: Certificate of Acceptance issued by Network Rail for the customised AE and vibration system built in-house, enabling trials to be performed at various site on the UK railway network.

8.5 Croppedy rolling stock wheel and axle bearing monitoring system

For the long-term evaluation of the capability of the integrated AE and vibration monitoring system in detecting wheel and axle bearing faults of in-service rolling stock a site at Croppedy was chosen for instrumentation, Figure 47. The site selected was adjacent to an existing commercial HABD. The installation of the customised system took place by a combined team of University of Birmingham (UOB), Network Rail and Krestos Limited engineers, including the author of this study. The installed system comprised 12 channels with 3 Agilent 2531A DAQs being employed. In the existing layout 7 channels were used in total as follows: four

channels for 4 AE R50a resonant sensors, two channels for 2 Wilcoxon industrial accelerometers and one channel for the industrial treadle used to trigger the acquisition once a train approached the sensors. The data acquisition was set to last for 18 seconds with sampling rates of 500 kSamples/s for each AE sensor and 25 kSamples/s for each accelerometer. The treadle activates the acquisition by closing an electric circuit whenever the trigger arm is pushed down by the flange of the first wheel of a passing train. The distance from the treadle to the first sensor is 18 metres. This gives sufficient time for the acquisition to start without missing any part of the train.

Although 18 seconds are sufficient for monitoring the entire length of passenger trains, freight trains which are up to 25 wagons long may not be captured in their entirety depending on how fast they are moving. This is due to the fact that a fixed acquisition time has been chosen. The system was installed in September 2015 and has been operating on a daily basis with very little maintenance since that time. It monitors approximately 200 trains each day.

The AE sensors have been ultrasonically coupled with araldite, also providing adhesion. For additional safety of the installation magnetic hold-downs have also been used. The industrial accelerometers have been installed with magnetic hold-downs alone at the rail foot.



Figure 47: Photographs showing the installation of the customised 12-channel AE-vibration system at the Cropredy site, direction from London towards Birmingham.

The schematic diagram in Figure 48 shows the sensor layout used in the instrumented site at Cropredy.

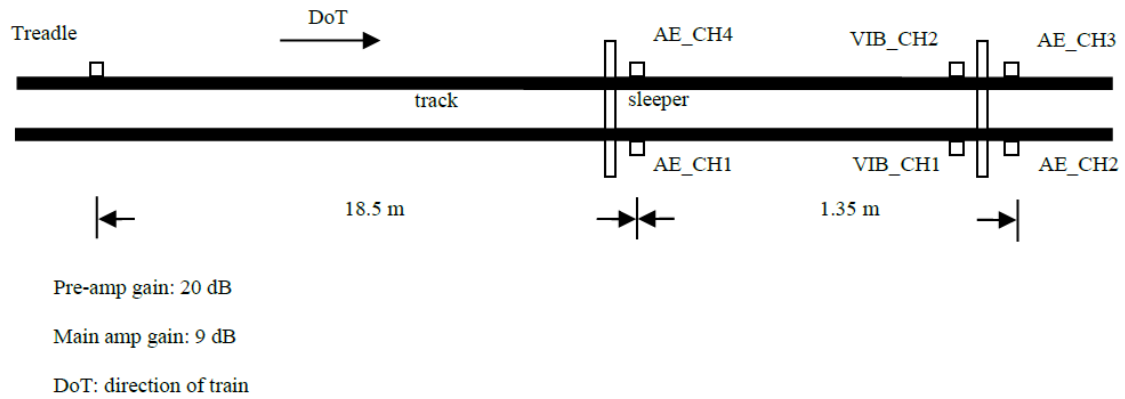


Figure 48: Schematic diagram of the Cropredy system sensor layout.

8.6 Chapter 8 Summary

This chapter provided the details of the experimental methodology employed during this study. The work has been based on a combination of laboratory trials, field trials under simulated operational conditions held in Long Marston and field trials under actual operational conditions held at various sites selected across the UK railway network. The next chapter discusses the key results obtained from the experiments documented through this chapter.

CHAPTER 9: RESULTS AND DISCUSSION

9.1 Introduction

Chapter 9 contains the key results and discussion associated with the experiments carried out during this study. It should be emphasised that a very large number of tests have taken place, so the purpose of this chapter is not to present an exhaustive amount of data, but to provide evidence of the key findings arising. The chapter is split into sub-sections related to the individual sets of tests carried out, starting with laboratory experiments, moving to Long Marston field trials under simulated conditions and finally field trials on the UK railway network under actual operational conditions. From the results presented it becomes obvious that AE and vibration analysis are powerful monitoring tools which can provide advance insight of the actual condition of structural infrastructure and rolling stock components, including rails, crossings, wheels and axle bearings.

The AE and vibration data can be integrated with data from other commercial systems. Although integration of data obtained from other monitoring systems has not been the purpose of this study and hence has not been updated, it should be noted that Huang [19] has outlined in detail a realistic qualitative methodology for doing so. From the results obtained it is clearly possible to follow the relationship between the laboratory work and field trials, helping validate the techniques investigated and promote their gradual uptake by the industry at a commercial scale in the foreseeable future.

9.2 Three-point fatigue bending laboratory trials

The results of the fatigue tests carried out under laboratory conditions are detailed next. Fatigue crack growth tests were carried out using three-point bending tests on a reference mild steel sample with no notch and no known micro-cracks present, and cracked rail grade and cast manganese steel samples. All samples with the exception of the reference uncracked and unnotched sample were pre-cracked using a Vibrophore machine as discussed earlier in chapter 8.

During fatigue testing a DARTEC 50kN servo-hydraulic universal test machine was used. Crack growth was monitored throughout testing using a DCPD instrument. Sinusoidal loading patterns were used with a cyclic loading ratio maintained throughout the tests at $R=0.1$.

Two AE R50a piezoelectric sensors procured from PAC were mounted on the samples during testing using araldite, which also offered the ultrasonic coupling required for the measurements. The AE sensors are of the same type as those used in the field trials in Long Marston, Cropredy and the crossing sites measured. R50a sensors have an operating frequency of 100-700 kHz. One sensor was connected to the customised system and one to the PAC commercial system used for reference measurements. All samples with the exception of the reference sample were cyclic loaded until final failure. Crack growth during testing was recorded using the DCPD instrument as well as both the PAC and customised AE systems.

The data obtained with both the customised and commercial AE systems during the tests were very encouraging as shown by the results obtained.

Figure 49 shows the AE activity generated during cyclic loading of the mild steel reference sample with no known cracks present. As it is expected only the noise arising from the bending moments of the sample and hydraulic pump are visible in the AE signal acquired. Also, the peak-peak amplitude of the AE signal is no more than ± 0.11 V indicating no crack growth is occurring. It should be noted that the saturation AE signal has peak-peak amplitude of ± 10 V.

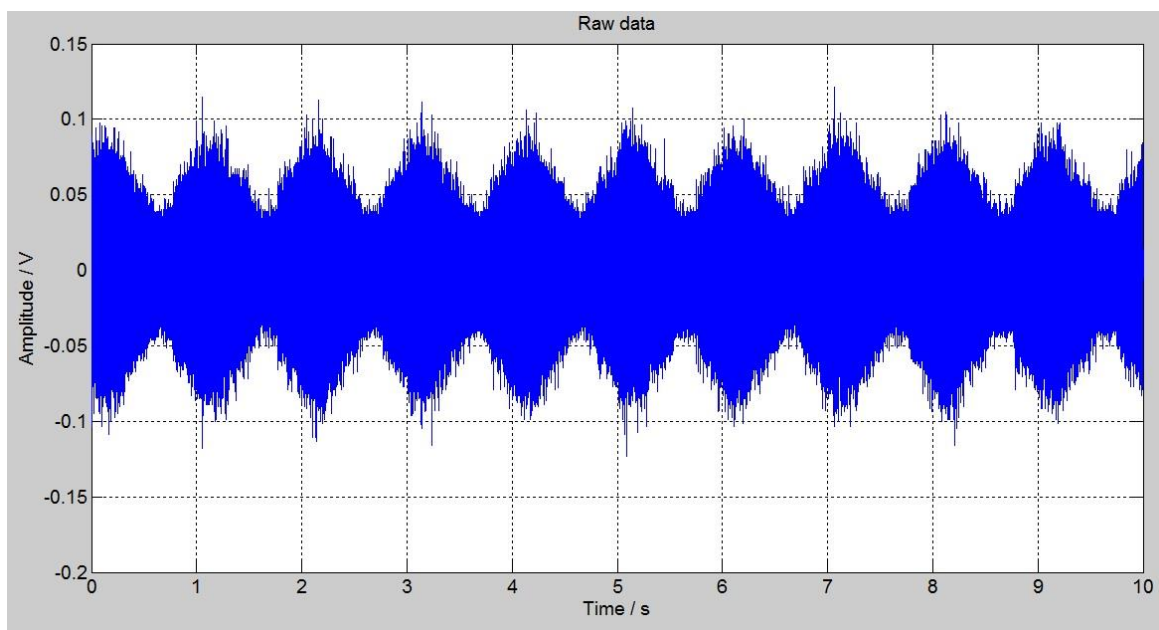


Figure 49: AE activity for the reference sample over 10s long acquisition at 1 MS/s. The thickening of the signal occurs during the loading stage and arises from the bending moments. During unloading the signal amplitude drops to background noise. There are no other visible peaks indicating crack growth. Some minor peaks visible in the signal are due to noise from the DARTEC servo-hydraulic mechanism. The peak-peak value does not exceed ± 0.11 V

The plots in Figure 50 show the raw AE data together with the processed results using moving RMS and Kurtosis algorithms for uncracked mild steel reference sample. As it can be seen the

values obtained for both RMS and kurtosis are extremely low, clearly indicating that there is no crack initiation or propagation occurring during the data acquisition.

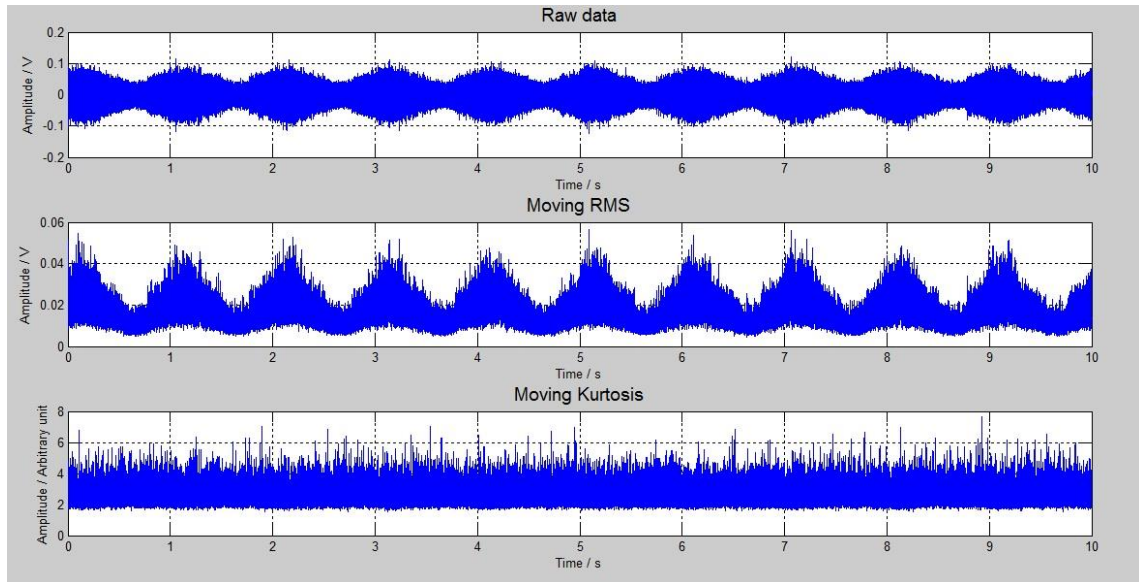


Figure 50: Raw dataset together with moving RMS and moving Kurtosis graphs. No crack indication is visible

Following from the test on the reference mild steel sample, testing on pre-cracked cast manganese steel samples was carried out. The plot in Figure 51 shows the crack growth in a pre-cracked cast manganese steel sample exposed to three-point fatigue bending. In this particular instance both AE sensors have been connected to the commercial system for calibration purposes. In the same plot the normalised cumulative AE energy detected from each AE sensor has been plotted in relation to the crack propagation.

It can be readily seen that the AE successfully follows the trend although with fluctuations in this particular instance. This is due to the fact that the sample is likely to be experiencing some level of plasticity at the crack tip as it is being loaded and unloaded. The sample tested had been

cut off from a cast manganese steel plate, which had a measured Vickers hardness of approximately $H_{V0.3}=277$. Hence, the sample had not yet attained its maximum hardness and could experience substantial work hardening during cyclic loading.

As a result, the elastic energy released from the crack tip is not the same throughout the test. This however, is not expected to be the case in samples, which have been explosion casted since they will already have obtained the optimum hardness. The Vickers hardness of explosion casted cast manganese steel should be in the range of 550 as per manufacturing requirements for crossings.

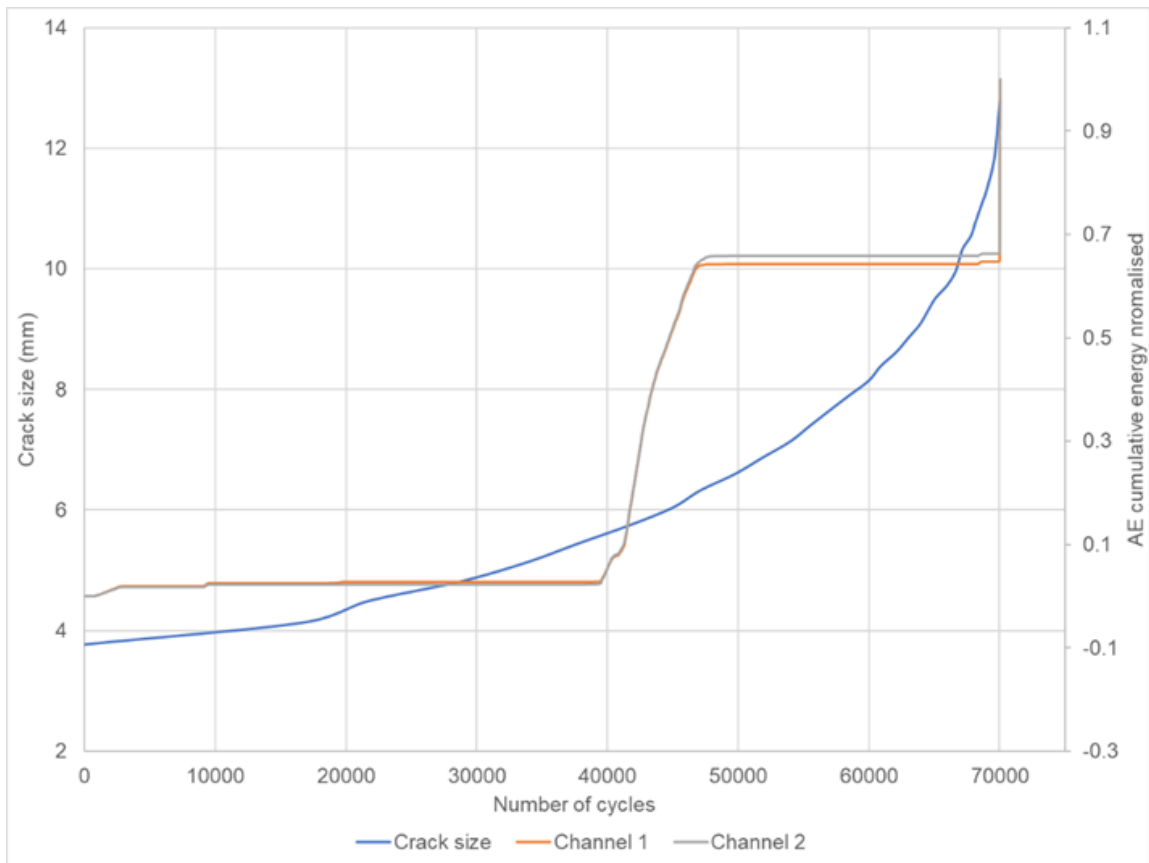


Figure 51: Plot showing crack growth with normalised cumulative AE activity up to the point of failure for a pre-cracked cast manganese steel sample.

Figure 52 shows the raw AE dataset for a pre-cracked cast manganese steel sample obtained using the customised AE system at the middle stages of the fatigue testing. As it can be seen from the plot the AE activity is clearly intense since the crack growth rate is progressing relatively rapidly at this stage. There is a clear peak for each loading cycle indicating a crack growth event, which has been successfully detected by the AE sensor.

The smaller peaks seen in some cases during the unloading stage of the cyclic loading process is likely to be related to crack closure and rubbing of the crack surfaces. These peaks could not be related to crack growth since crack propagation cannot occur during unloading. However, crack closure and rubbing of the crack surfaces is likely to be taking place. Such an event would indeed give rise to a peak, albeit of lower intensity as seen in the plot in Figure 52.

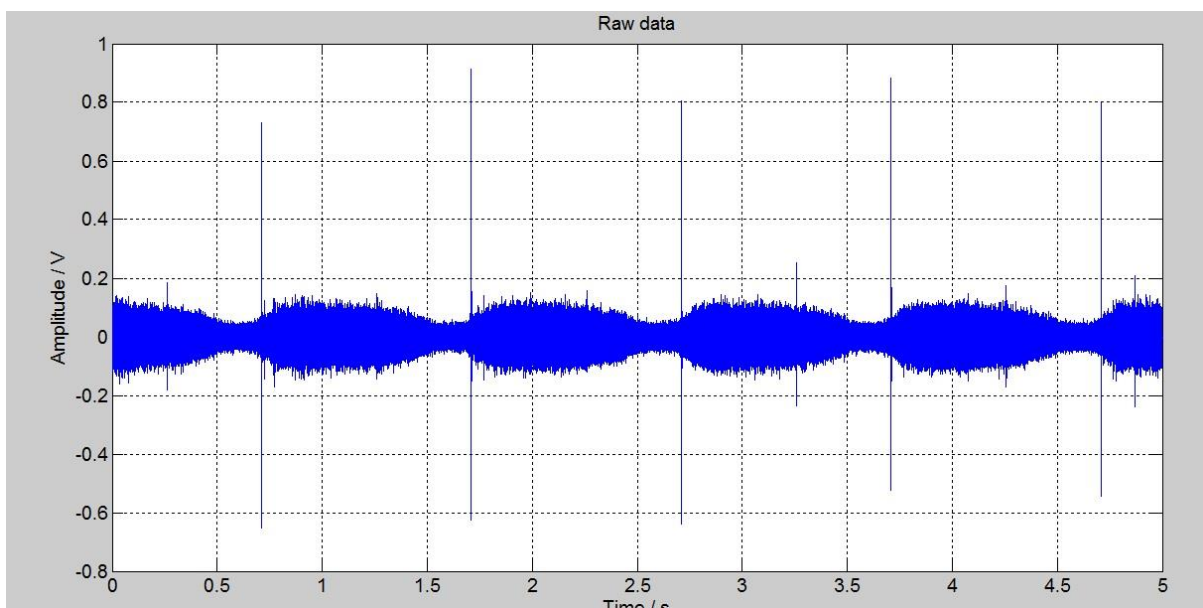


Figure 52: Raw acoustic emission dataset at mid-stages of the test for one of the pre-cracked cast manganese steel sample. The AE activity is clearly intense with crack growth occurring at every loading cycle.

The plots in Figure 53 shows the above raw AE dataset together with the moving RMS and moving Kurtosis values. Again, the crack growth events are clearly visible in the moving RMS plot but not in the moving Kurtosis plot only some peaks are observed. However, as the energy of the signal of the peaks intensifies the moving Kurtosis analysis will also reveal more clearly the crack growth events.

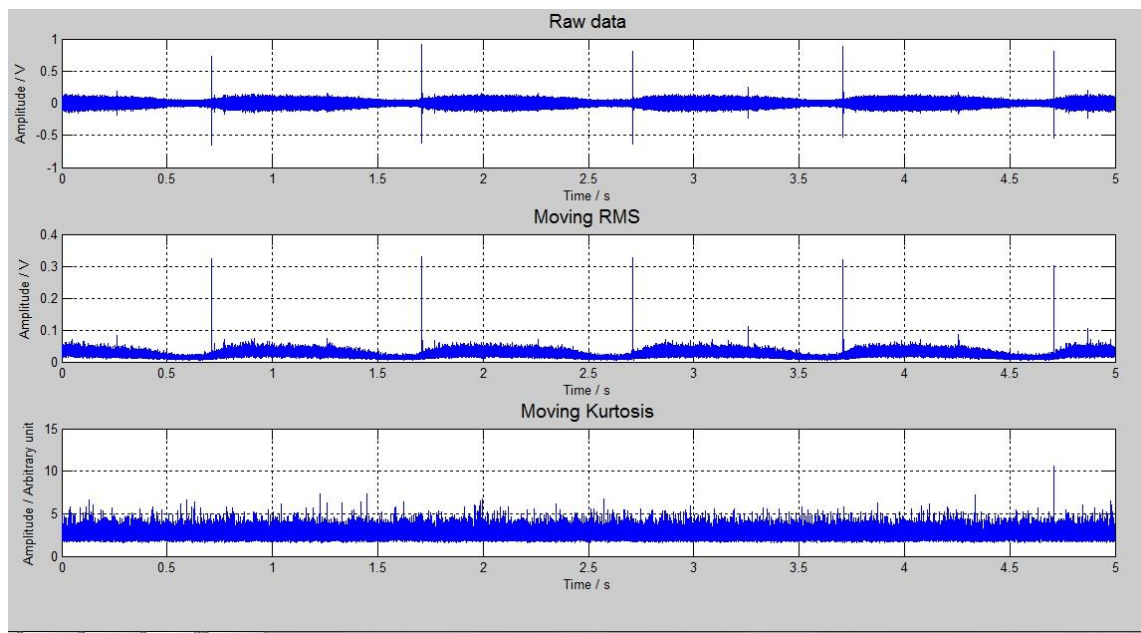


Figure 53 : Raw AE dataset, moving RMS and moving Kurtosis at the middle stage of the fatigue test for the cast manganese steel sample.

Fatigue crack growth testing was carried out on rail steel pre-cracked samples cut off from the web of R260 steel grade rails. As for the cast manganese steel samples, crack growth in the rail steel samples was monitored using a DCPD instrument and the commercial PAC system.

The Paris-Erdogan law for some of the samples tested is shown in Figure 54. The results for the Paris-Erdogan law are consistent with expectations and all samples are in close agreement with each other as expected.

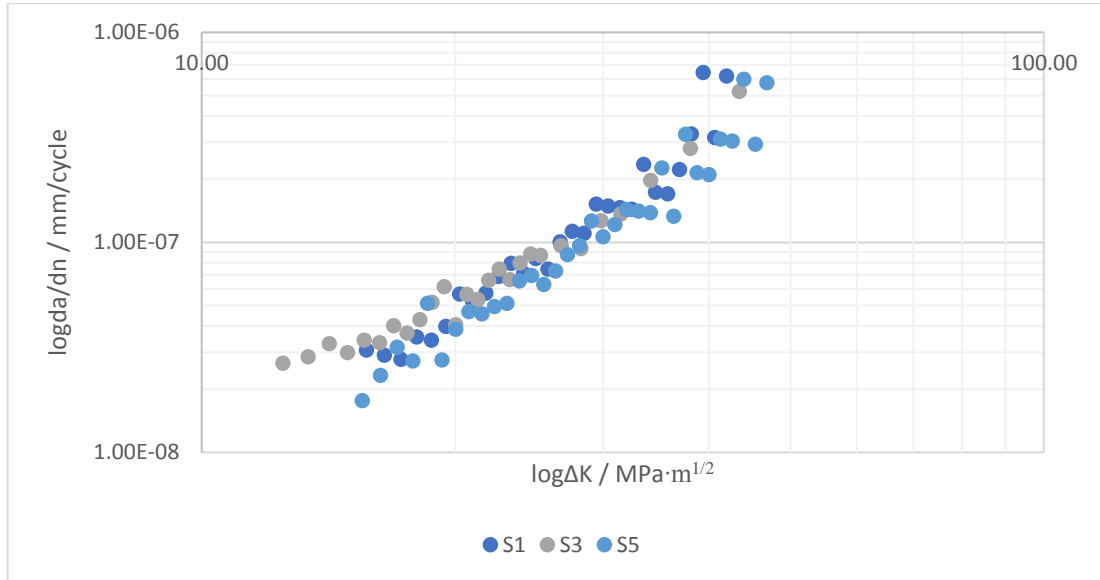


Figure 54: The Paris-Erdogan law plot for some of the R260 grade steel samples tested under three-point fatigue bending testing.

The following plots in Figure 55, Figure 56 & Figure 57 show the crack growth measurements for each of the samples together with the corresponding AE activity with increasing number of loading cycles. In sample S3 the AE plot for sensor 1 is not complete due to loss of coupling during the test. However, sensor 2 continued working nominally until the end of the test.

From the results obtained for all three samples, it can be seen that the trend between the AE and DCPD measurements is similar. Hence, it can be concluded that the AE is capable of successfully monitoring damage propagation in rails and crossings. By using the slope of

cumulative energy it is possible to obtain a more quantitative idea as to how far damage has propagated. This is true since AE activity intensifies as damage propagation reaches closer to critical dimensions and failure becomes imminent.

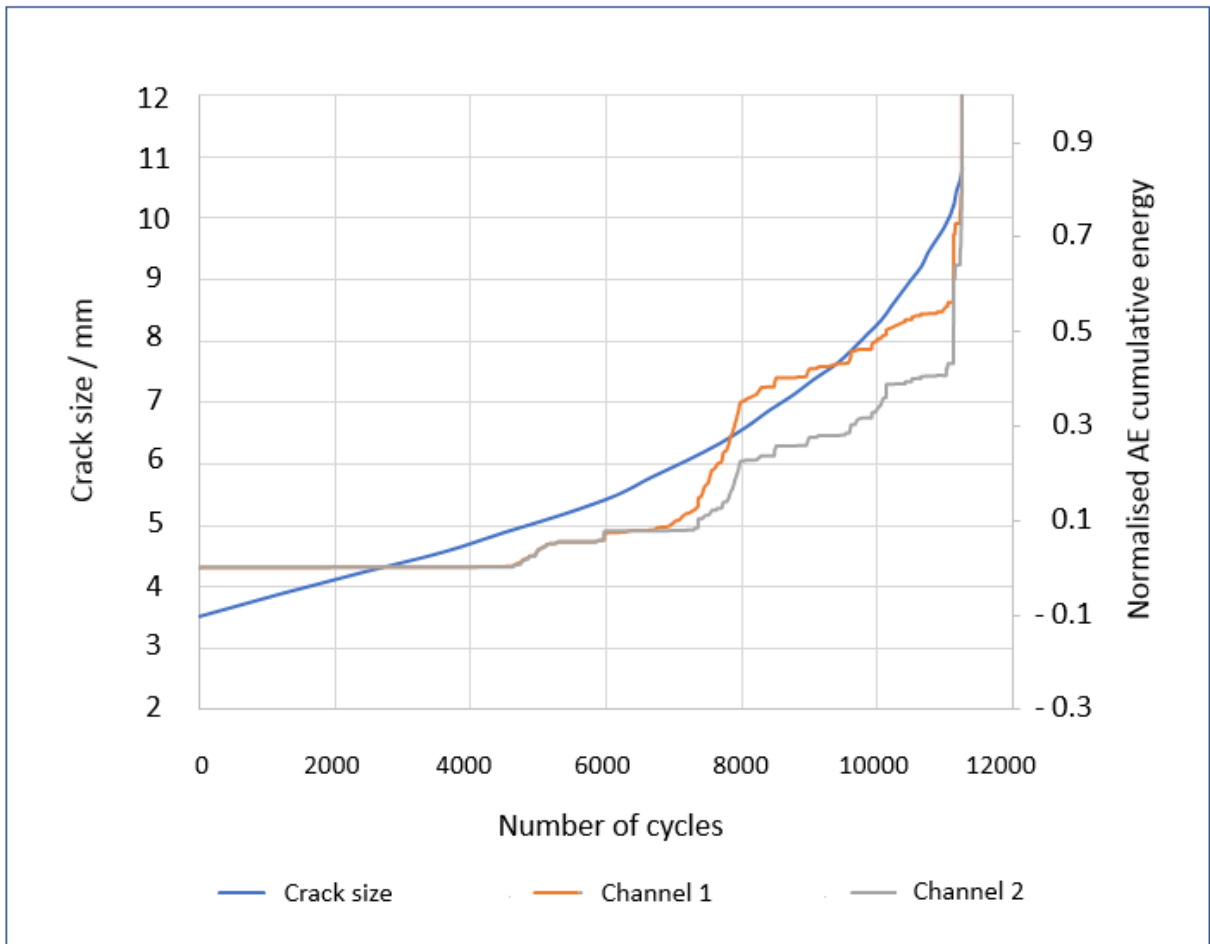


Figure 55: Normalised AE cumulative energy detected with respect to crack growth measured with DCPD and increasing loading cycles plot for R260 rail sample S1 up to final failure

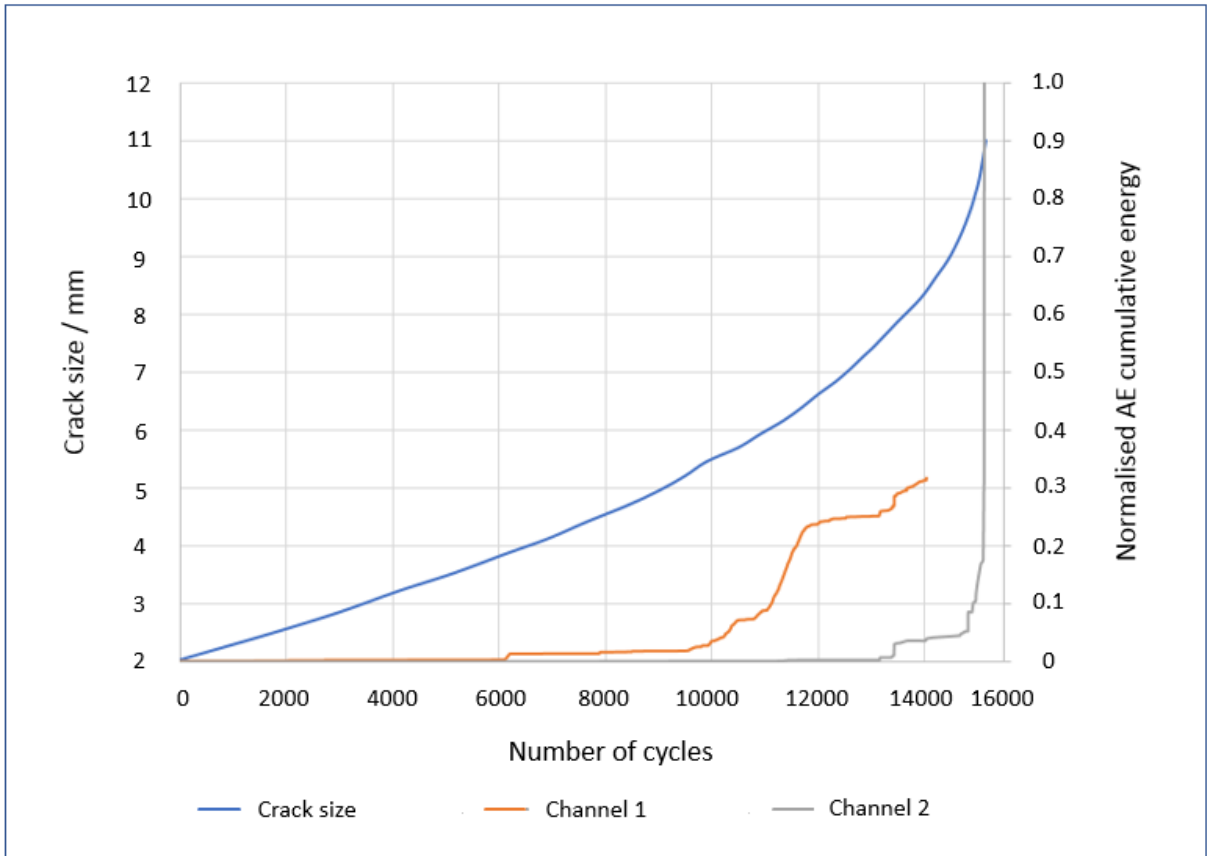


Figure 56: Normalised AE cumulative energy detected with respect to crack growth measured with DCPD and increasing loading cycles plot for R260 rail sample S3 up to final failure. Sensor 1 operation stopped earlier due to loss of coupling and hence the discrepancy in the trend also

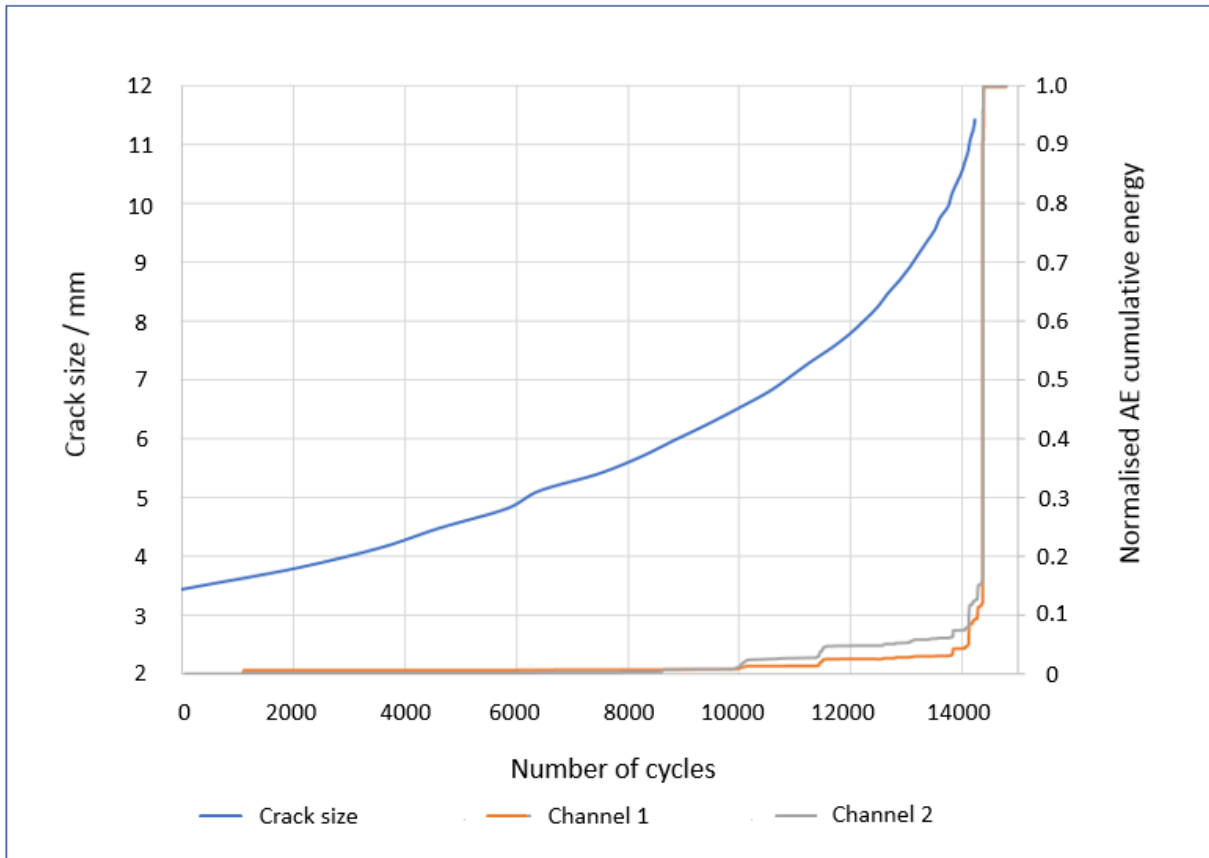


Figure 57: Normalised AE cumulative energy detected with respect to crack growth measured with DCPD and increasing loading cycles plot for R260 rail sample S5 up to final failure.

From the above tests it can be safely concluded that AE sensors can be used to effectively monitor damage propagation in rails and crossings in real-time. However, further work is required in order to reliably set quantitative thresholds of how far damage has propagated based on waveform measurements carried out with the customised system. One way of doing this is by trending the peak-peak values as well as the energy levels of these peaks within each measurement. This would be representative of the cumulative AE energy plots acquired during laboratory tests with the commercial PAC system.

9.3 AMSLER rolling tests

Rolling tests which are representative of wheel and bearing monitoring measurements in the field were carried out using an Amsler roller machine. Two sets of samples were employed during testing. Firstly, a set of cylindrical wheels with no defects on the surface of the tread, and secondly a set of cylindrical wheels where one of the samples contained an artificially induced defect on the surface of the tread which was approximately 1 mm deep. The experimental setup was monitored using an R50a AE sensor. Acquisition was carried out using the customised AE equipment. The sampling rate was set at 500 kSamples/s, acquisition at 6 s and amplification at 46 dB.

The plot in Figure 58 show the raw AE waveform acquired for the set of wheel samples with no defect present. As it can be seen the activity is low although some activity is evident. This is due to a bearing fault present in the Amsler itself which was also detectable using appropriate analysis.

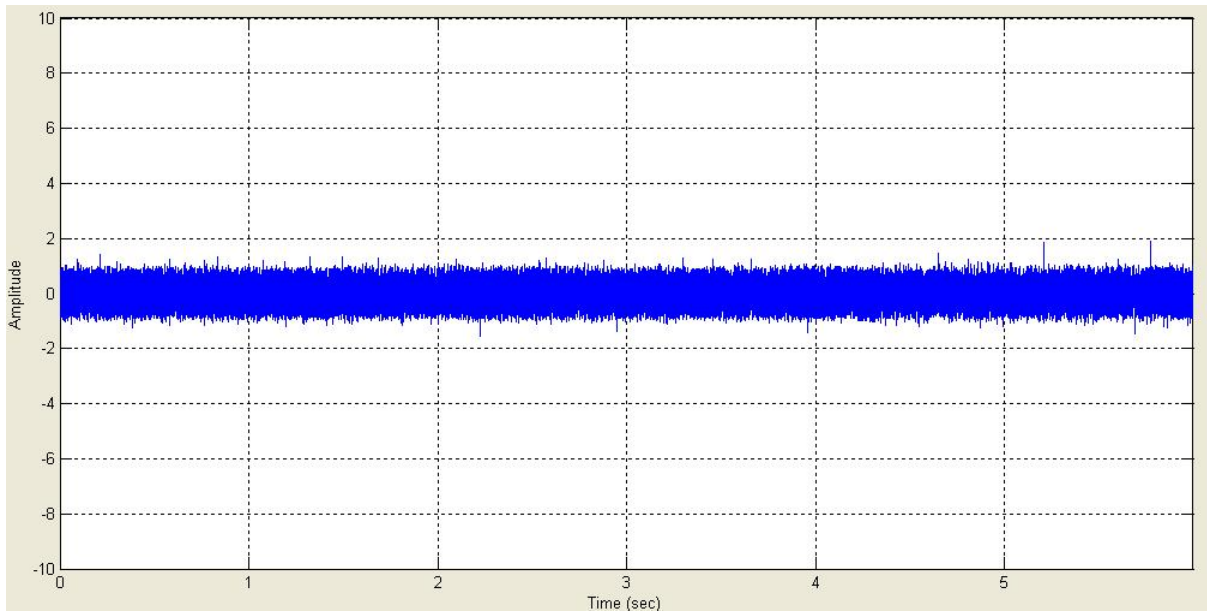


Figure 58: Raw AE waveform for Amsler test on wheel samples with no defects present.

The raw AE waveform above was analysed using various algorithms including moving RMS, spike energy and FFT. The plot in Figure 59 shows the result after the raw data set was processed with the moving RMS algorithm. Some peaks are evident, but they have low amplitude. These are very likely to be associated with the bearing fault present in the Amsler machine itself. However, the distance from the sensor is such that the transmitted energy is limited, albeit still detectable as low intensity peaks.

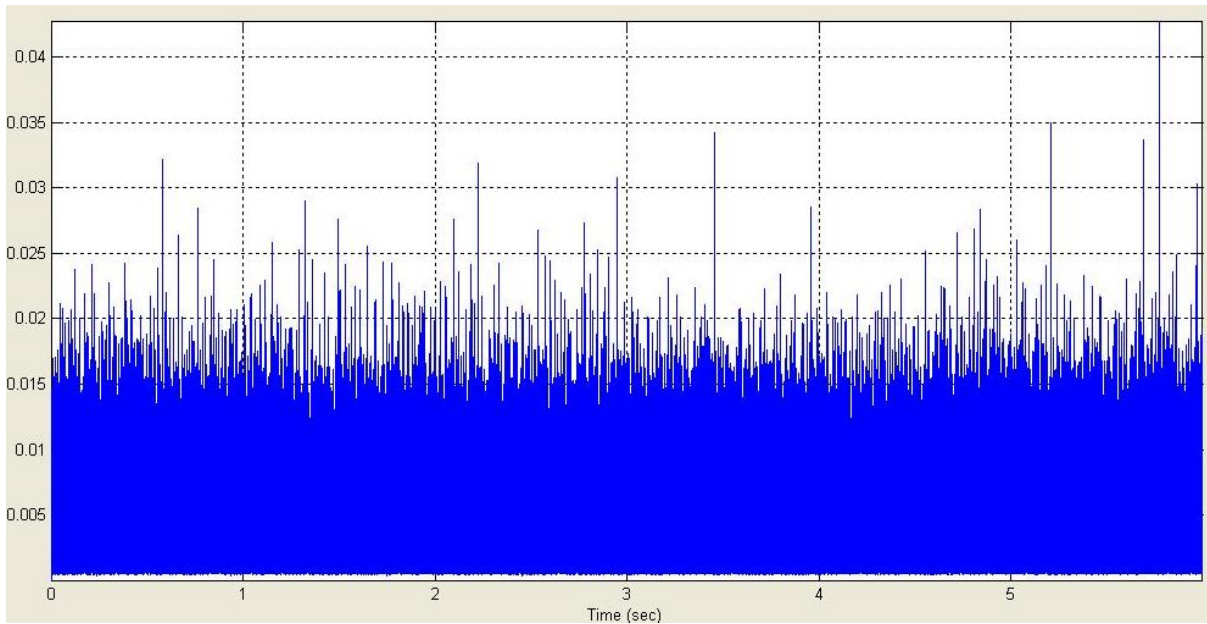


Figure 59: Moving RMS plot of the AE signal. The low intensity peaks visible are largely related to the background noise arising from a known faulty Amsler bearing and not from the sample wheels.

The power spectral analysis of the raw AE signal in Figure 60 has revealed some peaks at various frequencies including one higher intensity peak at approximately 55 kHz. These again are low amplitude peaks which are associated with the background noise arising from the Amsler rotating pieces, particularly the faulty bearing.

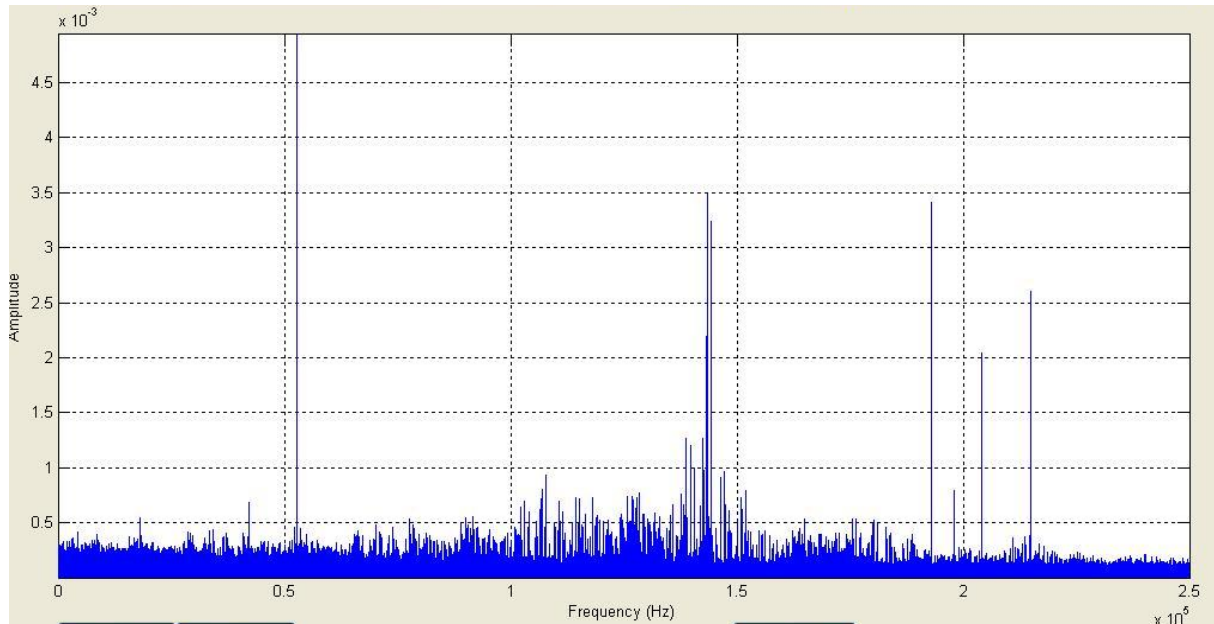


Figure 60: Power spectrum of the AE waveform captured for the wheel samples with no defects present. The peaks evident are associated with the background noise arising from the Amsler machine itself, particularly the known faulty bearing

Although in the raw waveform, the moving RMS and power spectral plots the faulty Amsler bearing is not clearly evident, this becomes much more obvious when the spike energy is used. As it can be seen in the spike energy plot in Figure 61 strong peaks associated with the faulty bearing frequency are evident. These peaks again have low amplitude, but they appear very clear in the signal, confirming the presence of a fault together with the rotational frequency that it occurs.

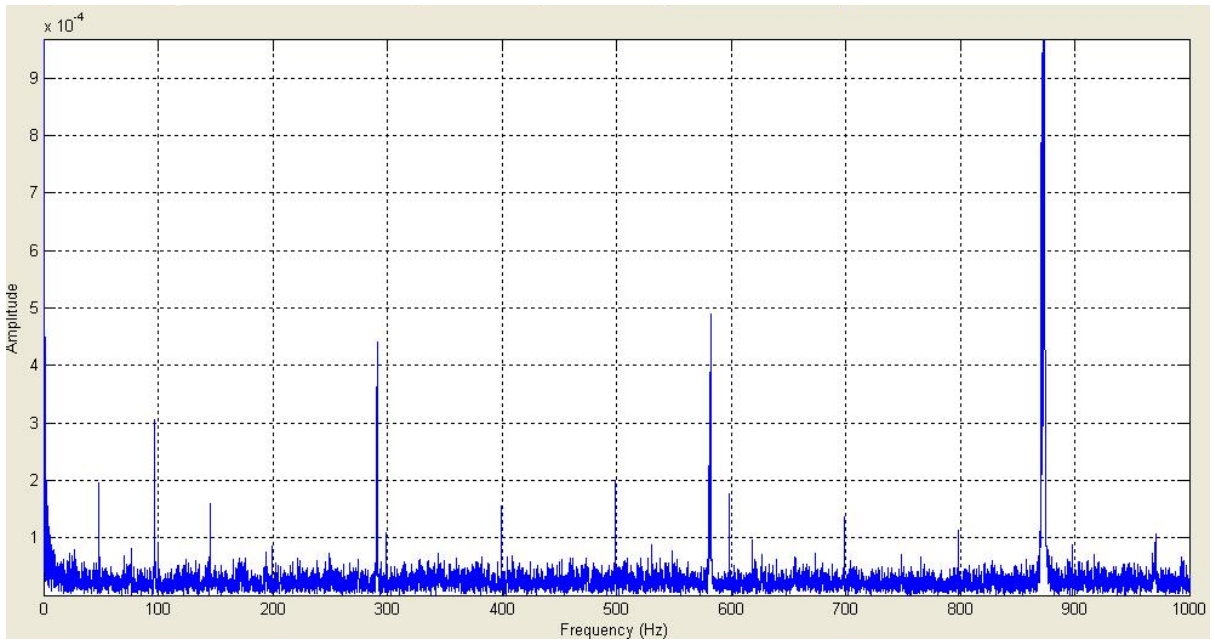


Figure 61: Spike energy plot showing some low intensity peaks (max amplitude does not exceed 10^{-3} V^2) which are associated with the bearing fault only in the Amsler machine itself and not the wheel samples which are in good condition.

If the load is removed, then the stress on the Amsler bearing is reduced even though the test wheels are still rotating against each other. This leads to peaks associated with the bearing fault disappearing as seen from the plots in Figure 62 to Figure 65.

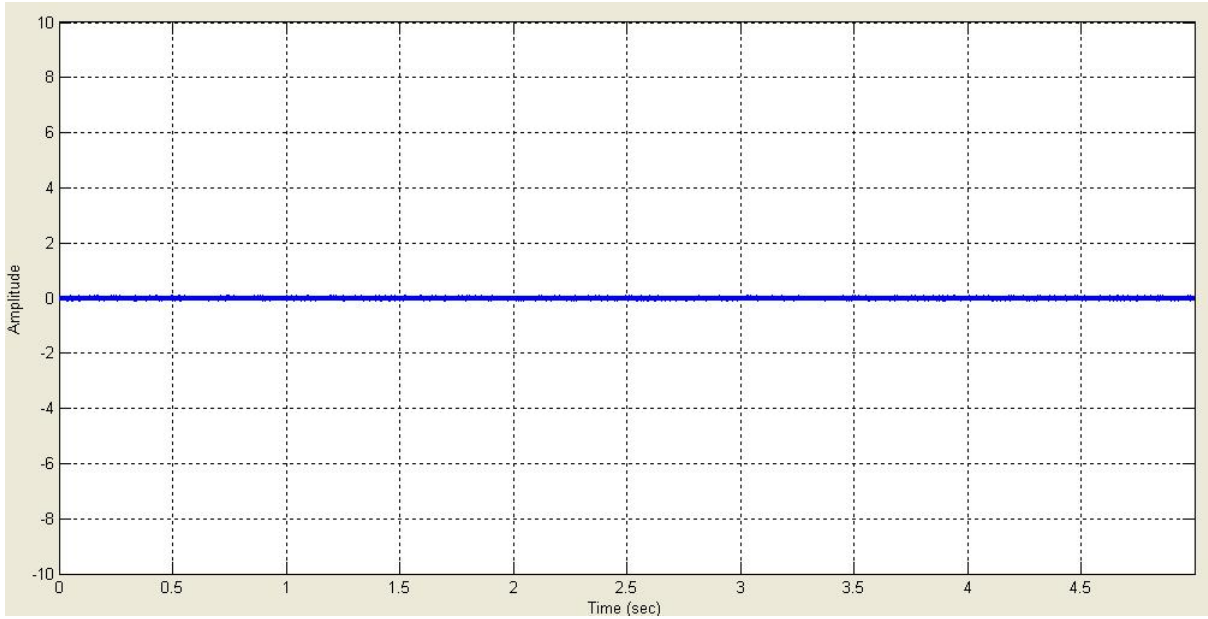


Figure 62: Raw AE waveform for the healthy wheel samples after load has been removed.

This leads to much lower background noise since the Amsler bearing does not get as stressed as when under load.

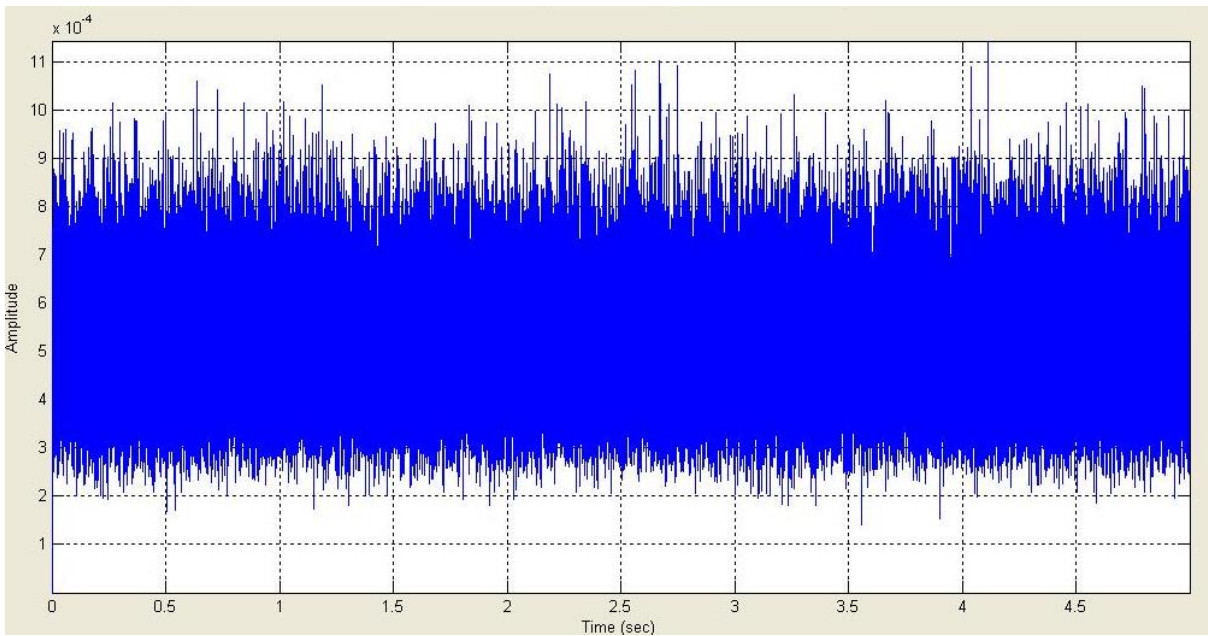


Figure 63: The moving RMS plot with no peaks related to the bearing being evident.

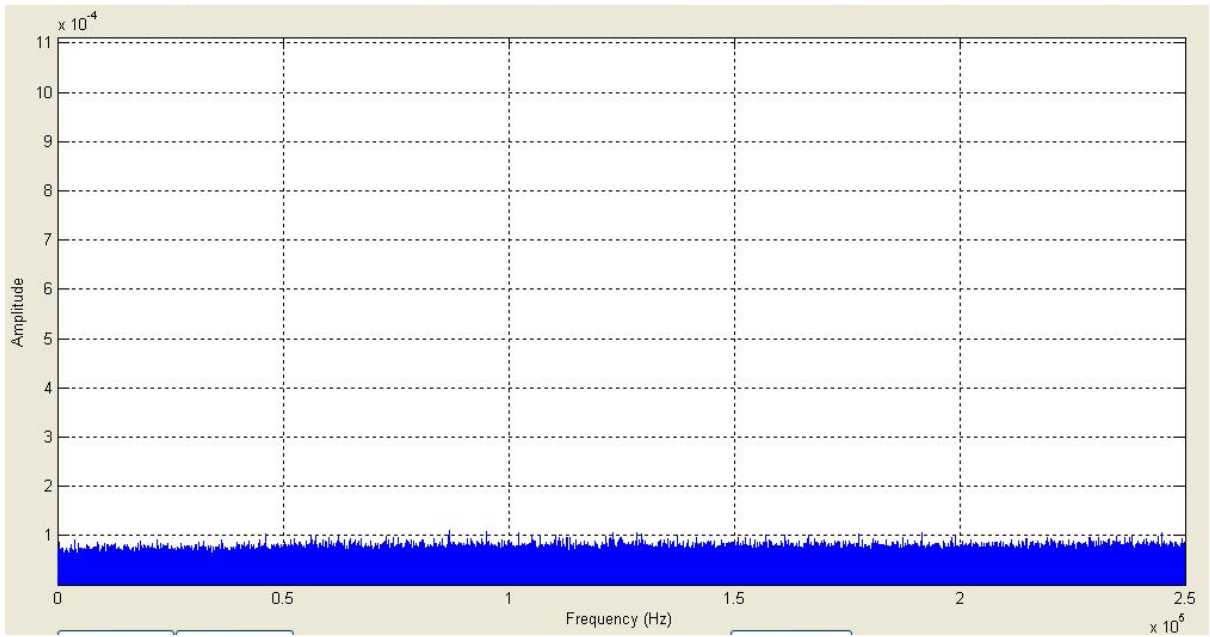


Figure 64: Plot of the power spectrum. It is evident that all peaks have disappeared, and the signal contains very little noise.

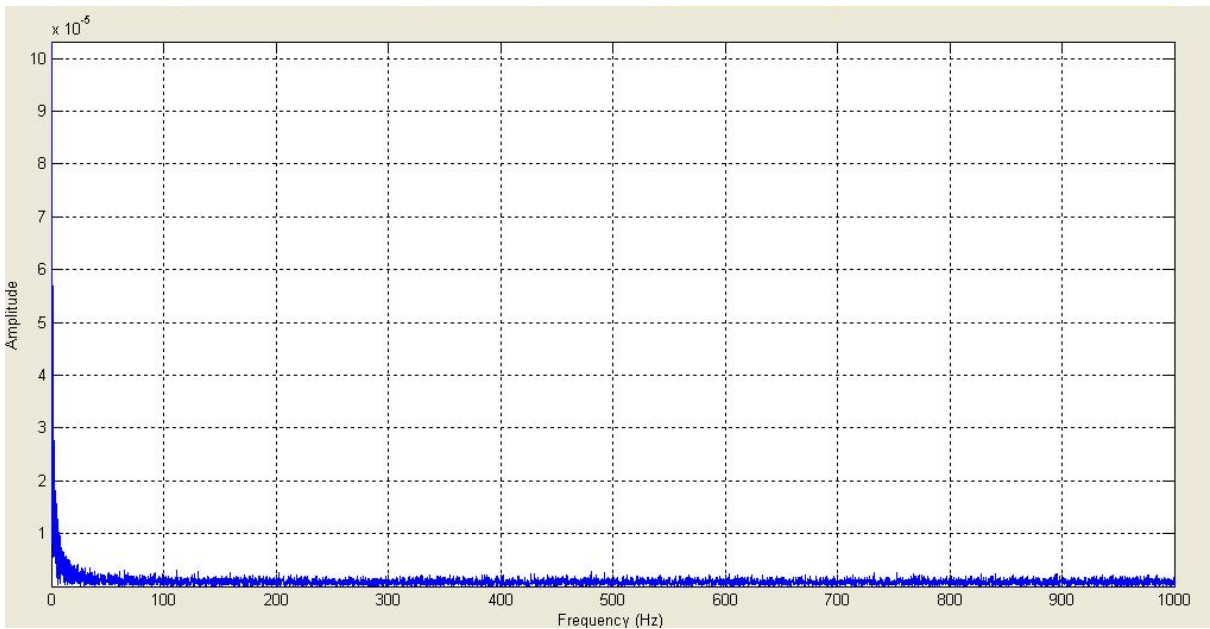


Figure 65: No peaks are evident in the spike energy plot either.

Subsequent tests were carried out on a set of wheels where one contained a 1 mm deep wear-type defect. Two different loads were applied to the testing configuration. In the first scenario an 8 kg load was applied whilst in the second scenario the load was increased to 150 kg.

The plot in Figure 66 shows the raw AE signal for the defective wheel setup with an 8 kg load applied. Some low intensity spikes are evident just above the background noise, which are associated with the presence of the tread wear defect present.

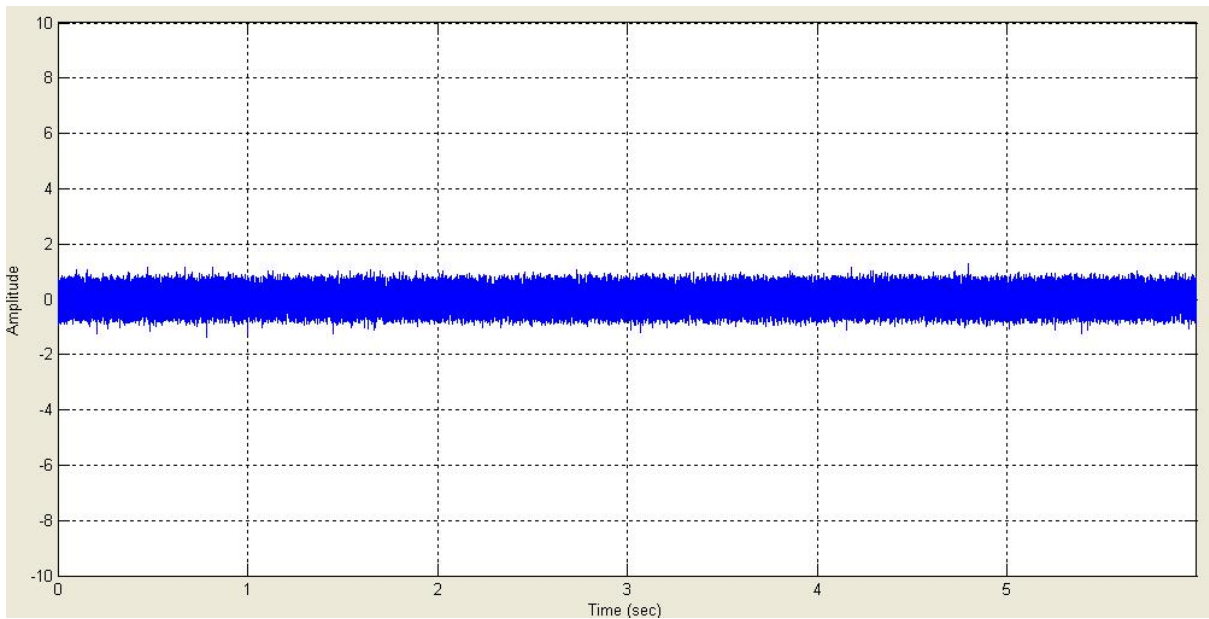


Figure 66: Raw AE waveform for the defective wheels after an 8 kg load has been applied.

Some low intensity peaks are evident just above the background noise.

The plot in Figure 67 shows the moving RMS result. Some low intensity peaks are evident, but they are higher than those seen in the moving RMS plot of the healthy test wheels.

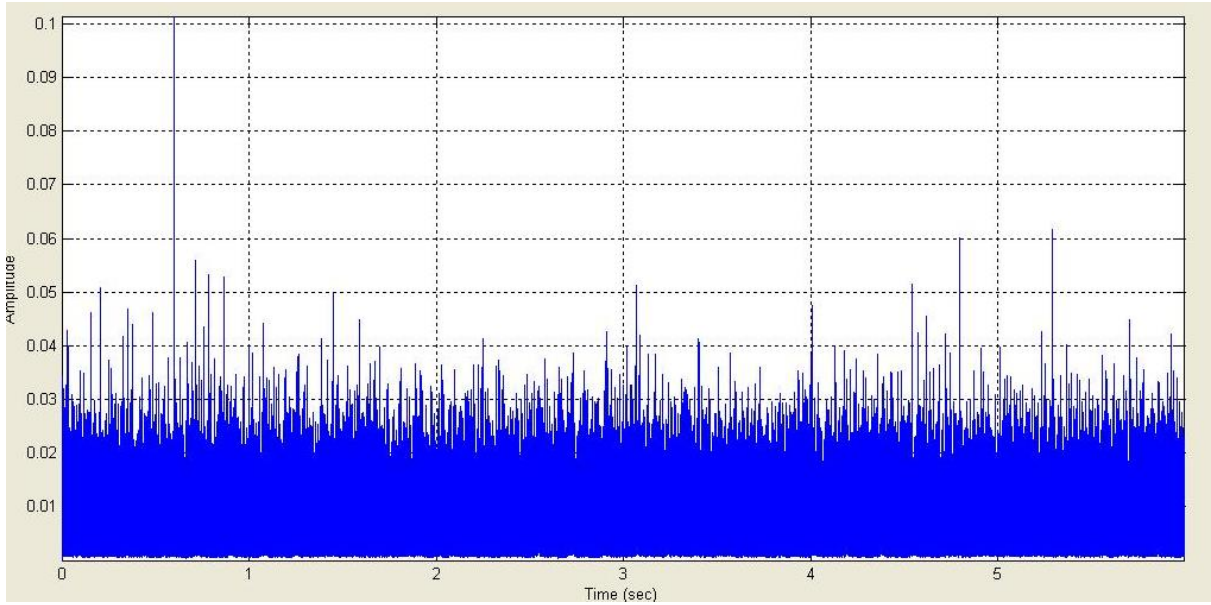


Figure 67: Moving RMS plot with several peaks present indicating the presence of a fault.

The power spectral analysis of the AE waveform for the faulty wheel setup under 8 kg loading has a higher frequency content associated with the presence of both the wheel tread defect as well as the faulty Amsler bearing defect, Figure 68.

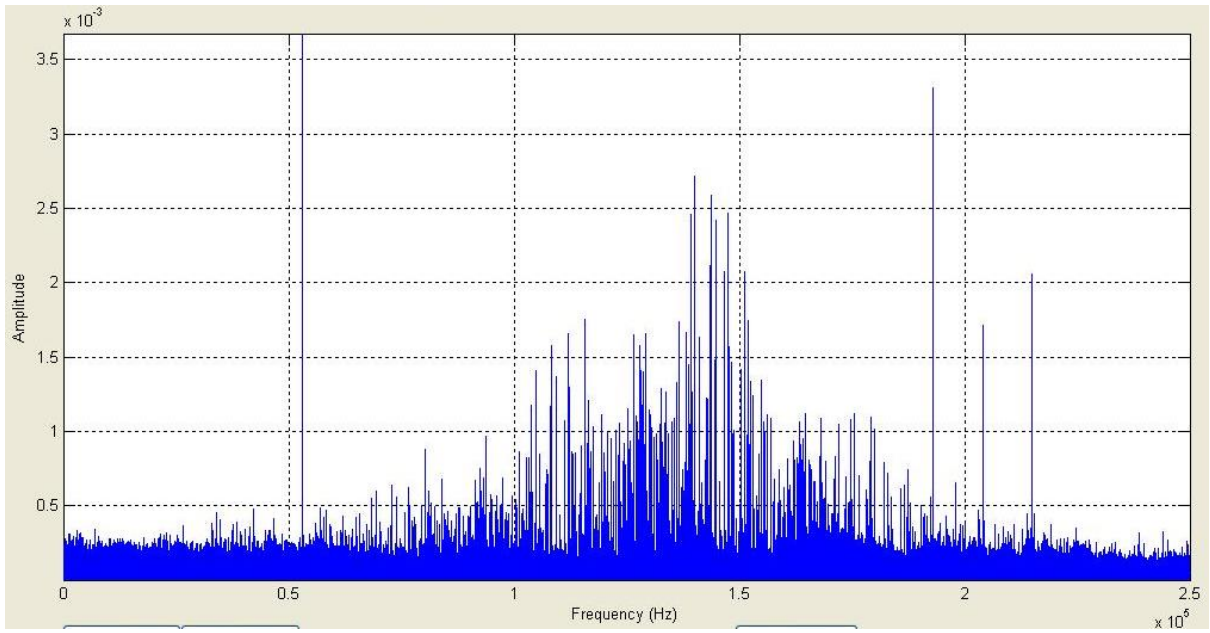


Figure 68: Power spectrum showing a much richer frequency content when the wheel defect is present in comparison with the healthy wheel setup.

The plot in Figure 69 shows the spike energy of the signal. Again, additional peaks associated with the defective wheel are present at additional rotational frequencies together with the peaks associated with the known Amsler bearing fault.

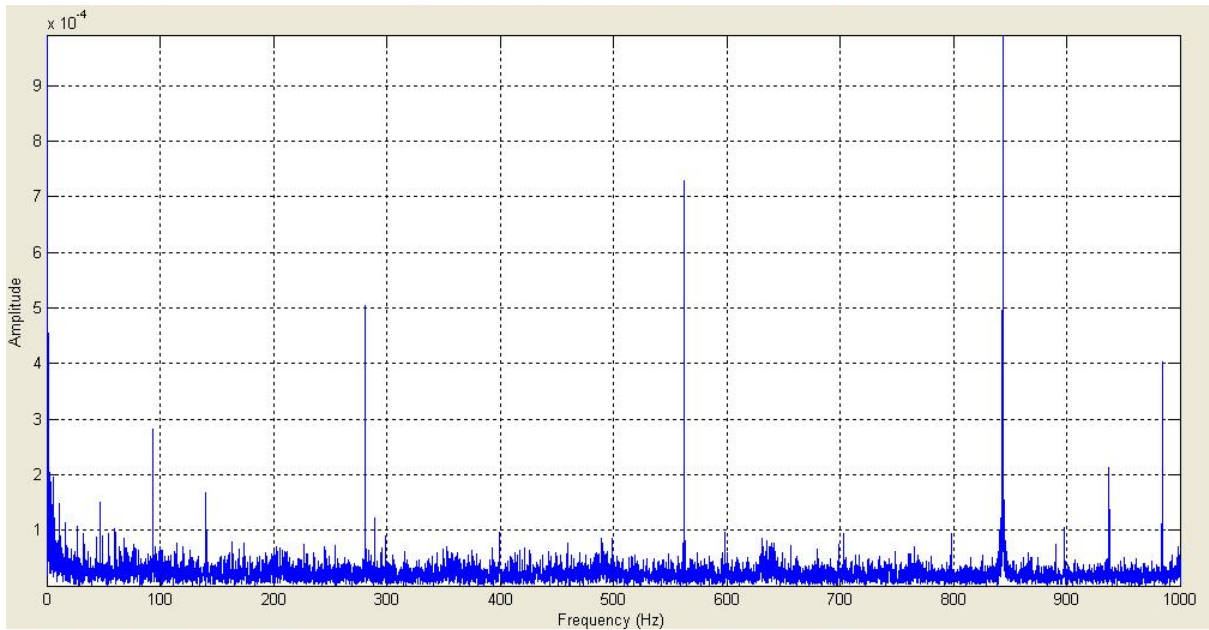


Figure 69: Spike energy plot indicating peaks at additional frequencies. However, the peaks for the bearing fault remain dominant.

The following plots in Figure 70 to Figure 73 show the raw AE wave form, moving RMS, power spectrum and spike energy for a load of 150 kg applied on the defective wheel setup. In this instance the peaks from the defective wheels become more dominant than the peaks arising from the faulty bearing.

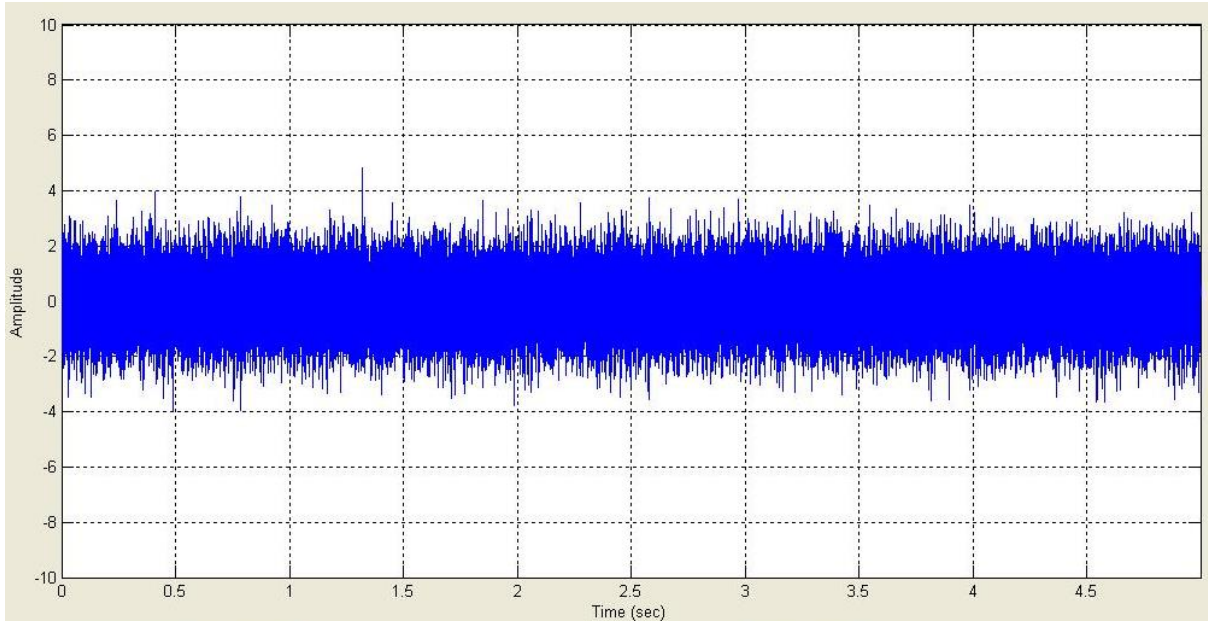


Figure 70: Raw AE waveform with multiple peaks evident above the background noise.

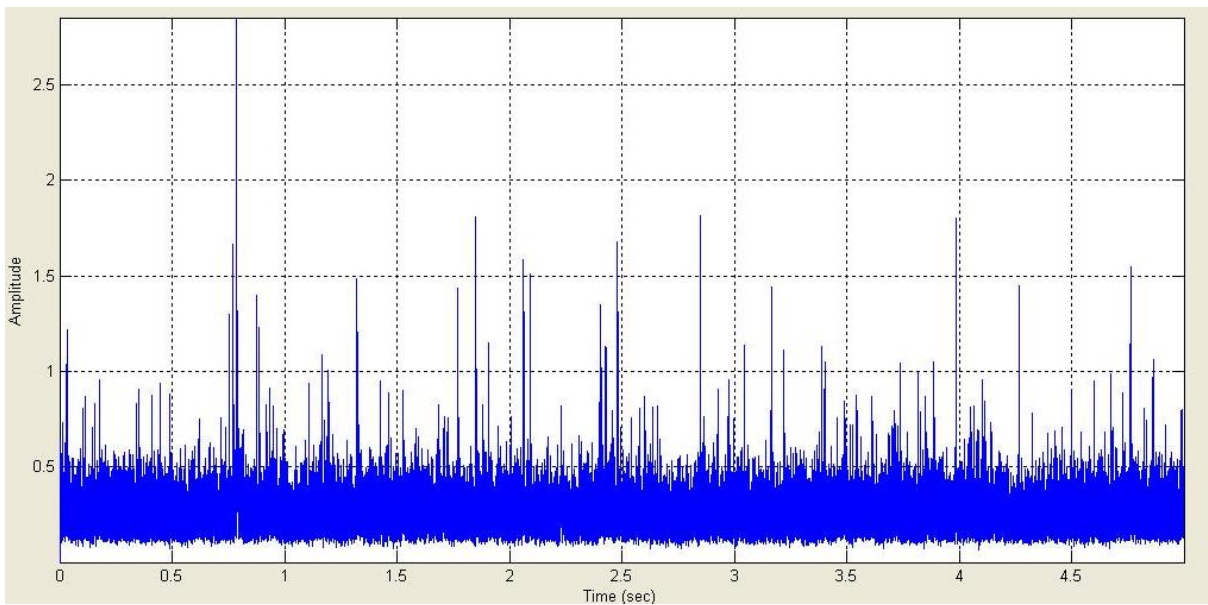


Figure 71: Moving RMS plot. Notice the much higher amplitude of the peaks present when higher load is applied on the experimental setup.

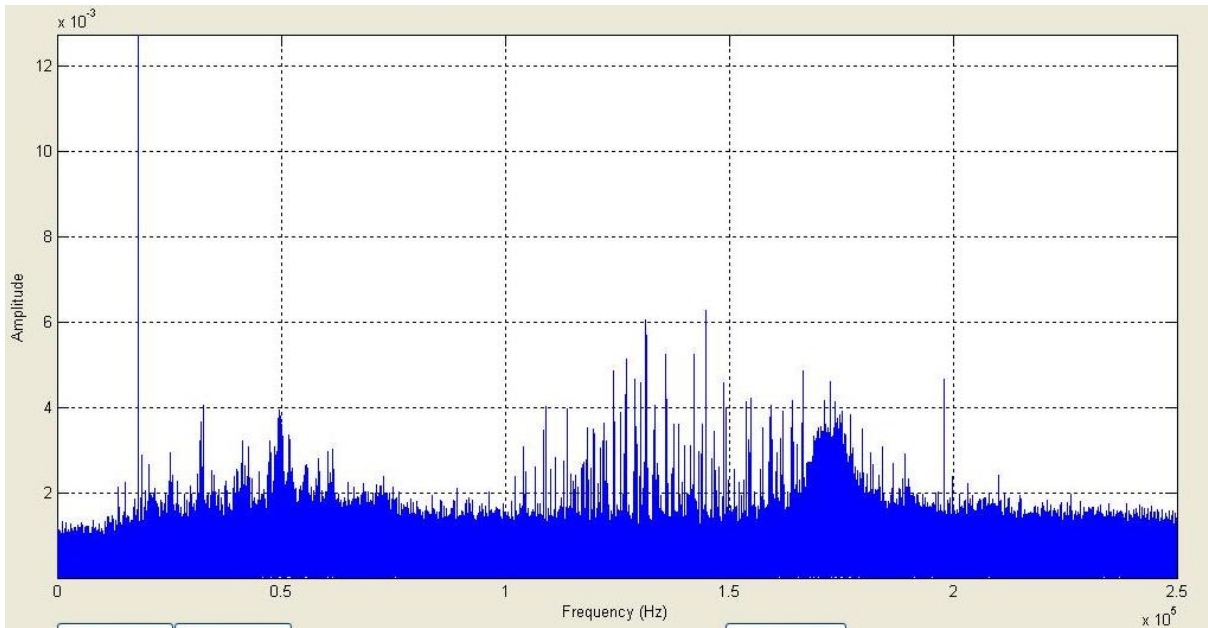


Figure 72: Power spectrum analysis of the AE waveform indicating an increase in the frequency content and some higher intensity peaks at certain frequencies.

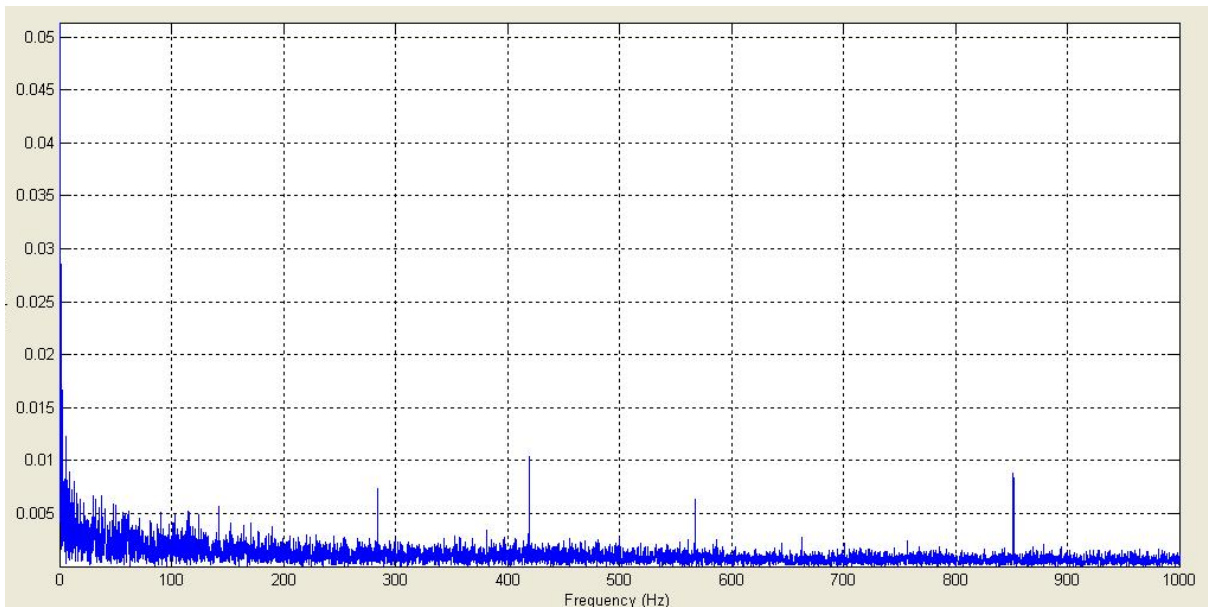


Figure 73: Spike energy plot with noticeable peaks at lower rotational frequencies associated with the rotation of the wheels. The peaks associated with the bearing fault are also still present but not as dominant as before in comparison with the wheel defect.

9.4 Long Marston Field Trials under simulated operational conditions

Field trials were carried out at Long Marston using the customised AE and vibration system both onboard and wayside. An industrial accelerometer and an AE sensor were mounted on the axle box in order to monitor the bearing condition of the test rolling stock.

The plot in Figure 74 shows the raw vibration signal taken onboard for a healthy bearing. Some minor peaks seen are associated with the impacts of the wheels as the train passes from one rail to the other over the joints.

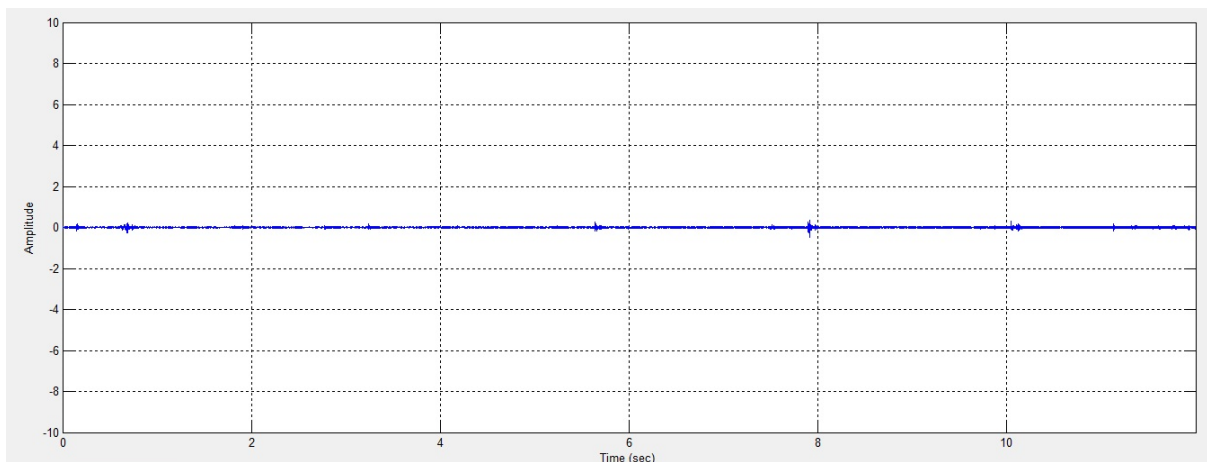


Figure 74: Onboard raw vibration signal for a healthy axle bearing.

The plot in Figure 75 shows the moving RMS. The peaks observed are related to the impacts as the train moves over the jointed rail track. Hence, these peaks are not associated with any bearing faults. Nonetheless, the fact that joints are detectable with vibration analysis suggests that certain infrastructure defects, such as wet beds and worn or broken rails, would also be detectable using an accelerometer attached on the axle box. Hence, the technique can be used for both monitoring axle bearings as well as the condition of infrastructure for more serious defects which may be present.

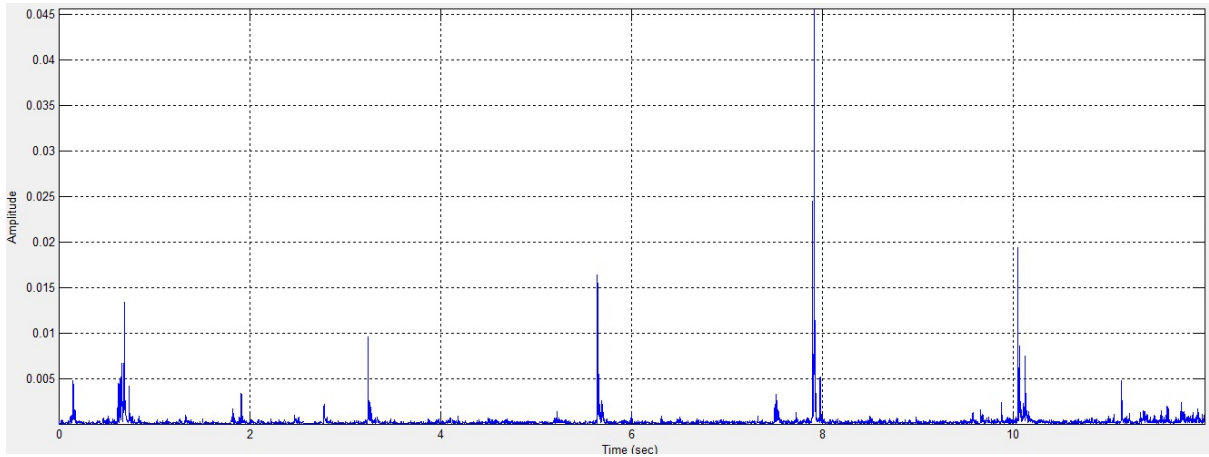


Figure 75: Moving RMS of the onboard vibration signal. The peaks are associated with joints on the track as the test train moves over them.

The plot in Figure 76 is the power spectrum of the vibration signal. Some of the peaks evident are clearly associated with the vibration arising from the movement over the joints and not an axle bearing fault.

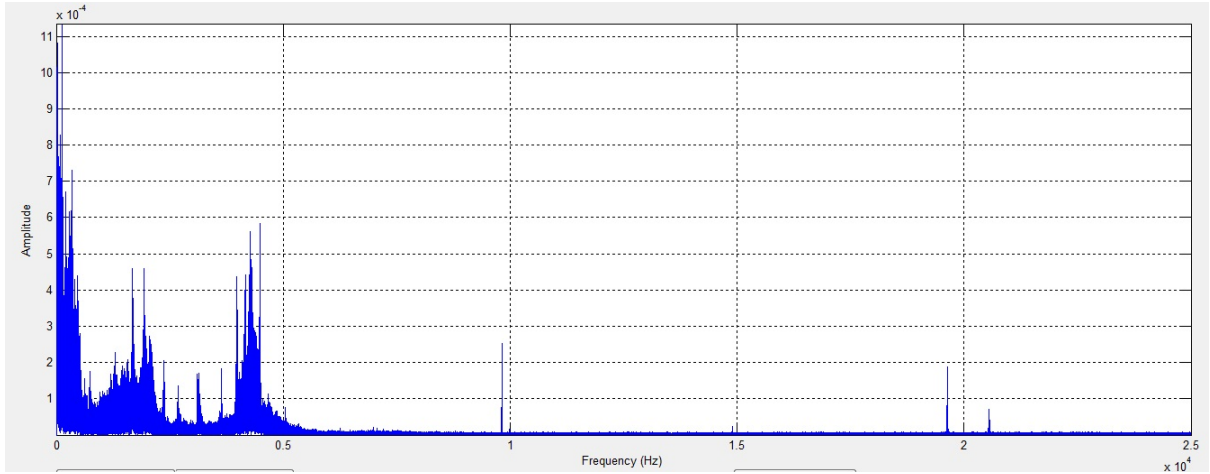


Figure 76: Power spectrum of the vibration signal. Some peaks evident are associated with the vibration arising from the movement over the joints.

The fact that the peaks are associated with the joints alone and that there is no bearing defect present is confirmed by the spike energy plot in Figure 77. It is evident that there are no peaks present at any rotational frequency and hence, no bearing defect.

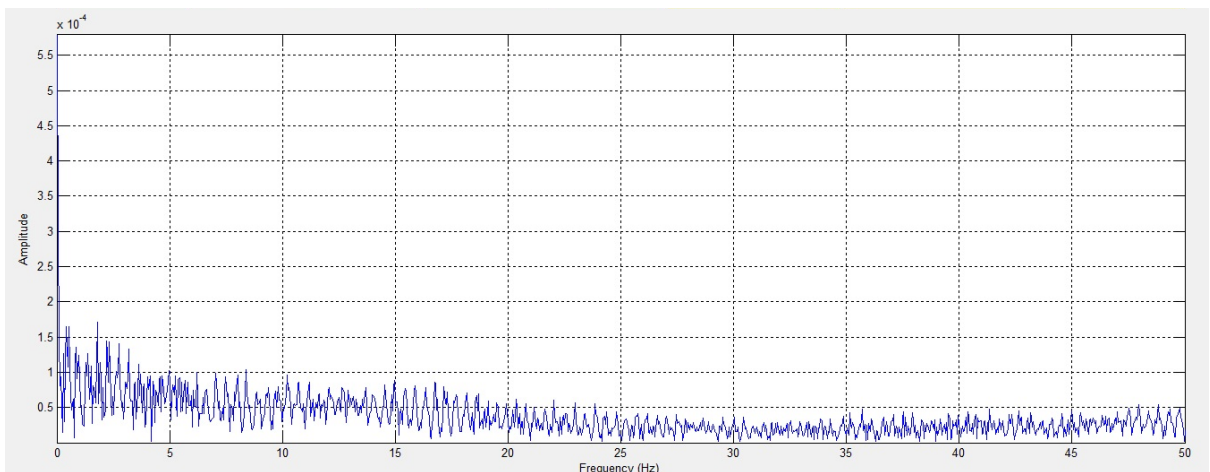


Figure 77: Spike energy plot with no peaks evident, suggesting that the monitored bearing is healthy.

The plot in Figure 78 shows the raw vibration signal taken onboard for a faulty bearing. The fault simulated in this case is contamination of the bearing lubricant causing poor rotational performance. Qualitatively the raw vibration signal for the faulty bearing is very similar to the healthy one, hence not much information can be extrapolated from this plot.

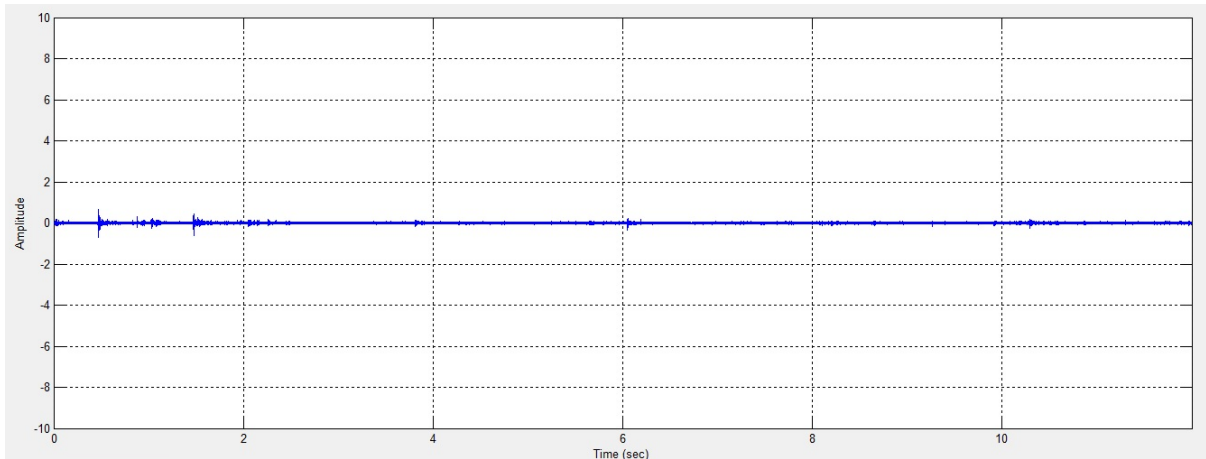


Figure 78: Raw vibration signal plot for faulty bearing. No much difference in comparison with the vibration signal for the healthy bearing is evident.

Similarly, the moving RMS plot shown in Figure 79 gives a similar response to the healthy axle bearing, being dominated by the impacts at the joints of the track as the train moves over them.

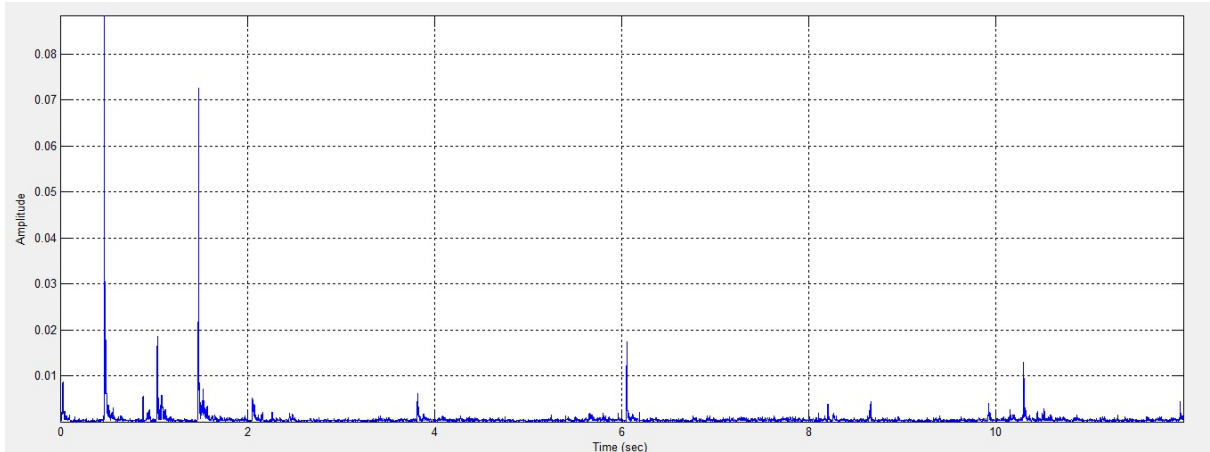


Figure 79: Moving RMS of the vibration signal for the faulty bearing. Again, the plot resembles that of the healthy bearing, with peaks associated with the transition over the track joints.

The power spectrum plot however, shown in Figure 80 is considerably different. This is due to the fact the bearing fault dominates the frequency content of the waveform giving rise to dominant peaks at certain frequencies that are associated with the bearing fault.

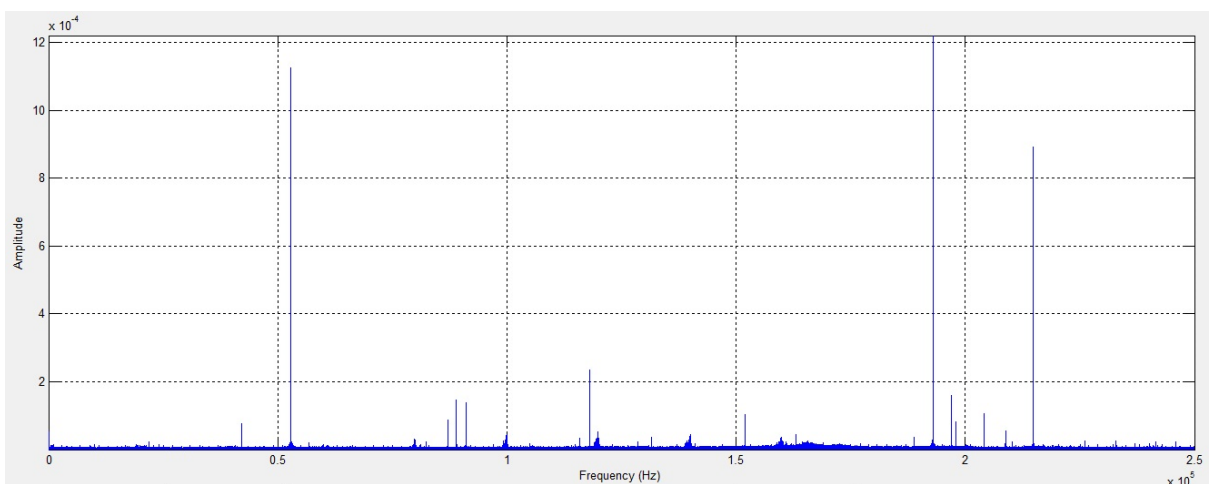


Figure 80: Power spectrum of the vibration signal for the faulty bearing showing considerable peaks at particular frequencies which are associated with the bearing fault rather than the impacts arising during the transition over the jointed parts of the track

The plot in Figure 81 shows the spike energy result. Again, there is clear indication of peaks at particular rotational frequencies which are associated with the faulty bearing and were absent previously in the healthy condition signal.

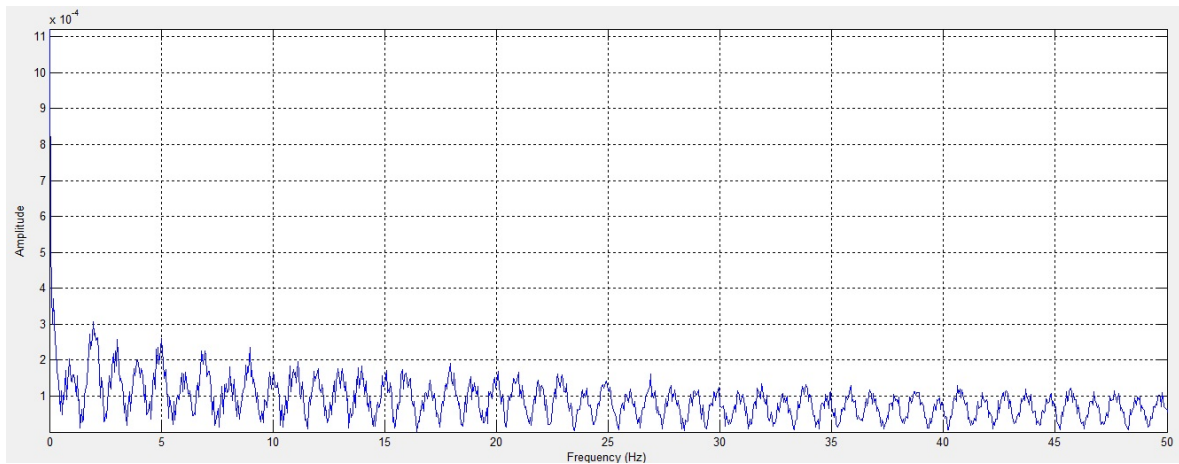


Figure 81: Spike energy plot for the vibration signal associated with the faulty bearing.

The plots in Figure 82 to Figure 85 show the raw AE signal and corresponding moving RMS, power spectrum and spike energy for the measurements taken onboard for the healthy bearing.

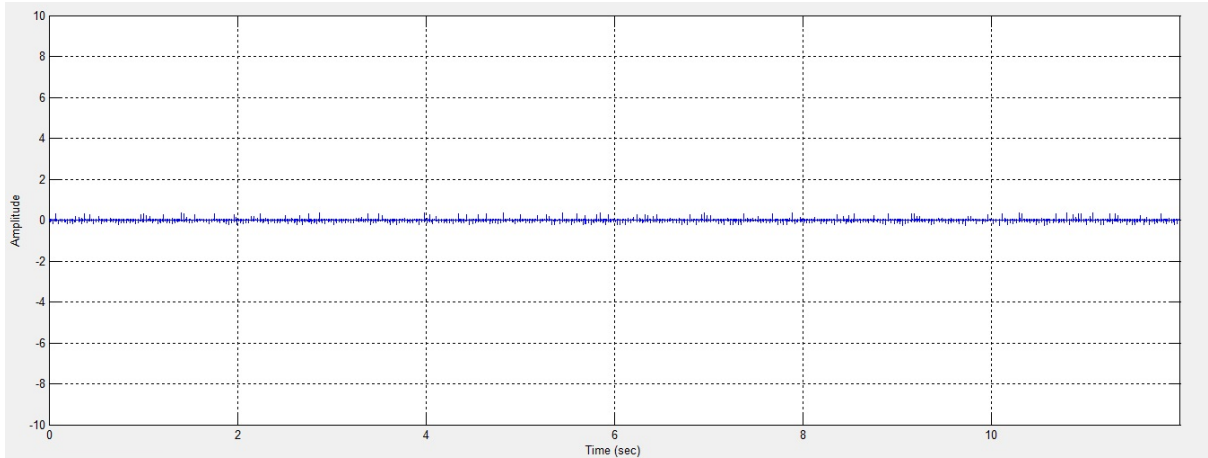


Figure 82: Raw AE waveform taken onboard for the healthy bearing. Notice the low level noise and almost complete absence of peaks associated with the jointed track.

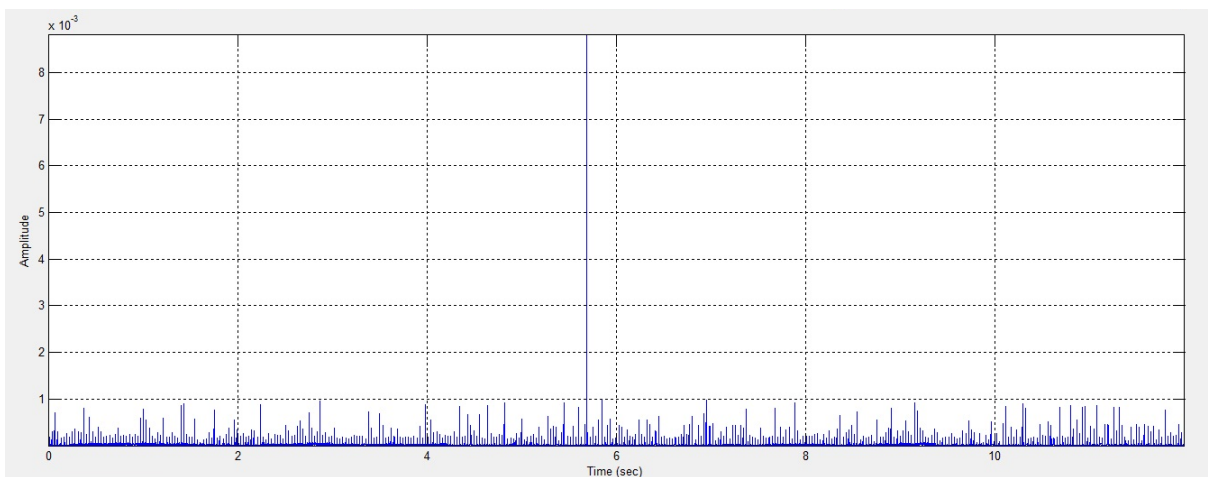


Figure 83: Moving RMS indicating very low amplitude peaks indicating that there is no fault present.

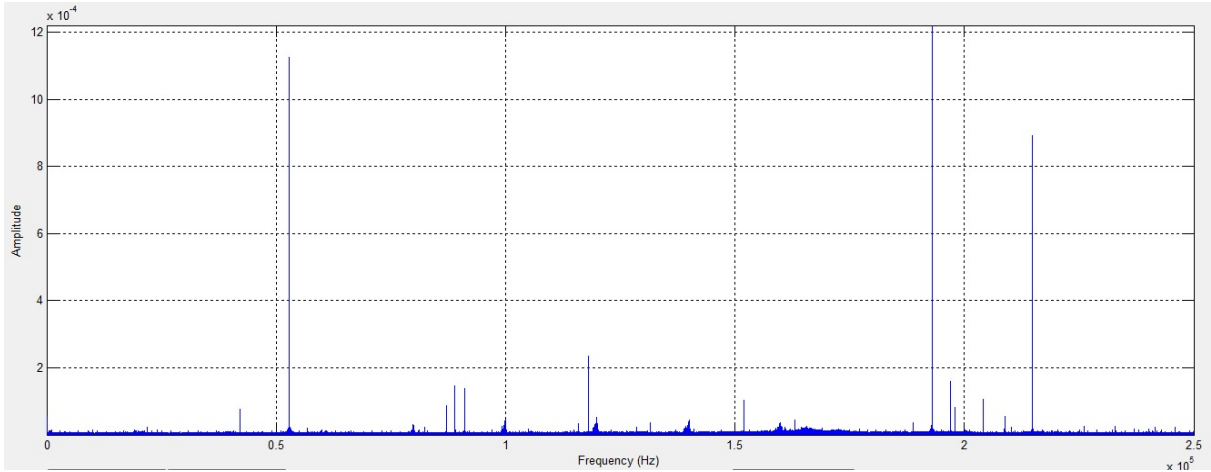


Figure 84: Power spectrum of the AE waveform. Notice the almost complete absence of frequency information in the power spectrum with the exception of a few low amplitude peaks at certain frequencies associated with background noise arising from the movement of the train.

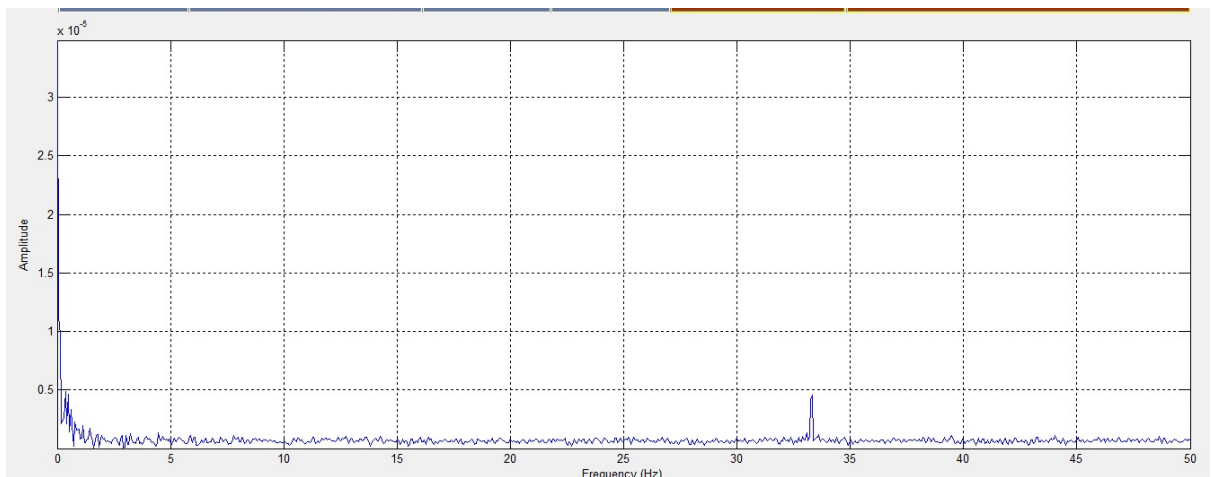


Figure 85: Spike energy plot of the AE signal. Notice the absence of any peaks with the exception of a very low amplitude peak at approximately 33.5 Hz. It is unknown what has given rise to this particular peak, but it is likely related to a background source, possibly the power axles of the locomotive pulling the test freight wagon.

The following plots in Figure 86 to Figure 88 show the AE measurement taken for the faulty bearing with contaminated lubricant. The characteristics of the signal are evidently different to those for the healthy condition, which makes apparent the presence of the fault.

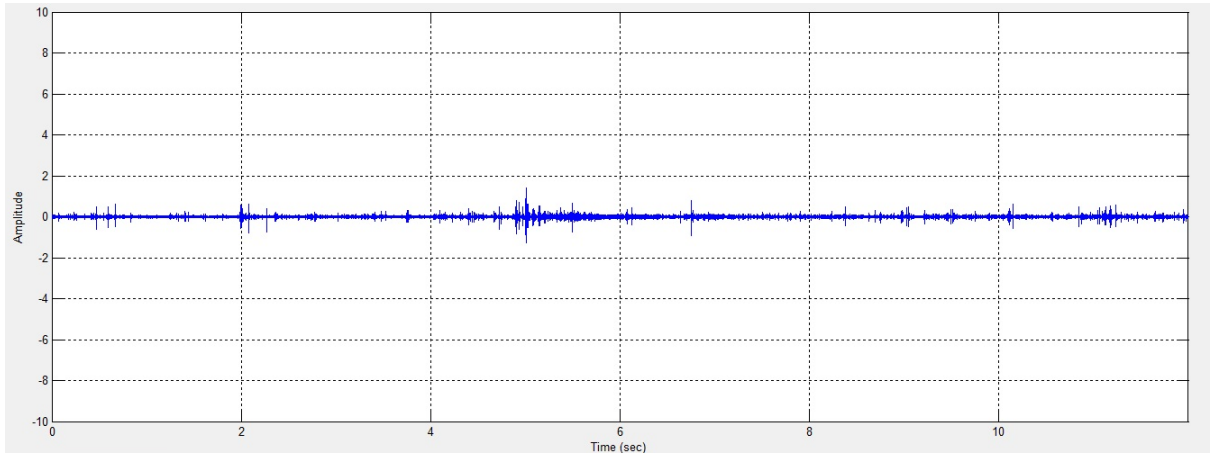


Figure 86: Raw AE waveform with multiple peaks present above the background noise level.

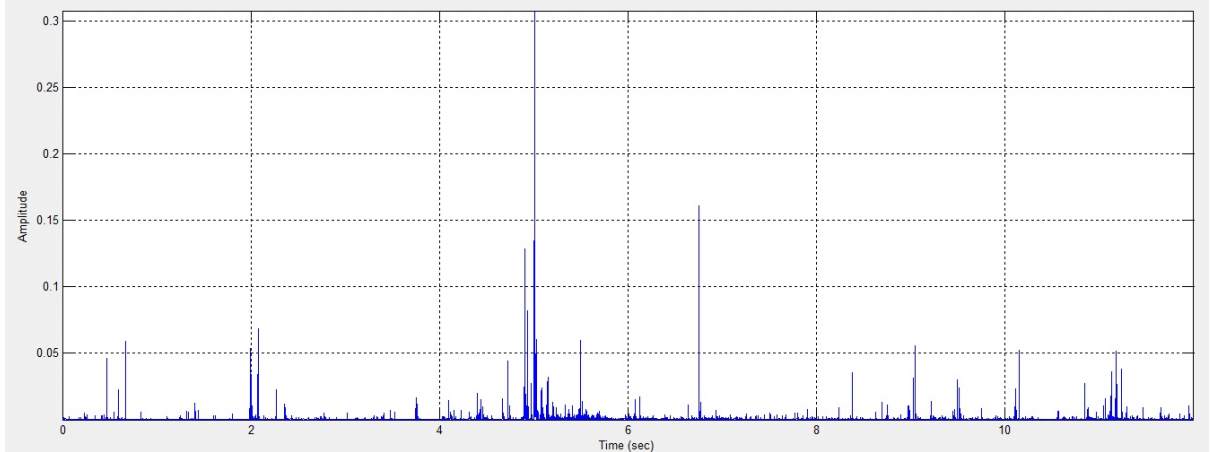


Figure 87: Moving RMS plot with several peaks present. These peaks are clearly associated with the bearing defect present.

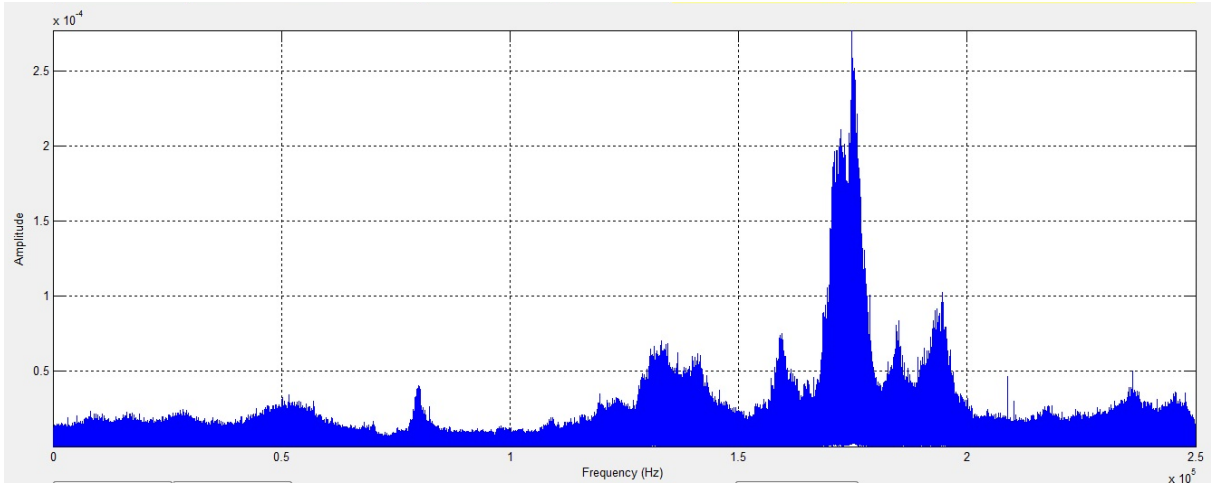


Figure 88: Power spectrum of the AE waveform for the faulty bearing. Notice the rich frequency content of the signal particularly between 130 kHz to 200 kHz in comparison with the power spectrum for the healthy condition.

The spike energy plot does not yield any clear indications, which is not however unexpected. Depending on the level of stress suffered by the bearing spike energy may or may not detect a defect present clearly. However, when multiple measurements are taken the power spectrum should clearly reveal the rotation frequency at which the fault occurs, highlighting its exact nature and hence the exact part of the bearing (race, roller, etc.) which has been damaged.

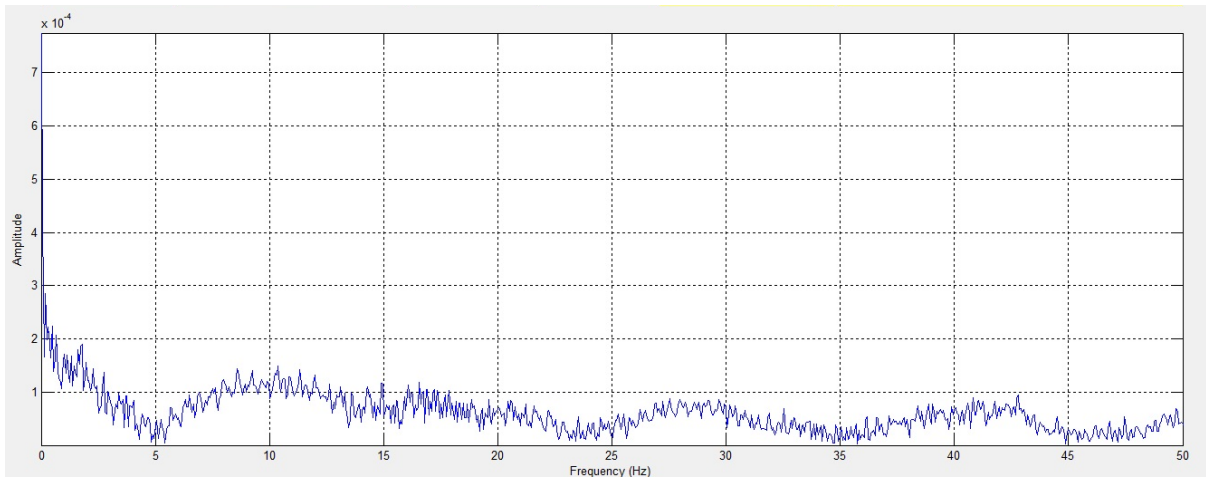


Figure 89: Spike energy plot not showing any useful information in this particular instance.

The following set of plots shows the vibration signal wayside measurement for the test train consisting of the locomotive and two freight wagons. One of the freight wagons has defective bearings from both sides of the track so there is no healthy side in this particular measurement.

High intensity peaks well above the background noise are evident. These are associated with the movement of the train over the joints as well as the presence of the axle bearing defects, which cause additional vibration to be induced from the passage of the train to the track. This has been detected by the accelerometer as shown from the plot in Figure 90. The associated moving RMS plot also clearly indicates high energy peaks as seen in Figure 91.

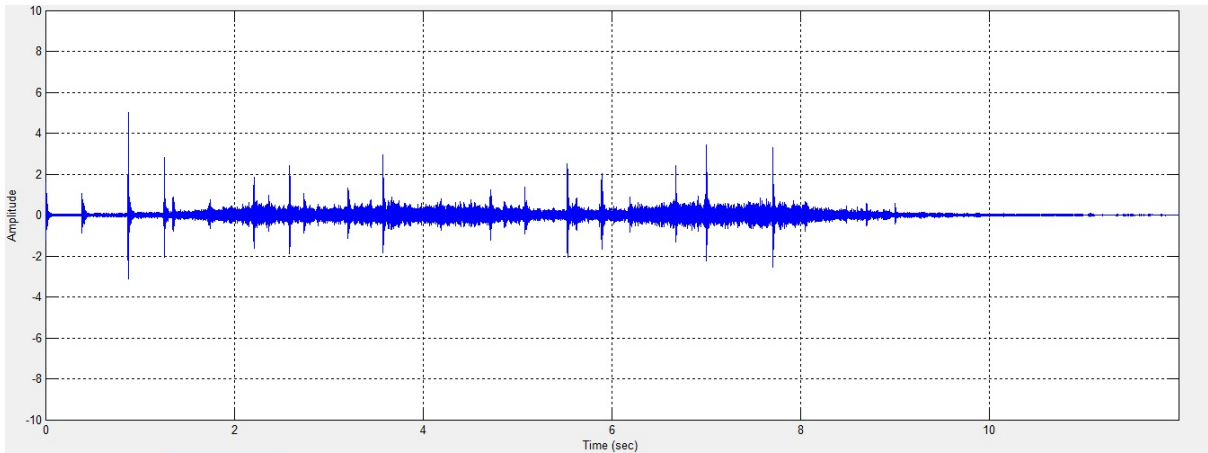


Figure 90: Wayside vibration signal for rolling stock with contaminated axle bearings. Clear peaks above the background noise are detectable.

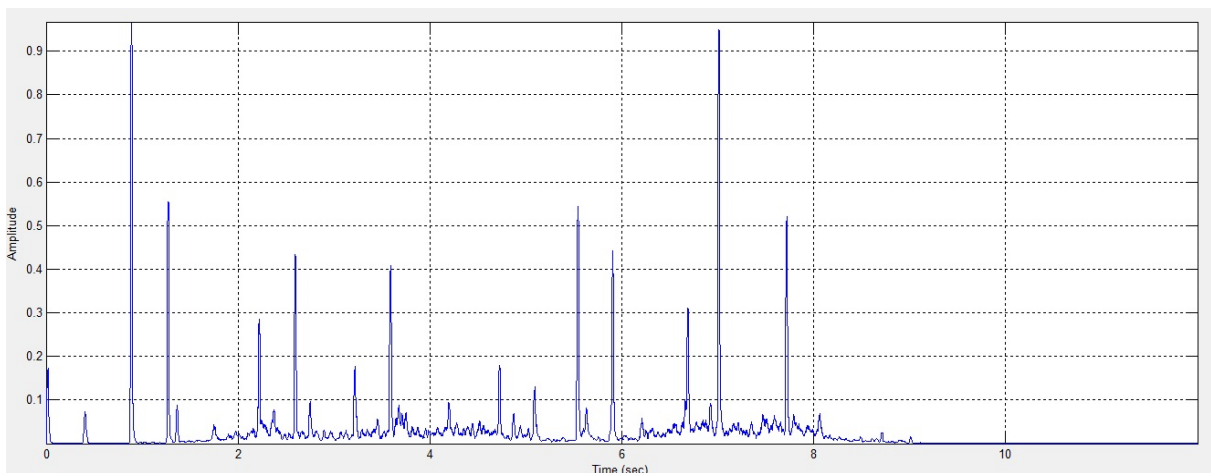


Figure 91: Moving RMS of the vibration signal indicating the high energy content of the peaks observed in the raw AE signal. These are associated with the axle bearing defect as well as the vibrational response to the transition of the wheel trains over each joint along the track section being monitored.

The plot in Figure 92 shows the corresponding AE waveform during wayside measurements. Multiple peaks can be clearly seen associated with both the bearing fault as well as the movement over the joints.

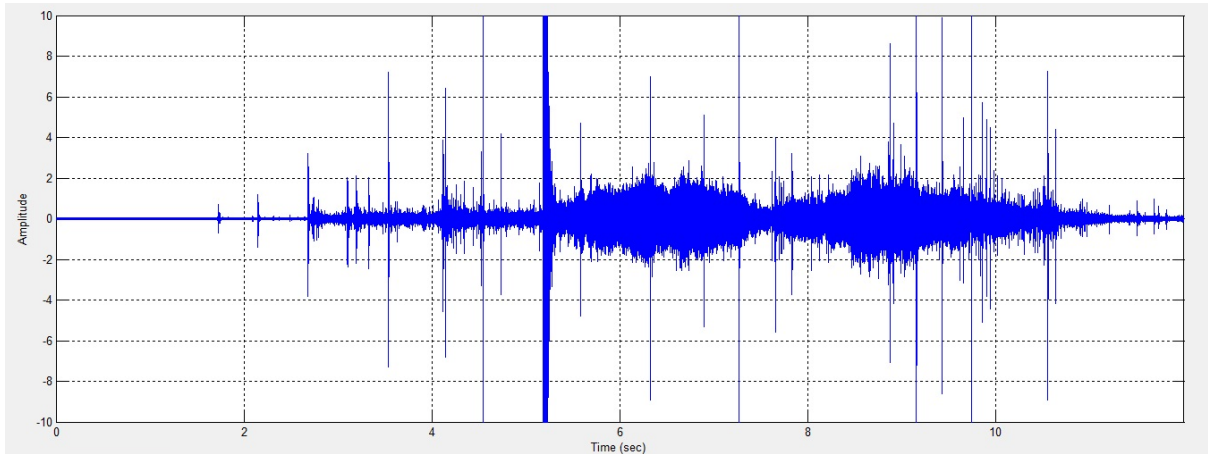


Figure 92: Raw AE waveform taken wayside. Multiple peaks are clearly observed

Subsequent analysis using the moving RMS algorithm and an appropriate window size which in this case was defined at 1000 data points indicates the presence of two major peaks which are clearly associated with the faulty bearings, Figure 93. The other peaks in the raw AE signal despite their high amplitude have disappeared, suggesting they contained low energy and were associated with a wheel flat artificially induced prior the AE measurements rather than the axle bearing defects themselves.

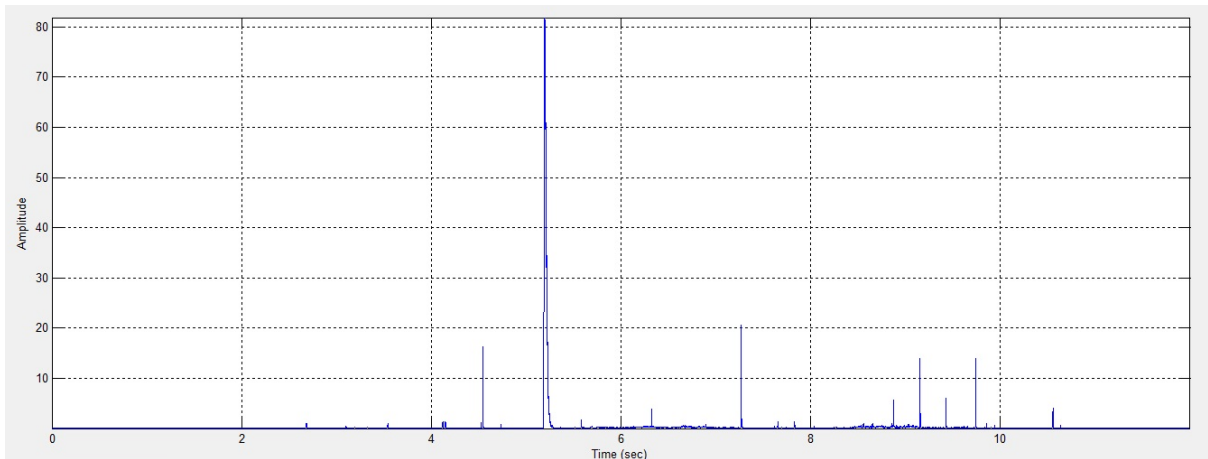
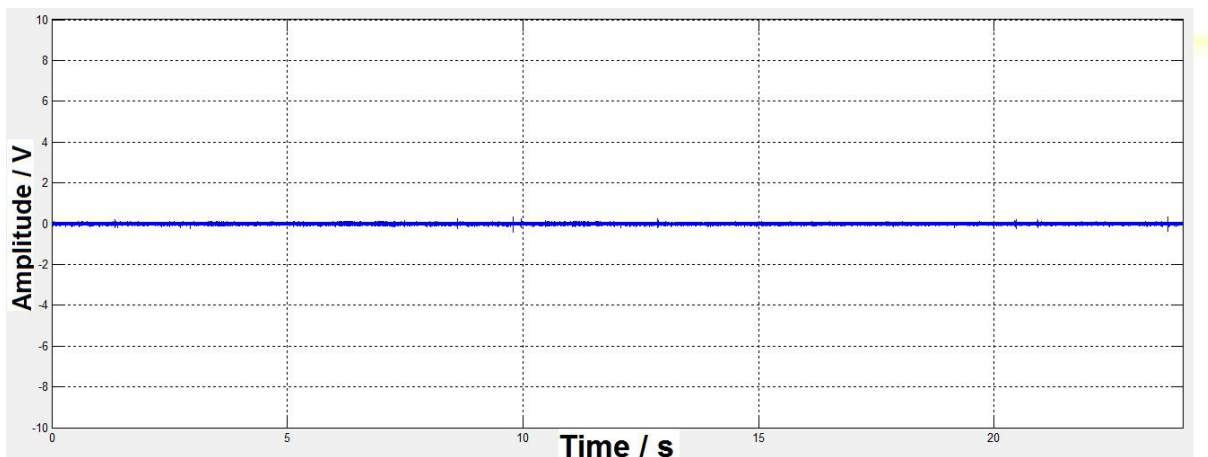


Figure 93: Moving RMS signal showing the presence of the axle bearing defects as well as the presence of the artificially induced flat in one of the wheels of the test train.

Some further key results obtained at Long Marston using alternative testing configurations are given in the following plots. The plot in Figure 94 (a) shows the onboard raw AE measurement of a healthy bearing. The plot in Figure 94 (b) shows the normalised moving RMS of the signal filtered using a time window of 60 points. It is evident that the AE signal contains very little noise.

a)



b)

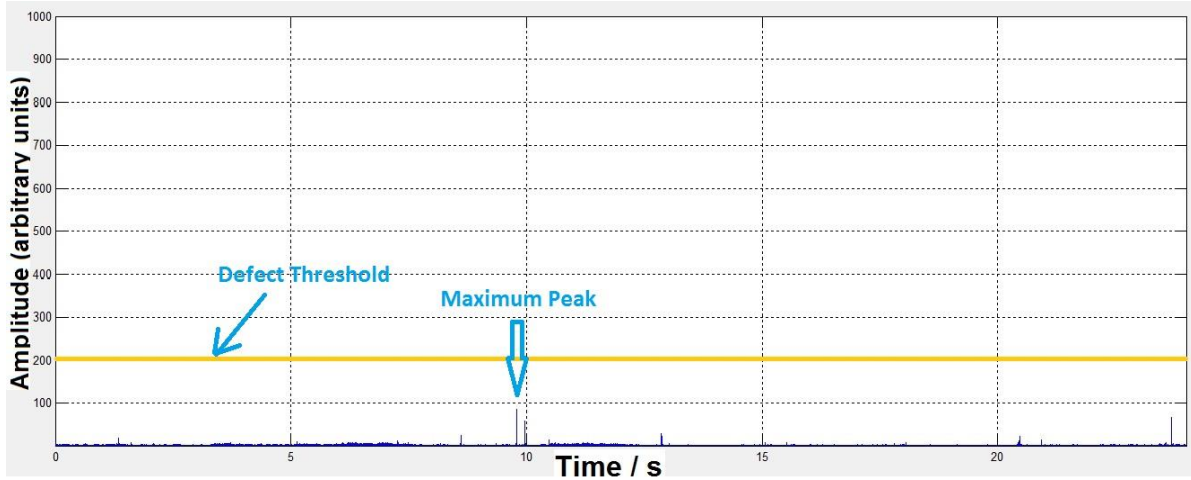
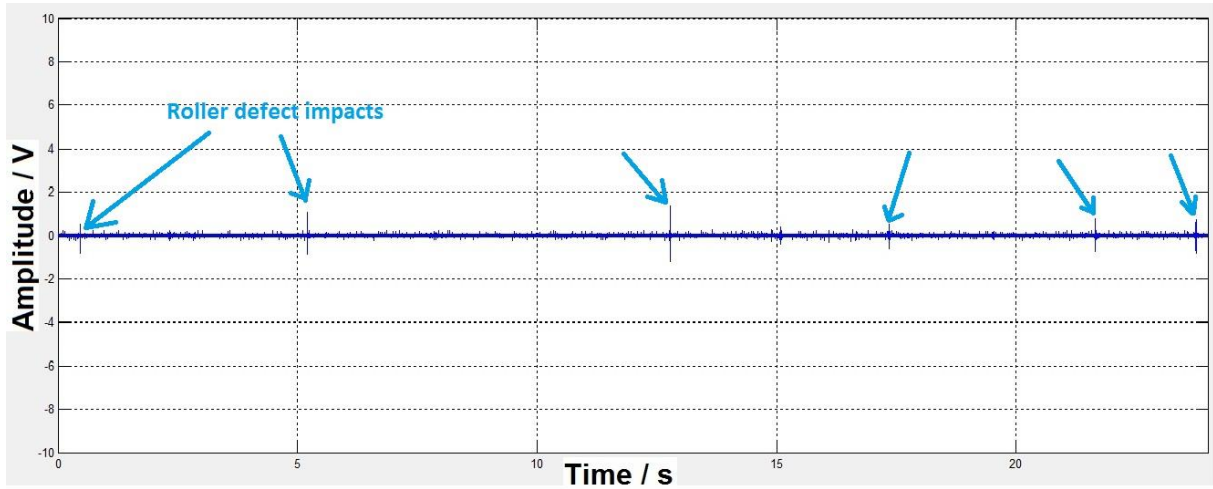


Figure 94: a) Raw AE data acquired from a healthy bearing and b) its moving RMS plot using a filtering time window of 60 points.

The plot in Figure 95 (a) shows the onboard AE measurement for the 4 mm roller defect. The signal appears to be slightly noisier than the healthy one. The peaks seen in the raw AE dataset correspond to the impact of the defective roller as the bearing rotates. By converting the raw data to normalised moving RMS we can see that a number of peaks are evident in the Figure 95 (b) plot, some of which exceed significantly 200 units indicating the presence of a defect. Peaks of no more than 200 units have been determined after the analysis of several tests in the field and laboratory to be associated with noise rather than actual defects. The highest peak for the 4 mm roller defect has a maximum RMS amplitude of 2000 units, well above the predefined threshold [90].

a)



b)

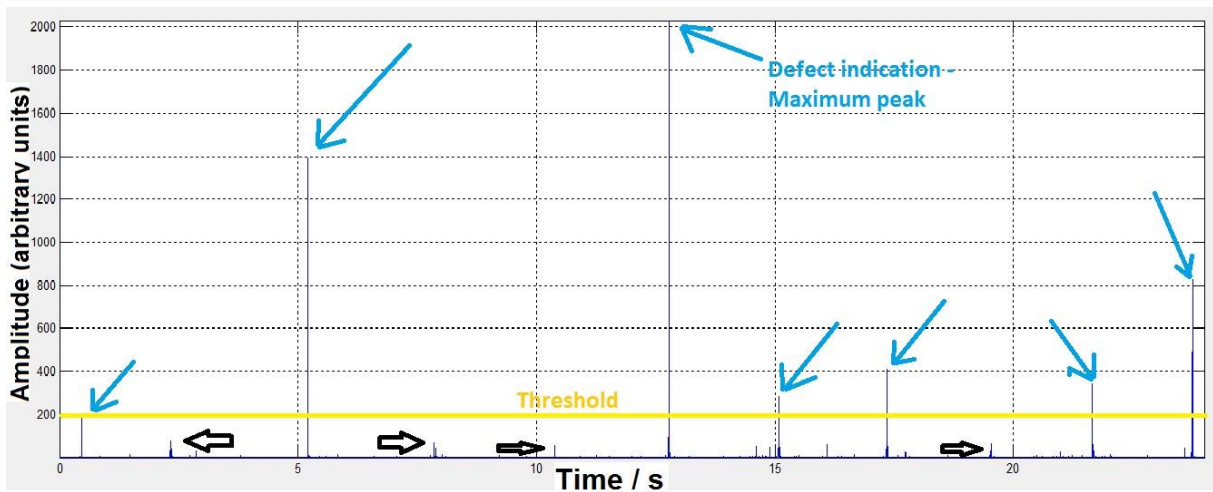


Figure 95: a) Raw AE data acquired from a bearing with a 4 mm roller defect and b) RMS processed results. Notice the amplitude of the strong RMS peaks

9.5 Cropredy site field trials under actual operational conditions

A similar signal processing approach as in the case of Long Marston measurements has been employed for the analysis of Cropredy site field trials. The results which follow are indicative since tens of thousands of measurements have been taken since the installation of the

customised system at the site. In certain cases, defects have been suspected but it has not been possible to validate them. This is an activity pending for future work.

The plot in Figure 96 shows the AE waveform obtained for a passenger train moving over the instrumented site. The peaks are associated with power axles rather than any wheel or axle bearing defect as confirmed with further analysis using moving RMS, FFT and spike energy.

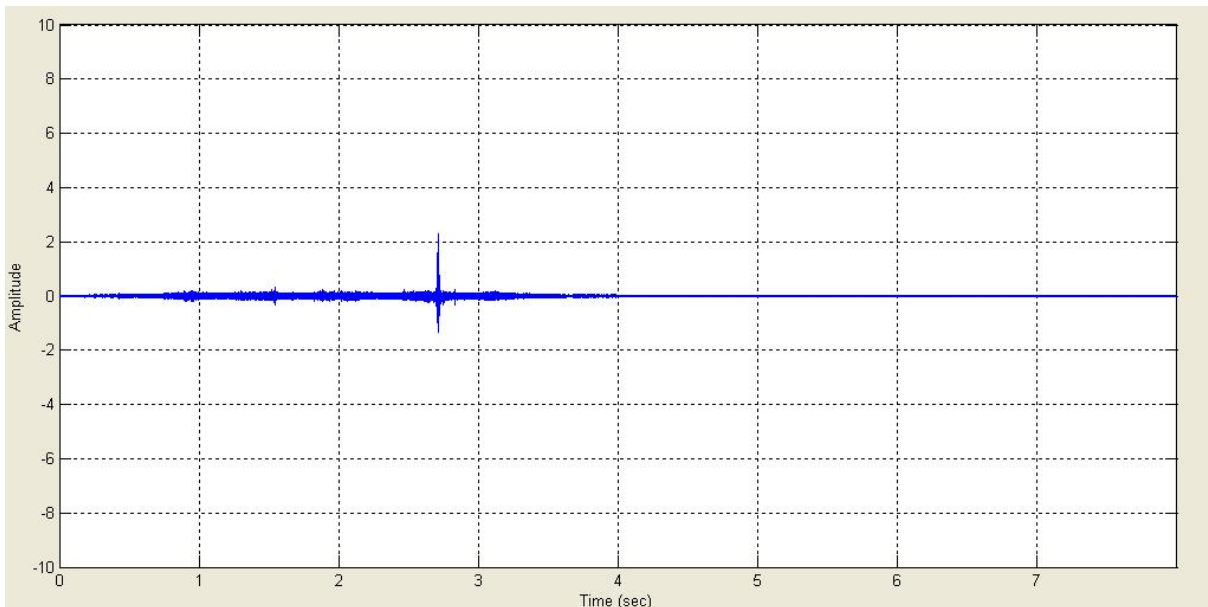


Figure 96: Raw AE signal for passenger train. The peak observed at the end of the signal is associated with a power axle causing sliding of the wheel as it moves along the track, generating additional noise captured by the AE sensor.

The plot in Figure 97 shows the corresponding moving RMS signal. The bogies of each carriage can be seen including the powering of the axle towards the end of the train. However, these are

all very low amplitude peaks clearly indicating that they are associated with background noise rather than an actual defect.

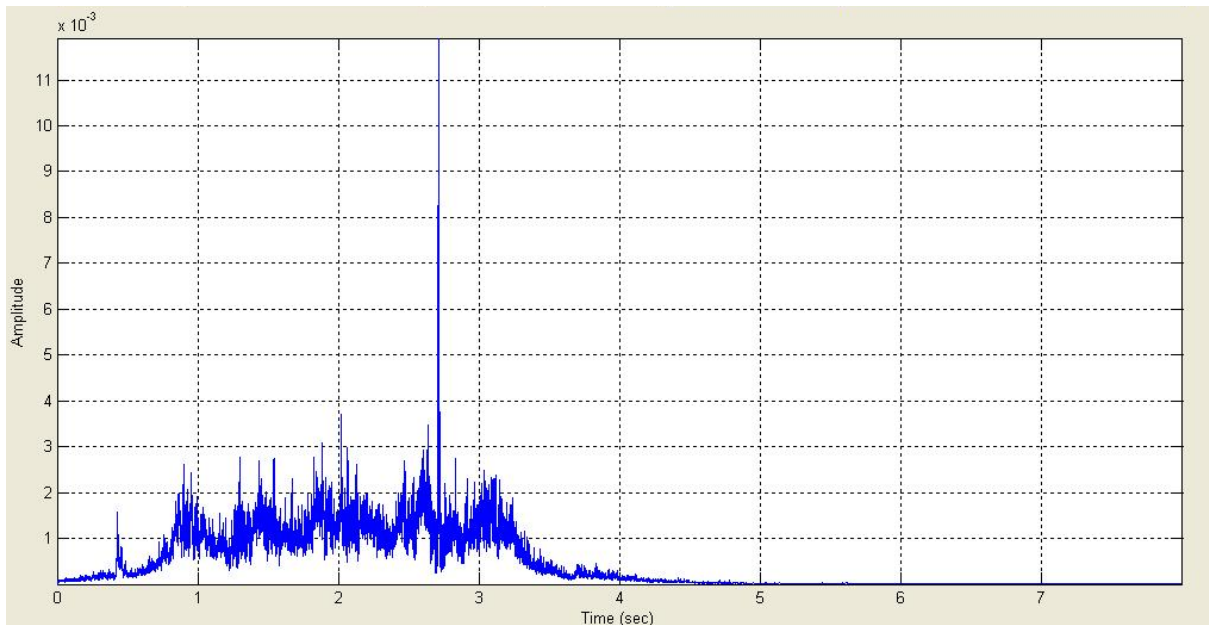


Figure 97: The corresponding moving RMS signal for a passenger train moving over the instrumented site.

The plot in Figure 98 is the corresponding power spectrum of the captured AE waveform.

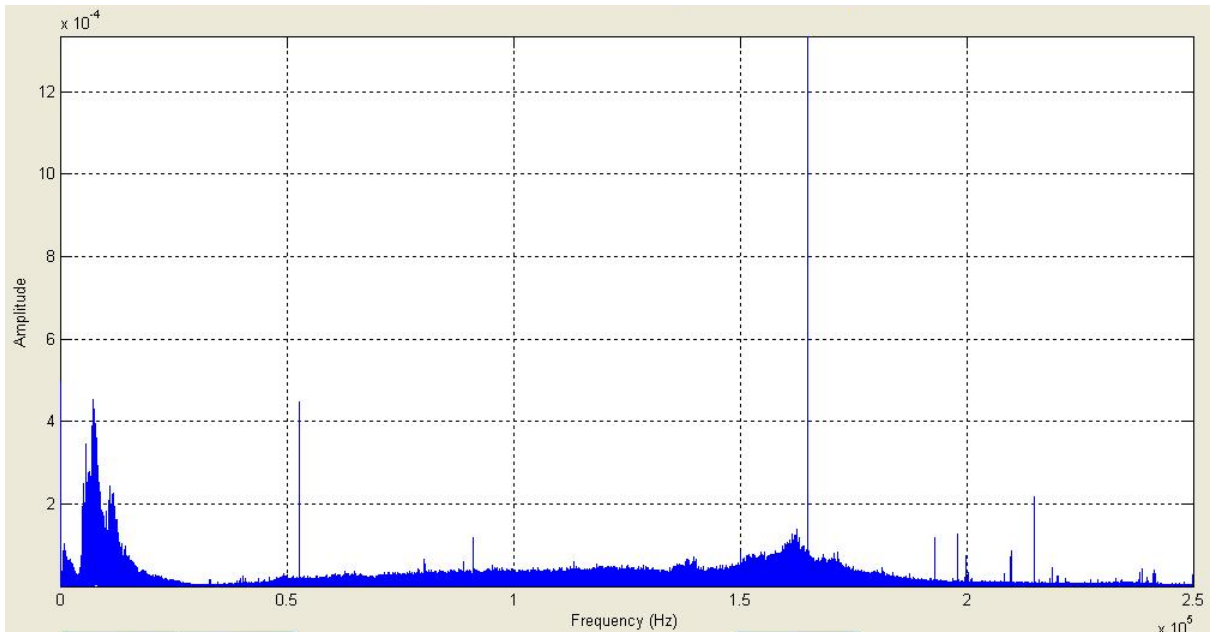


Figure 98: Power spectrum with relatively low amplitude peaks associated with background noise sources alone.

The plot in Figure 99 shows the associated spike energy signal. Again, the rotational frequency information is very low indicating the absence of any wheel or axle bearing defects. If such defects were present, peaks at the relevant rotational frequencies would have been evident.

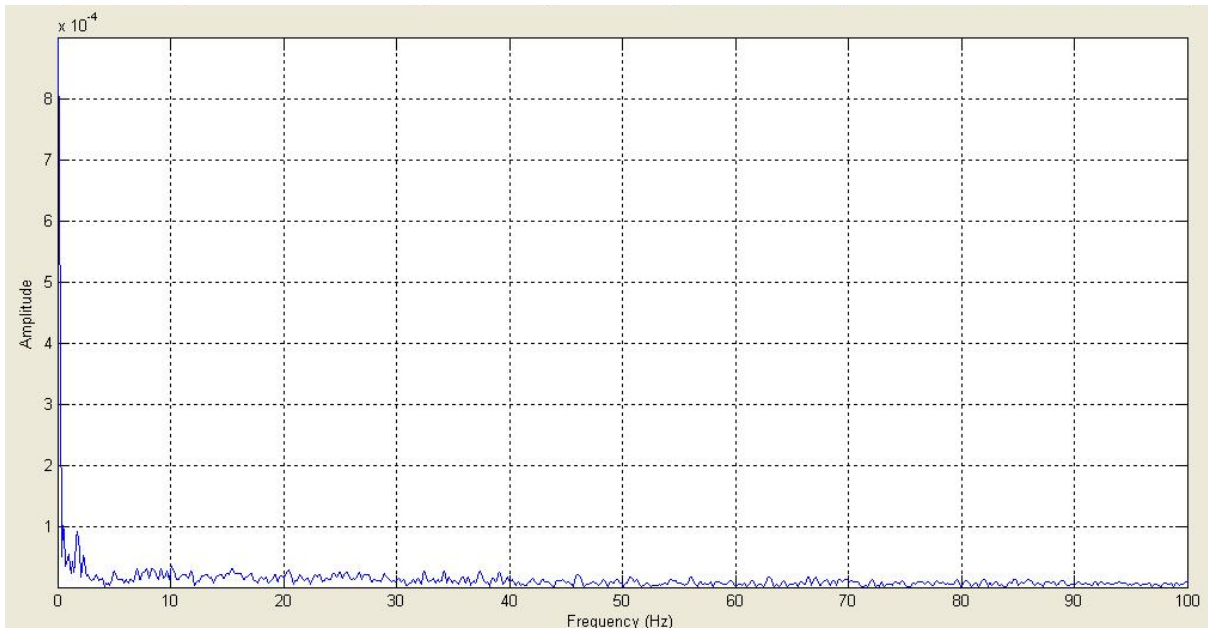


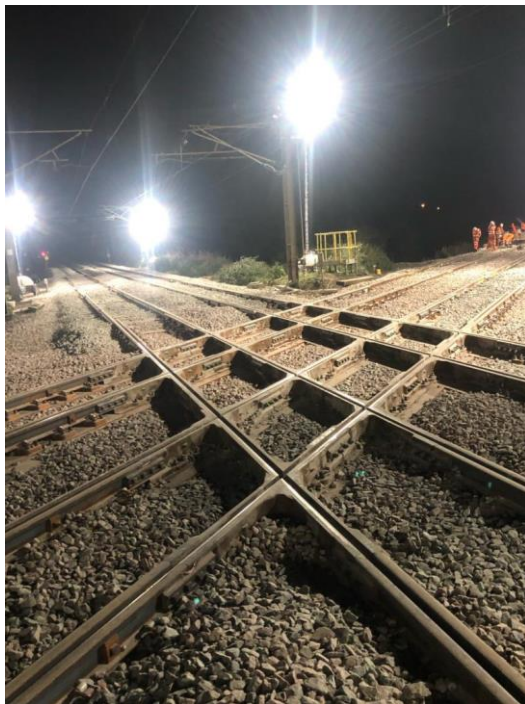
Figure 99: Spike energy plot indicating no wheel or axle bearing defect is present.

9.6 Cast manganese crossing trials under actual operational conditions

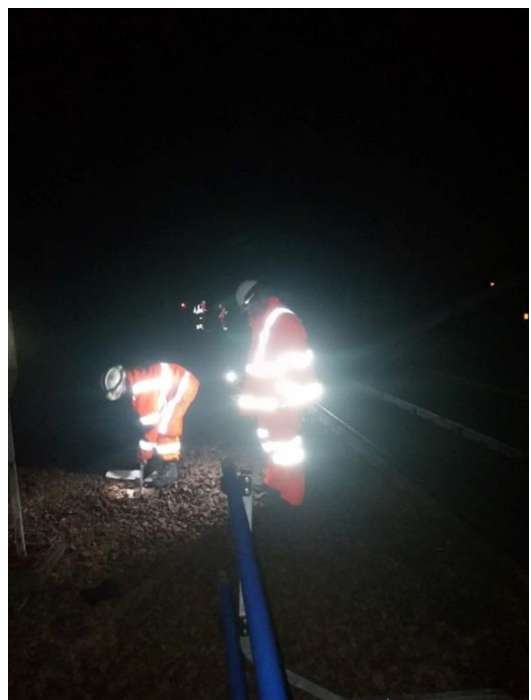
Network Rail makes extensive use of cast manganese crossings manufactured using advanced explosive casting technology. This enables the optimum operational hardness to be obtained during the manufacturing process of the crossing. Without explosive casting the attainment of optimum hardness is dependent on repeated loading cycles arising from the wheels of trains running over the crossing until the work hardening process of the cast manganese steel has been completed.

The microstructure of cast manganese steel is austenitic. The retention of austenitic microstructure at room temperature is possible due to the high manganese content (11-14 % in wt) which is an austenite stabilising alloying element in steels. Manganese increases the overall hardness of the material and promotes rapid work hardening behaviour.

Newark flat crossing is located on the East Coast Main Line. The maximum permissible train speeds are 125MPH up (towards Lincoln) and 100MPH down (towards Newark). From East to West the maximum permissible train speeds are 25 MPH and 50 MPH from West to East. The crossing is used by both passenger and freight trains. The photograph's in Figure 100 show the Newark crossing and the measurement setup.



a)



b)



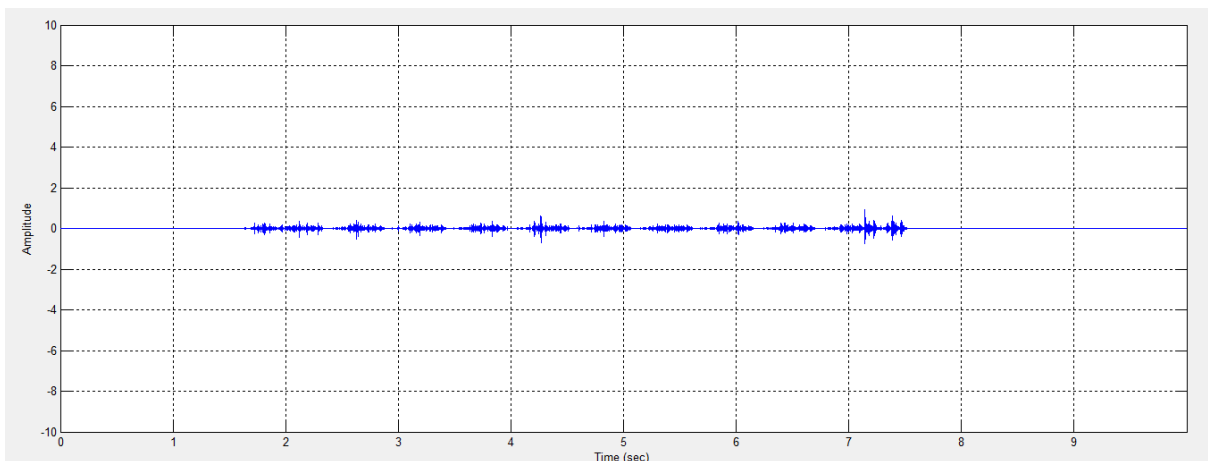
Figure 100: a) Photograph of the Newark flat crossing, b) the installation process of the AE system overnight and c) measurement setup and example rolling stock moving over the crossing at normal operational speed.

Network Rail had decided to replace the Newark flat crossing after approximately 15 years in service. Before replacing the aforementioned crossing, Network Rail had decided to evaluate the structural integrity while it was still in-service using AE.

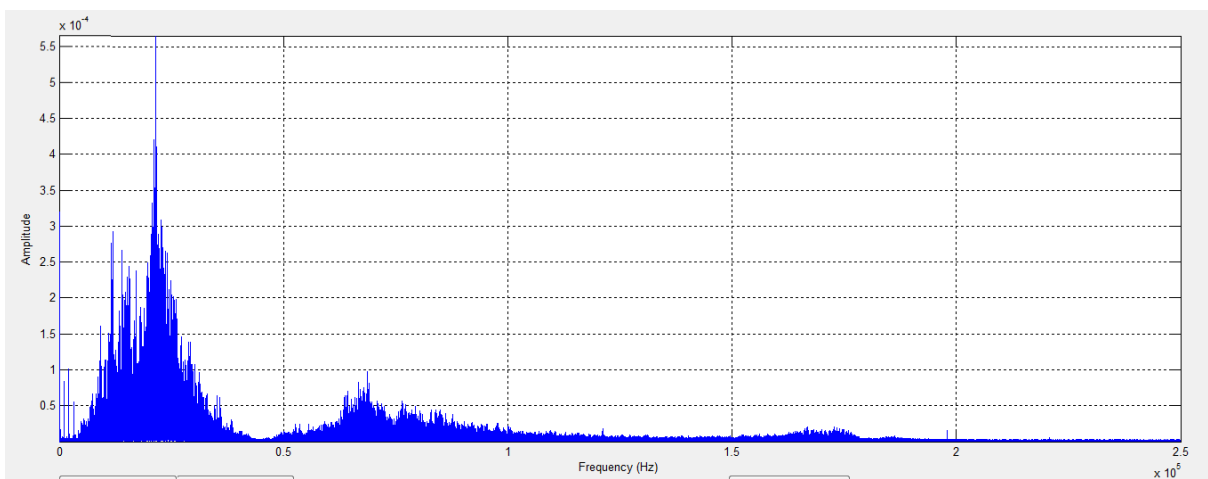
A customised AE system was installed on the crossing in order to evaluate its structural integrity in real-time. The installation of the system took place during night-time while the line was blocked. Measurements were carried out throughout the following day when normal traffic had resumed. The acquisition was triggered manually when a train approached at a pre-determined distant from any direction. Sampling rate was set at 500 kSamples/s and acquisition time was set at 10s. The loading cycles during AE measurements arose from the wheels of approximately 50 trains of various types, including freight trains.

Following from the analysis of the obtained AE measurements it was concluded that the crossing is in good condition. No active crack propagation was detected. The plots in Figure 101 show indicative raw AE measurement plots and their corresponding power spectra. As it can be seen from the power spectra the majority of activity is at low frequencies, which is related to mechanical noise arising from the wheels and motorised axles of the passing trains. There are no peaks evident above 100 kHz where crack-related activity would be expected to be seen in this type of material.

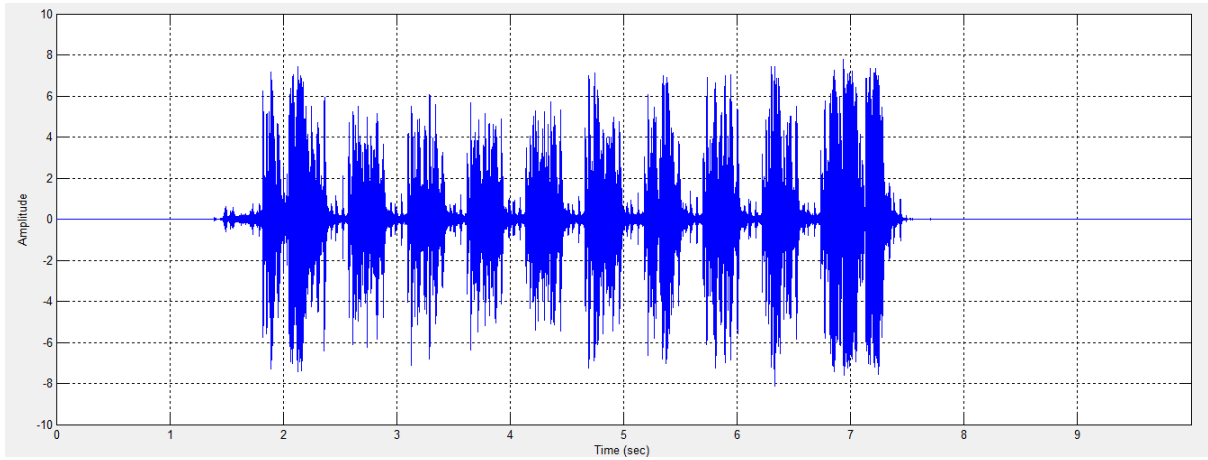
a)



b)



c)



d)

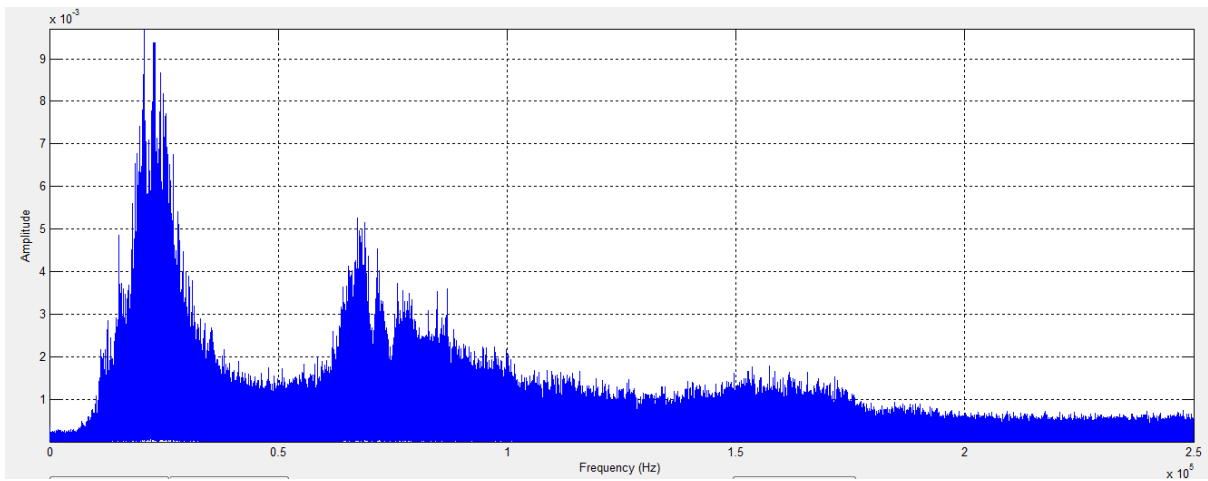


Figure 101: a) and c) raw AE waveforms acquired at Newark flat crossing and b) and d) corresponding power spectra indicating low frequency content above 100 kHz. This suggests that there is no crack propagation occurring which would result in peaks at higher frequencies being clearly observed.

Therefore, it was safely concluded that the structural integrity of the crossing following a large number of AE measurements and corresponding analysis was in good condition and there was no risk of immediate failure.

The photographs in Figure 102 show the crossing measured in the area of Wembley, on the West Coast Main Line. The crossing had been recently replaced and hence, no defects were expected to be found. This was also confirmed by the AE measurements. The plots in Figure 103 provide very similar results to those observed for the crossing at Newark. In this particular case the sampling rate has been set at 1 MSamples/s.

a)

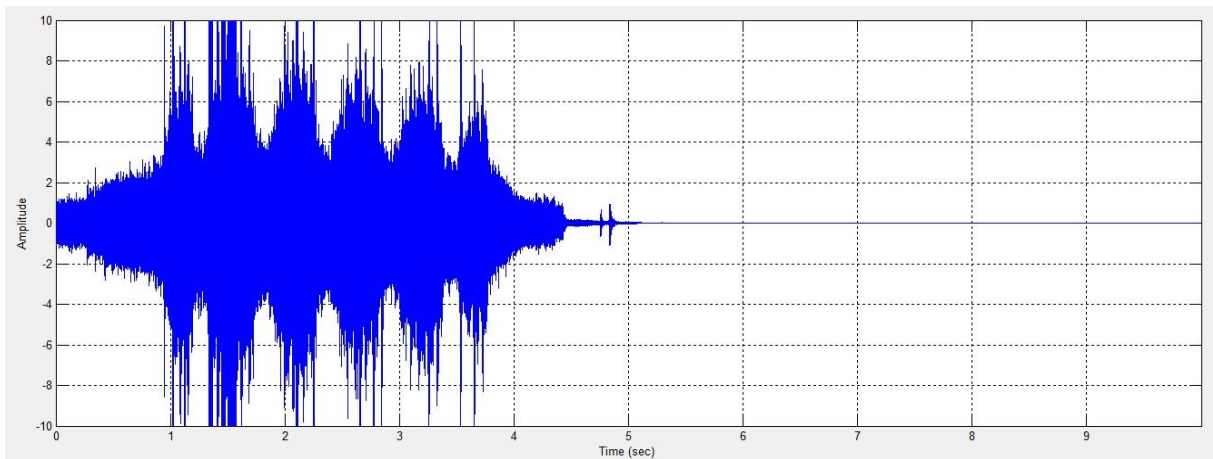


b)

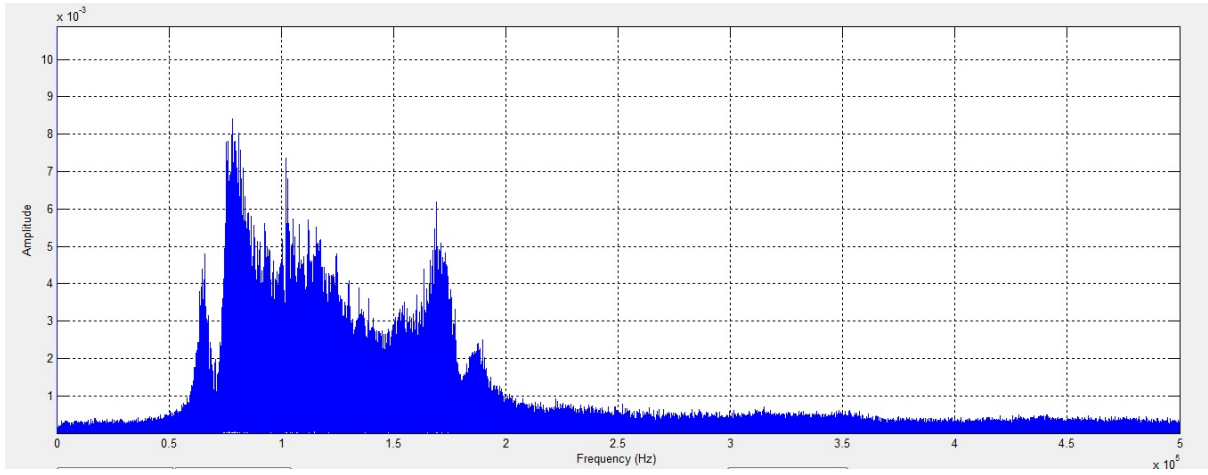


Figure 102: Photographs showing the: a) the crossing measured and b) indicative traffic.

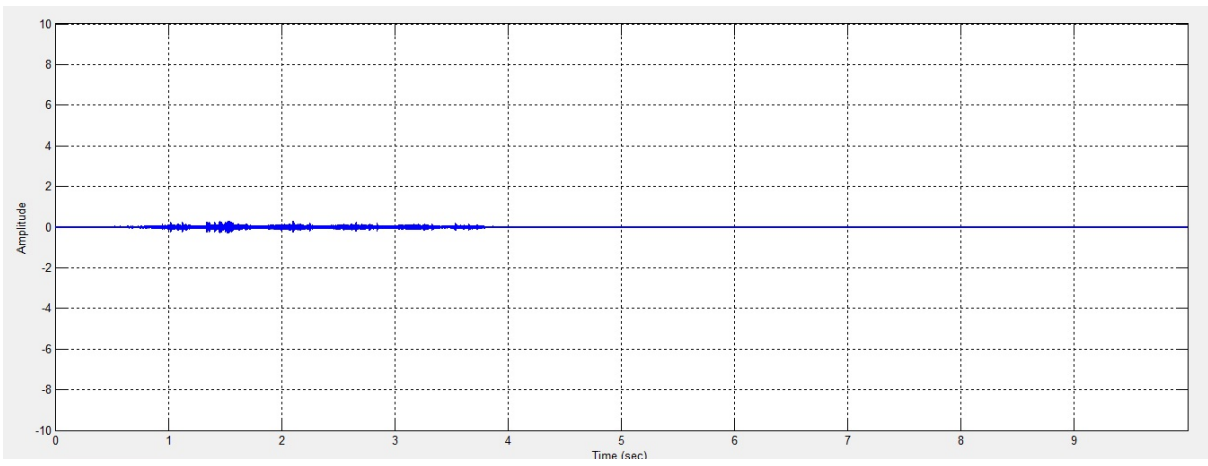
a)



b)



c)



d)

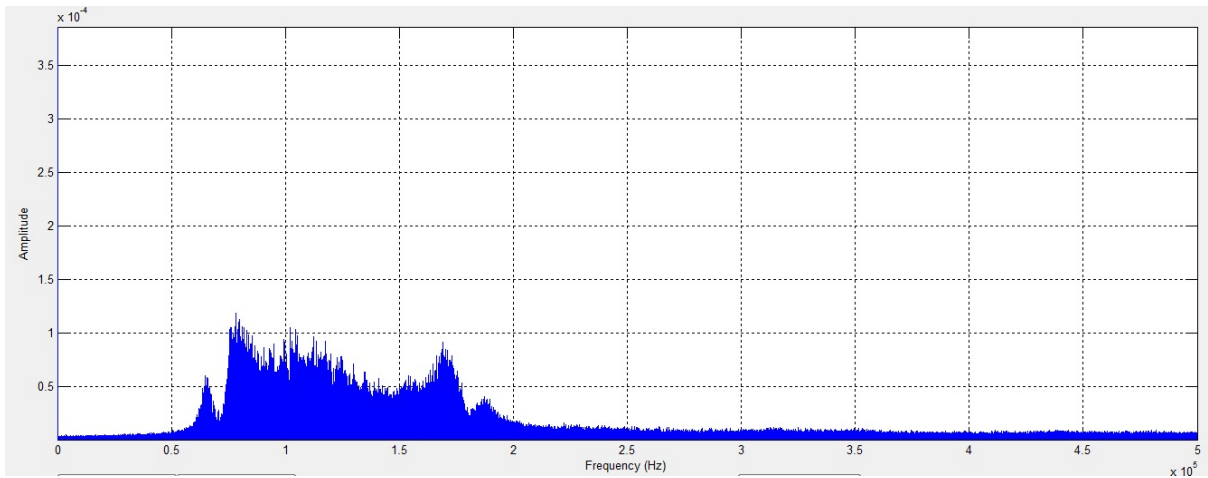


Figure 103: a) and c) raw AE waveforms acquired at Wembley crossing and b) and d) corresponding power spectra indicating low frequency content above 100 kHz. This suggests that there is no crack propagation occurring which would result in peaks at higher frequencies being clearly observed.

Another crossing measured on the West Coast Mainline in the area of Watford was identified as severely damaged and was due for replacement by the maintainer. There was substantial interest to monitor this particular crossing with AE. The experimental setup and defective crossing in Watford are shown in the photographs in Figure 104. Although passenger trains did not yield any additional damage, when the crossing was loaded by a heavy freight train clear peaks were detected on the AE waveform captured. These peaks and overall signal characteristics were identical to those signals observed for the cast manganese steel samples tested under three-point bending fatigue conditions.

a)



b)



c)

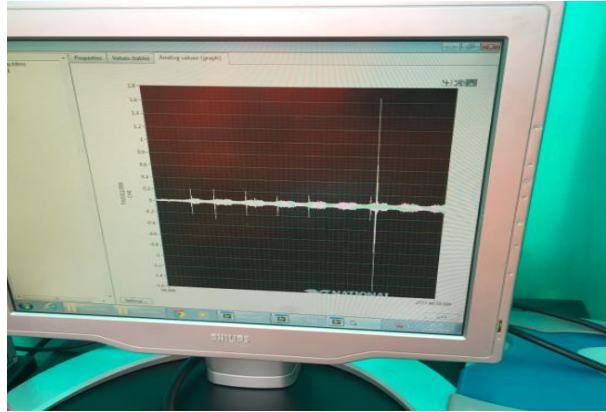


Figure 104: Photographs of a) defective crossing in Watford, b) experimental setup and c) captured signal indicating clear crack growth when the crossing was loaded by a heavy freight train.

The plot in Figure 105 shows the raw AE waveform indicating crack growth occurring with each loading freight wagon going over the defective crossing. The characteristics of the signal are identical to those observed in the laboratory.

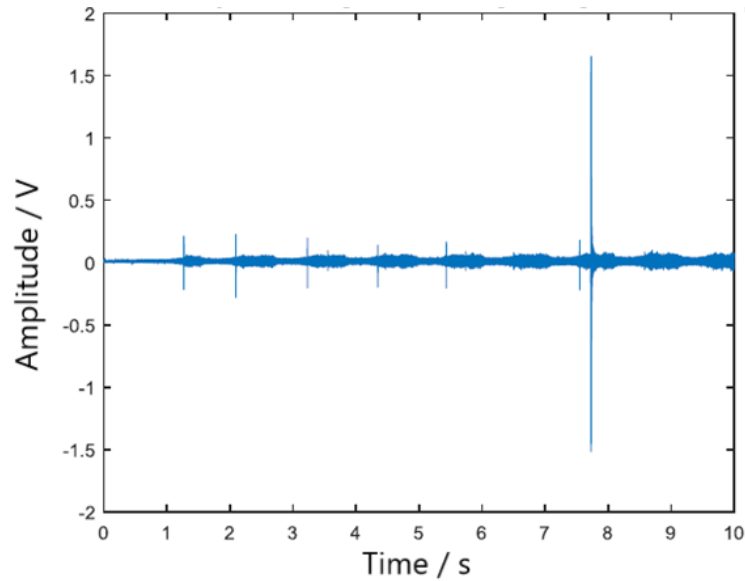


Figure 105: Raw AE signal indicating crack growth events occurring.

9.7 Chapter 9 Summary

Chapter 9 provided a critical overview of the key results obtained during this research study. From the results obtained, the strengths and weaknesses of AE and vibration analysis techniques have been ascertained. It has been confirmed that AE and vibration analysis can be used to monitor different types of defects effectively. However, quantification is a more complex proposition although it has been shown to be possible. Nonetheless, further verification is required, comparing findings with onsite evaluation of actual defects detected in order to reliably confirm the thresholds to be set in a commercially employed version of the collaboratively developed customised vibroacoustic monitoring system. Chapter 10 summarises in detail the main conclusions drawn from this study and provides useful recommendations for future work based on the knowledge built to date from the results already at hand.

CHAPTER 10: CONCLUSIONS AND FUTURE WORK

10.1 Conclusions

This research study has been driven by the strong industrial need for modern railways to adapt to the reality of current and future demand for increased seamless and environmentally friendly mobility capability. Modern railway networks are inherently environmentally friendly. This is particularly true for rail lines that are electrified since the power required by electric trains to operate can be provided by sustainable energy sources. An example of such a case are the Danish railways, which are currently powered in their entirety by wind energy. The UK has been committed to drive down its carbon footprint.

The transport sector is one of the key industries of the economy, which is receiving particular attention in terms of its carbon footprint. In recent months, there has been an increasing focus on the carbon footprint of air travel. Short routes have come under scrutiny followed by suggestions that alternative transport means should be used instead, with the main obvious proposition being rail transport.

Given present developments with respect to environmental activism, it is correct to anticipate that railway transport demand will experience further growth, putting extreme pressure on existing capacity. There will be a need for railway infrastructure managers to increase the availability of rail lines and operate at higher traffic densities than before. This will also put a higher burden on rolling stock operators who will be required to operate rolling stock for more hours per day making maintenance planning more difficult.

Conventional inspection procedures for identifying structural defects based on UT and MFL will become obsolete, being replaced with in-situ real-time monitoring processes. Of course UT, MFL and other types of inspection being used today will continue to serve the railway infrastructure managers well into the future but instead of being deployed as a primary inspection tool they will be employed instead as a verification tool once a defect has been detected and located by in-situ monitoring sensors.

There has been a continuous drive towards improving capacity, enhancing traffic density, accommodating more passengers and freight capacity whilst maintaining punctuality at the highest possible level. Especially in the case of freight transport, the just in time principle that several industries operate under, including automotive, mean punctuality will become increasingly important and costly if it is not maintained.

The passenger rolling stock operators are already required to accommodate the costs of compensation schemes in case of delays beyond thirty minutes, with full refunds being available in the event where delays exceed one hour. Similarly, Network Rail is required to compensate rolling stock operators for delays caused due to infrastructure-related issues. Therefore, there is already strong evidence that punctuality is of primary concern for the entire railway sector. Hence, business as usual cannot remain sustainable in the long-term unless new technologies are put in place in time to address reliability, availability, maintainability and safety requirements of 21st century railway networks.

Within this study, current methodologies and equipment have been discussed and analysed. This has put into the operational context of the modern railway network the existing technical capabilities as well as the key limitations and technical barriers that need to be overcome.

Furthermore, a novel methodology based on the integration of AE and vibration analysis has been investigated. Experiments have been conducted at three different levels starting from basic laboratory trials, field trials under simulated conditions carried out in the test track in Long Marston, and field trials carried out under actual operational conditions on the UK railway network at several sites. The pinnacle of the present work has resulted in the issuing of a Certificate of Acceptance from Network Rail, permitting the installation of a customised system developed in collaboration with other researchers within the NDT group, which has been installed on the Chiltern railway line at Cropredy since September 2015. The system has remained operational since the time of its installation with very little maintenance required in between. Other trials performed on the network include measurements at crossing sites in Wembley (West Coast Main Line), Hatton (Chiltern Rail Line), Watford (West Coast Main Line) and Newark (East Coast Main line).

The results obtained from the various sets of experiments have been particularly encouraging highlighting the potential of the technology developed for monitoring both critical infrastructure and rolling stock components. It has been proven that AE in particular is a powerful tool for monitoring structural degradation of rails and crossings as well as for evaluating faults in wheels and axle bearing of rolling stock. Vibration analysis has been shown

to be a useful integration to AE data, helping increase confidence and confirm the presence of certain defects, which may generate similar AE responses.

10.2 Future Work

There is ample scope for future work on AE and vibration analysis applications in the railway industry. This includes the development of wireless AE sensors and accelerometers powered by novel energy harvesting systems. Energy harvesting systems can be adapted in ways that promote the conversion of the environmental energy to electric in order to power the RCM sensors installed on the network as well as associated data processing and communications electronics. Wireless sensors will also open new possibilities, increasing operational flexibility and reducing the cost required to cover the entire railway network which extends to tens of thousands of kilometres and includes remote areas.

Advances in signal processing will continue towards the direction of Artificial Neural Networks (ANNs) [121-122], artificial intelligence (AI) and machine learning, opening vast new possibilities for processing large amounts of big data being generated across the vastness of a railway network such as the one in the UK. Furthermore, it will enhance the reliability of the analysis, reducing the likelihood of misinterpretation or missed faults. Data fusion from multiple sensors of various types will become more important, particularly in the context of identifying or verifying different faults in a wide range of critical railway infrastructure and rolling stock components.

There is hence, clearly a significant potential for further research and development of the subject. It could be considered by some that the interesting part is about to begin from where this research study just stopped. Time will tell what new developments will come around in the future and how many of them will have a relationship with the work reported herewith.

Research has been on-going in parallel with this project on sensor fusion by E. Giannouli [124]. This project looks into analysing signals from multiple sensors simultaneously in order to improve reliability as well as the amount of information gained regarding the condition of rolling stock wheelsets.

The rail network is a massive system generating a significant amount of data. The digitalisation of all information gained from various sensors needs to take place centrally. This is already one of the key aims of Network Rail through the establishment of a cloud-based system where all data will be trended and related to each other maximising the information gained regarding the overall condition of the various parts of the network.

REFERENCES

1. M. Papaelias, Chapter 2: An integrated strategy for efficient non-destructive evaluation of rails, Fault Detection: Classification, Techniques and Role in Industrial Systems, Fausto Pedro Garcia Marquez and Mayorkinos Papaelias (Eds.), Nova Science Publishers, 2013.
2. P. Vallely & M. Papaelias “A Qualitative Comparison of Advantages and Disadvantages of Structural Health Monitoring of Railway Infrastructure over Conventional Inspection Methods”. Proceedings of the 12th European Conference of Non-Destructive Testing (ECNDT2018), Gothenburg, Sweden 11th - 15th June, 2018.
3. J Davies, P Vallely, M Papaelias & Z Huang “Addressing future rail network performance challenges through effective structural health monitoring” Proceedings of the 2018 ASME Joint Rail Conference (JRC2018), Pittsburgh, PA, USA, April 18th - 20th 2018.
4. P. Vallely “The UK Experience with RCM” 2nd invitation Presentation at British Council- TUBITAK Knowledge Transfer on RCM for Railways Workshop, December 2017, Istanbul, Turkey.
5. P. Vallely and M. Papaelias “Integrating Remote Condition Monitoring of Railway Infrastructure with High Speed Inspection” In Proceedings of WCCM 2017, London, UK, June 2017.
6. Network Rail, “Technical Strategy 'A future driven by innovation',” London, 2013.
7. L. Peterson, “What we're doing,” Network Rail, 13th June 2014. [Online]. Available: <http://connect/communities/orbis/key-themes.aspx>. [Accessed 13th October 2014].
8. P. Lattimore, “Fail Safe,” Rail Professional, no. 152, p. 22 to 25, 2009.

9. Department for Transport, "Achieving VfM From a Railway Systems Authority," Risk Solutions, 2011.
10. M. Papaelias, C. Roberts, C. Davis, A review on non-destructive evaluation of rails: State-of-the-art and future development, Proceedings of the IMechE: Part F – Journal of Rail and Rapid Transit, 222, 4, pp. 367-384.
11. P. Yilmazer, Structural health condition monitoring of rails using acoustic emission techniques, M.Res. Thesis, University of Birmingham, Birmingham, UK 2012.
12. M. Papaelias, A. Amini, R. Culwick, J. Heesom, Z. Huang, V. L. Jantara Junior, S. Kaewunruen, S. Kerkyras, M. Kongpuang, F. P. Garcia Marquez, S. Shi, A. Upton, P. Vallely "Advanced remote condition monitoring of railway infrastructure and rolling stock". In Proceedings of the 1st International Conference on Welding & NDT, Athens, Eugenides Foundation, 22-23 October 2018.
13. P. Vallely, M. Papaelias, Z. Huang, S. Shi, S. Kaewunruen, J. Davies "The Stephenson Conference: Research for Railways". IMechE, April 2017, London, UK.
14. T. Anderson, "Analysis of Past Derailments," 6th May 2011. [Online]. Available: http://www.google.co.uk/url?url=http://www.era.europa.eu/Document-Register/Documents/Item%25204%2520-%2520DNV%2520-%2520Part%25201%2520Analysis%2520of%2520past%2520derailments%2520v2.ppt&rct=j&frm=1&q=&esrc=s&sa=U&ei=_oUFVclf1bFp4q-C4Ak&ved=0CByQFjAA&usg=. [Accessed 14th September 2014].

15. F. D. G. V. F. & M. R. C. Ulianov, "Overview of freight train derailment in the EU. Causes, impacts, prevention, and mitigation measures," Transport Research Arena, Paris, 2014.
16. Papaelias, M. Train wheelsets and wayside condition monitoring, Engineering Applications Seminar, The University of Birmingham, 29 January 2013.
17. Papaelias, M., Papailias, F., Kerkyras, S. & Graham, K. , The future of railway inspection, In the Proceedings of the British Institute NDT 2012 International Conference, 11-13 September 2012, Daventry, UK.
18. A. Amini, Ph.D. Thesis, University of Birmingham, 2017.
19. Z. Huang, Ph.D. Thesis, University of Birmingham, 2018.
20. Okamoto, I. 1998, How bogies work. *Japan Railway & Transport Review*, 18, 52-61
21. SafeRail, "SafeRail," TWI Ltd, [Online]. Available: <http://www.saferail.net/project/background.jsp>. [Accessed 12th March 2015].
22. S. L. Dedmon, "The process of spalling in railroad wheels," The American Society of Mechanical Engineering, vol. RTDF2011, no. 67030, pp. 167 - 172, 2011.
23. R. L. a. T. V. S. Teimourimanesh, "Breaking capacity of Railway wheels - State of the art survey," in 16th International World Congress (IWC16), Cape Town, RSA, 2010.
24. R. Smith, "The 19th Jenkins Lecture," 23rd September 2006. [Online]. Available: <http://www.soue.org.uk/souenews/issue6/jenkinlect.html>. [Accessed 10th June 2014].
25. S. L. Grassie, *Mechanics and Fatigue in Wheel/Rail Contact*, New York: Elsevier Science Publishing Company Incorporated, 1991.
26. S. M. C. & D. Lauro, "Inspection of Tread Damaged Wheelsets," in Rail Technology Division Fall Technical Conference, Chicago, 2008.

27. NSW RailCorp, Wheel Defect Manual, NSW RailCorp, 2013.
28. G. Tyler, "Summit Tunnel Fire," Fire West Yorkshire, 20th December 1984. [Online]. Available: <http://www.firewestyorkshire.com/summittunneldec20th.htm>. [Accessed 04th March 2015].
29. NBC News, "Europe on NBC New," Association Press, 30 June 2009. [Online]. Available: http://www.nbcnews.com/id/31638526/ns/world_news-europe/t/least-die-train-derails-explodes-italy/. [Accessed 12 March 2015].
30. J. Chen-Min, Microstructures and Properties of Materials, Volume 2 ed., Rochester: World Scientific, 2001, pp. 267 (paragraph 3.1) - 269 .
31. Burstow, M. 2010. Management of rail and wheel deterioration. In: SCHMID, F. (ed.) Wheel-Rail Best Practice Handbook. Birmingham University Press, A.N. Harris.
32. R. J. & T. C. D. Peng, "A study into crack growth in a railway wheel under thermal stop break loading spectrum," Engineering Future Analysis, vol. 25, pp. 280 - 290, 2013.
33. J. Peng, G. Y. Tian, L. Wang, X. Gao, Y. Zhang, Z. Wang, Rolling contact fatigue detection using eddy current pulsed thermography, 2014 IEEE Far East Forum on Nondestructive Evaluation/ Testing (FENDT), Chengdu, China, 20-23 June 2014.
34. R. Yang, Y. He, B. Gao, G. Y. Tian, J. Peng, Lateral heat conduction based eddy current thermography for detection of parallel cracks and rail tread oblique cracks, Measurement, Vol. 66, April 2015, pp. 54-61.
35. J. Peng, G. Y. Tian, L. Wang, Y. Zhang, K. Li, X. Gao, Investigation into eddy current pulsed thermography for rolling contact fatigue detection and characterization, NDT & E International, Vol. 74, September 2015, pp. 72-80.
36. M. Papaalias, F. P. G. Marquez, J. M. C. Munoz, C. Roberts, A B-spline approach to alternating current field measurement for railroad inspection, IEEE International

- Conference on Industrial Engineering and Engineering Management, IEEM 2008, 8-11 December 2008, Singapore, pp. 1385-1389.
37. M. Papaelias, C. Roberts, C. L. Davis, B. Blakeley, M. Lugg, High-speed inspection of rolling contact fatigue in rails using ACFM sensors, *Insight – Non-Destructive Testing and Condition Monitoring*, Vol. 51, Issue 7, 2009, pp. 366-369.
 38. M. Papaelias, M. Lugg, C. Roberts, C. Davis, High-speed inspection of rails using ACFM techniques, *NDT & E International*, Vol. 42, Issue 4, 2009, pp. 328-335.
 39. M. Papaelias, C. Roberts, C. L. Davis, B. Blakeley, M. Lugg, Further developments in high-speed detection of rail rolling contact fatigue using ACFM techniques, *Insight – Non-Destructive Testing and Condition Monitoring*, Vol. 52, Issue 7, 2010, pp. 358-360.
 40. M. Papaelias and M. Lugg, Detection and evaluation of rail surface defects using alternating current field measurement techniques, *Proceedings of the Institution of Mechanical Engineers Part F: Journal of Rail and Rapid Transit*, Vol. 226, Issue 5, 2012, pp. 530-541.
 41. J. M. C. Munoz, F. P. G. Marquez, M. Papaelias, Railroad inspection based on ACFM employing a non-uniform B-spline approach, *Mechanical Systems and Signal Processing*, Vol. 40, Issue 2, 2012, pp. 605-617.
 42. B. Sladojevic, “Ultrasonic testing of aluminothermic welding joints of rail tracks, Institute of Kirilo Savic, Belgrade, 2001.
 43. Nielsen, J. C. & Johansson, A. 2000. Out-of-round railway wheels-a literature survey. *Proceedings of the Institution of Mechanical Engineers, Part F: Journal of Rail and Rapid Transit*, 214, 79-91.

44. C. F., A. I. J. Brizuela, "Railway wheel-flat detection and measurement by ultrasound," *Transportation Research, An International Journal*, vol. Part C, p. 10, 2011.
45. I. C. R. W. A. W. & D. V. N. Symonds, "Observing early stage rail axle bearing damage," *Journal of Engineering Failure Analysis*, vol. Special Edition journal, no. Sixth International Conference of Engineering Failure Analysis., 2015.
46. Railstaff Publishing Ltd, "Sound Investment," *The Rail Engineer*, no. 99, pp. 47 - 50, 2013.
47. Network Rail, *Train Detection (NR/SP/SIG/11752) Issue 2*, London: Network Rail, 2001.
48. C. B. & C. Roberts, "Developing System Models to Help Great Britain's Railways Embrace Innovation Technologies with Confidence," in *RRUKA Conference 2012*, London, 2012.
49. R. Clark, "Rail flaw detection: overview and needs for future developments," *NDT & E International*, 2004, 37, pp. 111-118.
50. Health and Safety Executive, "Train derailment at Hatfield 17th October 2000 Second HSE Interim Report," Health and Safety Executive, London, 2001.
51. S. L. Grassie, "Rolling Contact Fatigue on the British railway system: treatment," *Wear*, 2005, 258, pp. 1310-1318.
52. S. L. Grassie, "Squats and squat-type defects in rails: the understanding to date." *Proceedings of the Institution of Mechanical Engineers, Part F: Journal of Rail and Rapid Transit*, 226, 3, 2012, pp. 235-242.
53. Operational failure modes of S&Cs (Deliverable D13.1), Collaborative Project SCP3-GA-2013-60560, Increased Capacity 4 Rail network through enhanced and optimised operations, FP7-SST-2013-RTD-1.

54. P. Sweeting, "Track Geometry," Network Rail, 26th March 2010. [Online]. Available: <http://connect/communities/EngineeringDataNST/TrackGeometry.aspx>. [Accessed 14th October 2014].
55. S. Shi, Ph.D. Thesis, University of Birmingham 2019.
56. M. Papaalias, Z. Huang, S. Kaenwunruen, M. Kongpuang, S. Kerkyras, F. P. Garcia Marquez, S. Shi, P. Vallely "Online assessment of the structural integrity of railway crossings using high frequency acoustic emission sensors". Proceedings of the 6th Conference of the Combined Australian Materials Society, New South Wales, Australia, 27th - 29th November 2018.
57. Network Rail, Inspection of Cast Crossings and Cast Vees in the track (formerly RT/CE/S/054), London: Network Rail, 2004.
58. L. F. M. E. R. a. J. R. E. J. M. Hart, "Development of a Machine Vision System for the Inspection of Heavy-Haul Railway Turnout and Track Components," Rail Transportation and Engineering Center,, Illinois, 2015.
59. SKF Product Information 401, Bearing failures and causes, PI 401 E, SKF, 1994.
60. Vale, C., Interoperable monitoring, diagnosis and maintenance strategies for axle bearings - the MAXBE project, In the Proceedings, of Transport Research Arena 2014, Paris, 2014.
61. Lagneb, C. K., 2007, Evaluation of wayside condition monitoring technologies for condition-based maintenance of railway vehicles, Lulea University of Technology.
62. Lamari, A., 2008, Rolling stock bearing condition monitoring system, Queensland University of Technology.

63. Schobel, A. & Mirkovic, S. 2010. Flat Wheel Detection as a Part of Wayside Train Monitoring Systems. *Acta facultatis medicae Naissensis*, 27.
64. GE Transportation Systems Ltd., Hot Box and Hot Wheel Detection, Welwyn Garden City: GE Transportation Systems Ltd., 2006.
65. ITSS, "ITSS - Hot Axle Box, Hot Wheel and Flat Wheel Detectors," ITSS, Thursday February 2015. [Online]. Available: <http://www.railway-technology.com/contractors/engineering/itss-rail/>. [Accessed Thursday February 2015].
66. Brickle, B., Morgan, R., Smith, E., Brosseau, J. & Pinney, C. 2008. Wheelset Condition Monitoring-RSSB Report for Task T607. *TTCI (UK), Ltd.*
67. Schobel, A. & Mirkovic, S. 2010. Flat Wheel Detection as a Part of Wayside Train Monitoring Systems. *Acta facultatis medicae Naissensis*, 27.
- 68.E. Giannouli, Z. Huang, A. Amini, P. Vallely, S. Soua, F. P. Garcia Marquez, M. Papaelias "Remote condition monitoring of railway axle bearings based on data fusion from several sensors". In Proceedings of WCCM 2017, London, UK, June 2017.
69. Wasiwitono, U. et al., How useful is track acceleration for monitoring impact loads generated by wheel defects? 5th Australasian Congress on Applied Mechanics (ACAM 2007), 2007. *Engineers Australia*, 502-507.
70. Hajibabaia, H. et al., 2012. Wayside Defect Detector Data Mining to Predict Potential WILD Train Stops. Annual Conference and Exposition of the American Railway Engineering and Maintenance-of-Way Association Chicago, U.S.

71. Track IQ, “1,” Track IQ, [Online]. Available: <http://www.trackiq.com.au/railbam.html>. [Accessed 16th February 2015].
72. Southern, C., 2007, The successful use of non contact acoustic bearing condition monitoring, Condition Monitoring National Forum, Sydney, Australia
73. Bladon, K. et al., Predictive condition monitoring of railway rolling stock. Proc., Conference on Railway Engineering, 2004.
74. Jones, C. J. C. & Jones, R. 2010. Management of noise and vibration. In: SCHMID, F. (ed.) Wheel-Rail Best Practice Handbook. Birmingham University Press, A.N. Harris.
75. Snell, O. & Nairne, I. Acoustic bearing monitoring—the future RCM 2008. Railway Condition Monitoring, 2008 4th IET International Conference on, 2008. IET, 1-5.
76. Southern, C. et al., 2004. RailBAM-an Advanced Bearing Acoustic Monitor: Initial Operational Performance Results. CORE 2004: New Horizons for Rail, 23.
77. M. S. a. E. Morganti, “A geography of rail, road and air transport,” French Institute of Science and Technology for transport, development and networks, Paris, 2009.
78. Go-HS2, “Links and Downloads,” Go-HS2, [Online]. Available: <http://www.go-hs2.com/LinksAndDownloads/LinksAndDownloads.aspx>. [Accessed 12 March 2015].
79. H. E. ,. H. J. M. ,. H. M. T. & H. W. A. Rainer Pohl, “NDT techniques for railroad wheel and gauge corner inspection,” NDT&E International , vol. 37, pp. 89 - 94, 2003.
80. H. Rowshandel, M. Papaelias, C. Roberts, C. Davis, Development of autonomous ACFM rail inspection techniques, Insight-Non Destructive Testing and Condition Monitoring, Vol. 53, Issue 2, 2011, pp. 85-89.
81. G. Nicholson, A. Kostryzhev, H. Rowshandel, M. Papaelias, C. Davis, C. Roberts, Sizing and tomography of rolling contact fatigue cracks in rails using NDT technology

- potential for high speed application, 9th World Congress on Railway Research, Lille, France, 2011.
82. J. Al-Dalabeeh, C. Roberts, M. Papaelias, Analysis of alternating current field measurement rail inspection signals, 51st Annual Conference of the British Non-Destructive Testing, NDT 2012, Daventry, UK, 11-13 September 2012.
83. R. S. Edwards, C. Holmes, Y. Fan, M. Papaelias, S. Dixon, C. L. Davis, B. W. Drinkwater, C. Roberts, Ultrasonic detection of surface-breaking railhead defects, *Insight – Non-Destructive Testing and Condition Monitoring*, Vol. 50, Issue 7, 2009, pp. 369-373.
84. D. F. Cannon, K. Edel, S. L. Grassie, K. Sawley, Rail defects: an overview, *Fatigue Fract. Engng Mater. Struct.*, 2003, 26, pp. 865-887.
85. Ekberg, A., Sotkovzski, P., 2001. Anisotropy and rolling contact fatigue of railway wheels”, *International Journal of Fatigue*, 23, pp. 29-43.
86. Industrial Standard (Network Rail) NR/L2/TRK/001/Mod07: Inspection and maintenance of permanent way: Management of rail defects, 1/12/2012.
87. C. Turner, et al., A review of key planning and scheduling in the rail industry in Europe and UK. *Proceedings of the Institution of Mechanical Engineers, Part F: Journal of Rail and Rapid Transit*, 2015: p. 0954409714565654.
88. S. Shi, Z. Han, Z. Liua, P. Vallely, S. Souza, M. Papaelias “Quantitative monitoring of brittle fatigue crack growth in railway steel using acoustic emission (*Proceedings of the Institution of Mechanical Engineers*”. Part F: *Journal of Rail and Rapid Transit*).
89. S. Shi, Z. Huang, S. Kaewunruen, P. Vallely, S. Souza and M. Papaelias “Quantitative monitoring of brittle fatigue crack growth in railway steel

- using acoustic emission”. In Proceedings of WCCM 2017, London, UK, June 2017.
- 90.M. Papaelias, A. Amini, Z. Huang, P. Vallely, D. C. Dias, S. Kerkyras “Online condition monitoring of rolling stock wheels and axle bearings”. Proceedings of the Institution of Mechanical Engineers, Part F: Journal of Rail and Rapid Transit, Vol. 230, No. 3, pp. 709-723, March 2016.
- 91.M. Papaelias, Z. Huang, A. Amini, P. Vallely, N. Day, R. Sharma, S. Kerkyras, Y. Kerkyras “Advanced wayside condition monitoring of rolling stock wheelsets”. In the Proceedings of ECNDT 2014, Prague, Czech Republic, 2014, October 2014.
92. Amini, A., Entezami, M., Kerkyras, S. & Papaelias, M. 2013 Condition monitoring of railway wheelsets using acoustic emission, In the Proceedings of the 10th International CM conference, Krakow, Poland, June 2013.
93. Taylor, J. 1994. The Vibration Analysis Handbook: Vibration Consultants, Inc.
94. Barke, D. & Chiu, W., 2005, Structural health monitoring in the railway industry: a review. Structural Health Monitoring, 4, 81-93.
95. Howard, I. 1994. A Review of Rolling Element Bearing Vibration Detection, Diagnosis and Prognosis'. DTIC Document.
96. James L., et al. 1995. Acoustic emission analysis for bearing condition monitoring. Wear, 185, 67-74.
97. Kerkyras, S., Areias, M. Dias, D. Franco, A. Kerkyras Y. and Papaelias, M., Online evaluation of structural degradation of train wheel using vibration analysis techniques, 49th Annual conference of the BINDT Proceedings, June 2010, Cardiff, UK.

98. Maly, T. et al., New development of an overall train inspection system for increased operational safety. *Intelligent Transportation Systems, 2005. Proceedings, IEEE*, 188-193.
99. Maly, T. & Schobel, A. Concept for crossborder data exchange on wayside train monitoring systems. *9th International Conference on Intelligent Transport Systems Telecommunications, (ITST), 2009, IEEE*, 315-319.
100. Mba, D. & Rao, R. B., 2006, *Development of Acoustic Emission Technology for Condition Monitoring and Diagnosis of Rotating Machines; Bearings, Pumps, Gearboxes, Engines and Rotating Structures*.
101. Ouyang, Y. et al., 2009. Optimal locations of railroad wayside defect detection installations. *Computer - Aided Civil and Infrastructure Engineering*, 24, 309-319.
102. Watson, M. et al., A comprehensive high frequency vibration monitoring system for incipient fault detection and isolation of gears, bearings and shafts/couplings in turbine engines and accessories. *ASME Turbo Expo, 2007*.
103. P. Yilmazer, A. Amini and M. Papaelias, The structural health condition monitoring of rail steel using acoustic emission techniques, In the *Proceedings of NDT 2012 Conference, BINDT, UK, September, 2012*.
104. N. Dadashi, et al. A framework of data processing for decision making in railway intelligent infrastructure, In the *proceedings of IEEE First International Multi-Disciplinary Conference in Cognitive Methods in Situation Awareness and Decision Support (CogSIMA), 2011*.
105. D. O. Harris and H. L. Dunegan, Continuous Monitoring of Fatigue Crack Growth by Acoustic Emission Techniques, *Experimental Mechanics, Third SESA*

- International Congress on Experimental Mechanics, Los Angeles, California, U.S.A., 13-18 May 1973, pp. 71-81.
106. Avraham Berkovits and Daining Fan, Study of fatigue crack characteristic by acoustic emission. *Eng. Fract. Mech.* 51, 1995, pp. 401-416.
 107. T. M. Roberts and M. Talebzadeh, Acoustic emission monitoring of fatigue crack propagation, *J. Constr. Steel. Res.* 59, 2003, pp. 695–712.
 108. T. M. Roberts and M. Talebzadeh, Fatigue life prediction based on crack propagation and acoustic emission count rates, *J. Constr. Steel. Res.* 59, 2003, pp. 679–694.
 109. M. N. Bassim, S. ST. Lawrence and C. D. Liu, Detection of the onset of fatigue crack growth in rail steels using acoustic emission, *Engineering Fracture Mechanics* 41, 1994, pp. 207-214.
 110. Z. Han et al., Acoustic Emission Monitoring of Brittle Fatigue Crack Growth in Railway Steel, WCAE 2015, Hawaii, USA, November 2015.
 111. A. A. Pollock, Back to basics, Loading and stress in acoustic emission testing, American Society for Nondestructive Testing, March 2004.
 112. D. G. E. a. H. N. G. Wadley, “Acoustic Emission: Establishing the Fundamentals,” *Journal of Research of the National Bureau of Standards*, vol. 89, no. 1, p. 26, 1984.
 113. C. G. a. M. Ohtsu, *Acoustic Emission Testing Basic for Research - Application in Civil Engineering*, Berlin: Springer-Verlag, 2008.
 114. J. Yu, P. Ziehl, B. Zárata, J. Caicedo, Prediction of fatigue crack growth in steel bridge components using acoustic emission, *J. Constr. Steel. Res.* 67, 2011, pp. 1254-1260.

115. G. White, *Introduction to Machine Vibration*, Bainbridge Island: DLI Engineering Cooperation, 1995.
116. Curtis, G. 1974. Acoustic emission—4: Spectral analysis of acoustic emission. *Non-Destructive Testing*, 7, 82-91.
117. R. F. Dwyer, Detection of non-Gaussian signals by frequency domain kurtosis estimation, In *Proceedings of IEEE International Conference of Acoustics, Speech, and Signal Processing*, 1983.
118. C. Ottonello and S. Pagnan, Modified frequency domain kurtosis for signal processing. *Electronics Letters*, 30, 14, 1994, pp. 1117-1118.
119. S. Pagnan, C. Ottonello, and G. Tacconi, Filtering of randomly occurring signals by kurtosis in the frequency domain, In *Proceedings of the IEEE 12th IAPR International Conference on Pattern Recognition, Vol. 3: Signal Processing*, 1994.
120. J. Antoni, The spectral kurtosis: a useful tool for characterising non-stationary signals, *Journal of Mechanical Systems and Signal Processing*, 20, 2, 2006, pp. 282-307.
121. Godin, N., S. Huguet, and R. Gaertner, Integration of the Kohonen's self-organising map and k-means algorithm for the segmentation of the AE data collected during tensile tests on cross-ply composites. *NDT & E International*, 2005. 38(4): p. 299-309.
122. Godin, N., et al., Clustering of acoustic emission signals collected during tensile tests on unidirectional glass/polyester composite using supervised and unsupervised classifiers. *NDT & E International*, 2004. 37(4): p. 253-264.

123. Qazizada, M. E. and Pivarciova, E., Mobile robot controlling possibilities of inertial navigation systems. *Procedia Eng.*, 149:404-413, ICMEM 2016, (CC-BY-NC-ND-4.0).
124. E. Giannouli, Ph.D. Thesis, University of Birmingham, 2020.
125. Schlichting, Joachim & Ziegler, Mathias & Maierhofer, Christiane & Kreuzbruck, Marc. Flying Laser Spot Thermography for the Fast Detection of Surface Breaking Cracks. 18th World Conference on Nondestructive Testing, April 2012, Durban, South Africa.

APPENDIX 1

Institution of
**MECHANICAL
ENGINEERS**

Certificate for Best Presented Paper

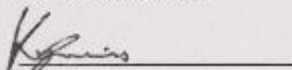
This is to certify that

PATRICK J VALLELY

Was voted the best presented paper at
The Stephenson Conference: Research
for Railways 2017

Kiesha Lewis

Events Executive



The Institution of Mechanical Engineers

Improving the world through engineering

